MILLER CYCLE COMBUSTION STRATEGY FOR DOWNSIZED GASOLINE ENGINES

TENGKU NORDAYANA AKMA

Aeronautical and Automotive Engineering Department

Loughborough University, UK

Submitted in partial fulfilment of the requirements for the award of

Doctor of Philosophy of Loughborough University

May 2017

ABSTRACT

In response to the global concerns towards oil scarcity and climate change, the automotive industry is currently focusing on improving fuel economy and reducing exhaust emissions. Modern downsized gasoline engines that come with a package that includes a boosting system, variable valve train and direct fuel injection system is effective for fuel economy improvement and emission reduction. However, the knocking issue becomes severe at high load operations as a result of the high intake boosting pressure. In regard to the part load conditions, the gas exchange process requires extra work to draw in air into the cylinder due to a lower amount of pressure in the intake manifold caused by the restriction of the throttle plate.

The Miller cycle is regarded as a potential strategy of knock control for downsized gasoline engines. Extensive works have sought to examine the performance improvement via the Miller cycle, yet only limited research has been conducted on the manner in which it can influence knock suppression. The focus of this thesis is to investigate early and late intake valve closing timings in terms of how they affect the compression process, the ability to suppress engine knock and meet the power output required at high loads for spark-ignited gasoline engines. Apart from that, this research also demonstrates the Miller cycle potential by utilising fully variable valve timing in controlling the load at the part load condition without using a throttle. The early intake valve closing with different valve lifts was tested in order to investigate the impact during the gas exchange process, particularly the pumping losses and the potential to improve fuel economy.

This study includes both experimental and simulation studies. A Lotus single-cylinder research engine referred to as SCORE was mainly used for the experimental component of the study. The simulation work was conducted using a one-dimensional spark ignition engine model built in the Ricardo WAVE software for naturally-aspirated and downsized engines. The engine model values are validated against the experimental values from the Lotus SCORE and Lotus SABRE engines. The combustion model with a reduced kinetics mechanism was validated using a Rover K-series engine. A broad matrix of the engine operations has been investigated combining a variety of engine speeds and engine loads.

The Miller cycle effects on knock suppression in a downsized engine environment have been investigated in three parts, namely the Miller cycle at different speed-load, knock suppression with extreme Miller cycle, and knock analysis with combustion kinetics. Through the works, the Miller cycle has demonstrated its capability to suppress engine knocking in a more efficient manner as opposed to the standard engine operation. This is contributed by the fact that early and late intake valve closings could affect the end gas condition at the end of the compression stroke, thus making it possible to suppress the engine knocking.

The experimental study for controlling load without using throttle under the naturally-aspirated condition found that the Miller cycle with an early intake calve closing strategy able to improve fuel consumption by reducing pumping losses. The downsized engine condition, which has been evaluated via modelling work, also showed an improved performance trend using the unthrottled Miller cycle strategy. The open cycle and close cycle efficiencies have improved through the Miller cycle implementation.

The contribution of this work is made in order to establish the comparison of the Miller cycle strategy in suppressing knocking between the early intake valve closing and late intake valve closing under a boosted environment. For the part load condition of the downsized engine, the research contributes to the existing body of knowledge by comparing the throttle-less Miller cycle and the standard throttled operation as a load control strategy.

Pursuit of happiness…

I am grateful for the amazing and inspiring people I have encountered throughout my journey.

ACKNOWLEDGEMENT

I would like to thank some of the people that I have been fortunate enough to have in my life and especially those who helped me throughout my PhD journey and the most challenging task of writing this thesis.

My first thank you is to my supervisor, Professor Rui Chen, for his encouragement and critical advice on my works throughout the research journey. My teammates in the combustion research group especially Sotiris and Dan. Thanks to Dr Graham Pitcher for his technical support on the SCORE engine and Farraen for helping me with the engine model. I would also like to express my thanks to the members of staff in the AAE workshop and other fellow researchers in the W189 PhD office.

My thanks also go to Loughborough University for the great experience and knowledge that I have gained here. I would like to express my gratitude to my sponsors; the Ministry of Higher Education Malaysia and the International Islamic University Malaysia. Not to forget to the Loughborough community for making my stay there was memorable.

Special thanks to my life partner, Kasyfi Mohamad Nor. The journey would not have been possible without his endless love and support. To my son, Tariq Mursyid, who has made this journey even more special. Also, thank you to my beloved parents and parents-in-law. And finally, thanks are also due to everyone else, whose names are not listed here, for their kind help and support.

TABLE OF CONTENTS

NOMENCLATURE

Symbols

C	Absolute gas velocity
c_p	Specific heat at constant pressure
c_v	Specific heat at constant volume
m	Mass
$\dot{m}$	Mass flow rate
N	Crankshaft rotational speed
P	Pressure
T	Temperature
Q	Heat transfer
λ	Ratio of expansion ratio to the compression ratio
γ	c_p / c_v
u	Specific internal energy
h	Specific enthalpy
V	Cylinder volume
R	Gas constant
l	Connecting rod length
a	Crank radius
s	Crank axis to piston pin distance
B	Cylinder bore
θ	Crank angle
η	Efficiency
ρ	Density

Abbreviations

1-D	One dimensional
AFR	Air-fuel ratio
BDC	Bottom dead centre
BMEP	Brake mean effective pressure
BSFC	Brake specific fuel consumption

CI	Compression ignition
CO_2	Carbon dioxide
DF	Downsizing factor
DISI	Direct injection spark-ignited
EIVC	Early intake valve closing
EU	European Union
FVVT	Fully variable valve timing
GCR	Geometric compression ratio
GDI	Gasoline direct injection
GECR	Geometric effective compression ratio
HRR	Heat release rate
IMEP	Indicated mean effective pressure
ISFC	Indicated specific fuel consumption
IVC	Intake valve closing
LIVC	Late intake valve closing
LSPI	Low speed pre-ignition
MBF	Mass burned fraction
MEP	Mean effective pressure
NA	Naturally-aspirated
NO_x	Nitrogen oxide
PFI	Port fuel injection
PMEP	Pumping mean effective pressure
SFC	Specific fuel consumption
SI	Spark ignition
SOI	Start of injection
VCR	Variable compression ratio
VVT	Variable valve timing
WOT	Wide open throttle

LIST OF FIGURE

LIST OF TABLE

Chapter 1

INTRODUCTION

1.0 Overview

This chapter briefly explains the current situation and future direction of internal combustion engines. Throughout the chapter, a brief overview of internal combustion engines (ICE) and their future development will be provided so that we would understand and appreciate why it is still relevant to conduct research in this technological branch, while facilitating the improvement of green technologies in order to achieve a sustainable transportation system. The motivation behind this study and the research direction of the project will also be clarified.

1.1 Current situation of ICE

For over a century, the revolution of internal combustion engines has been accurately reflecting the expansion of the automotive industry and modernisation of the world. The development of the engine technology could be clearly observed in the automotive industry. Apart from conventional engines, a more extensive commercialisation strategy has been implemented in the case of fuel cell vehicles, electric vehicles, and hybrid vehicles. Nevertheless, it is predicted that in the near future, these technologies would still be considered as very challenging for full operationalisation. There are no limits in predicting the future of engine advancement, but as of now, the internal combustion engine is expected to remain the dominant power plant of the vehicles, with improvements being made in terms of fuel quality and engine efficiency.

The main commercialised internal combustion engines can be classified into two broad categories: spark ignition (SI) engines, which are powered by gasoline fuel, and compression ignition (CI) engines, which generate power from diesel fuel. Apart from gasoline and diesel, many alternative fuels are nowadays being tested on SI and CI engines in order to replace the dependency on fossil fuel. Significant efforts have been made by researchers and manufacturers in achieving feasible and superior internal combustion engine technologies. Despite achieving some significant milestones, they are

still struggling to break the physical limitations of the mechanisms and are consistently facing difficulties in the process.

It is important to understand how the energy flows in the car from the moment fuel is filled in the tank. Figure 1.1 shows the energy flows of a midsize gasoline-powered vehicle for urban and highway driving. An efficiency rate of only 13 – 20 % is finally transmitted to the wheel from the fuel energy [1]. The amount of fuel consumed by a vehicle is affected by the driving conditions and the vehicle efficiency itself in converting chemical energy into mechanical energy to drive the wheels. From a total percentage of energy of 100 % in the fuel tank, 62 - 69 % is associated with engine loss. Significant further improvements could be made to the existing engine technology in order to fully utilise the energy produced, despite views holding that the development of internal combustion engines has already reached its limit.

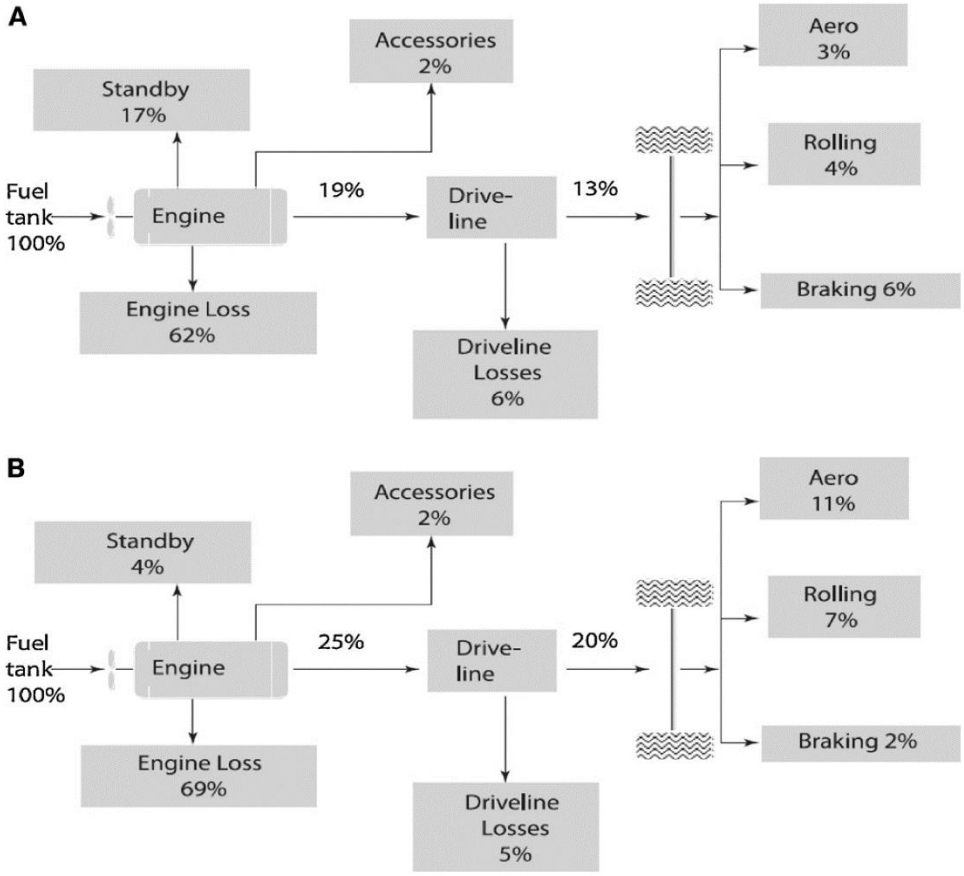

Figure 1-1 Energy flows of a car: A) Urban driving, B) Highway driving [1]

Figure 1.2 shows the average losses and efficiency between three tested engines, which represent the currently available engines in the market. It is a project conducted by MAHLE in order to identify the potential for energy efficiency in different operating points of the speed-load. Engines *#1* (1.6 L, CR 12.1:1) and *#2* (1.8 L, CR 11.2:1) are NA engines with port fuel injection, while engine *#3* (1.6 L, CR 11.0:1) is a turbocharged engine with direct fuel injection.

The average efficiency from the three engines is calculated at 29 % [2]. The graphs indicate that thermal losses are dominating with more than 50 % for all three engines and constitute a challenge for the ICEs in terms of reaching higher efficiency. The turbocharged engine *#3* shows a good reduction in thermal losses and increment in the overall efficiency, as compared to the NA engines. However, the value for thermal losses is still considered to be high because it exceeds 50 %. The aforementioned findings clearly demonstrate that a significant amount of potential energy has been lost to the thermal losses. Further developments are required in order to improve the overall efficiency and cut the losses. This is to make sure that the internal combustion engine is still relevant in today's world, where it must compete with other new technologies, such as electric driven and fuel cell powered cars.

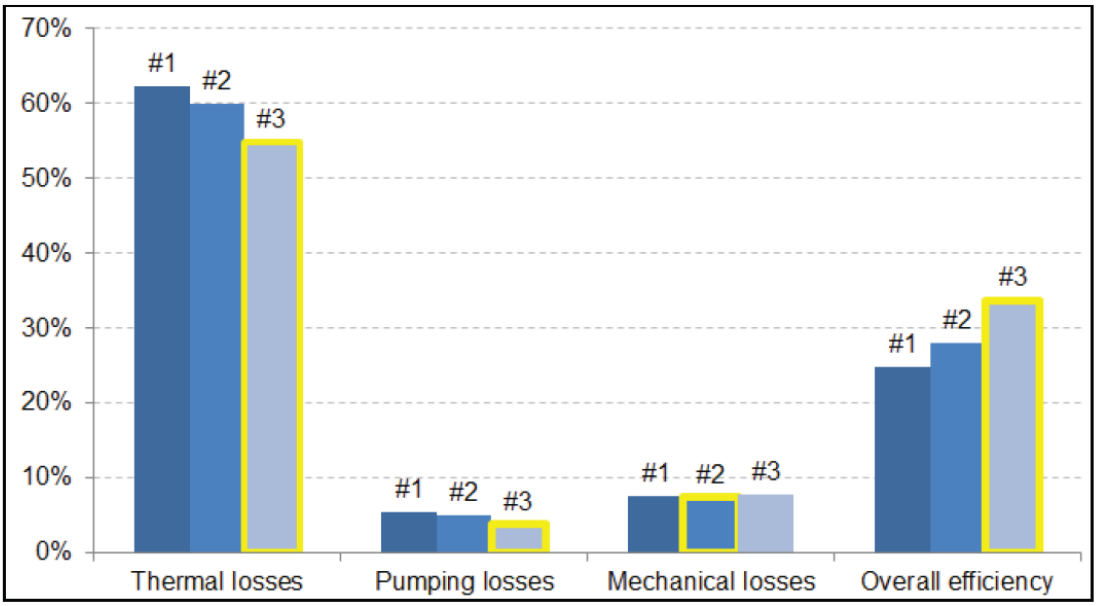

Figure 1-2 Average losses and efficiency [2]

1.2 Future direction of ICE

Most of the major vehicle markets have introduced energy efficiency regulations for the vehicle manufacturers to follow. Figure 1.3 illustrates the target for the new vehicles based on the amount of carbon dioxide (CO_2) emissions. The European Union (EU) target is 95 g CO_2/km by the year 2021. As two of the largest developing economies, China is targeting 117 g CO_2/km by the year 2020 and India is targeting 113 g CO_2/km by the year 2021 [3].

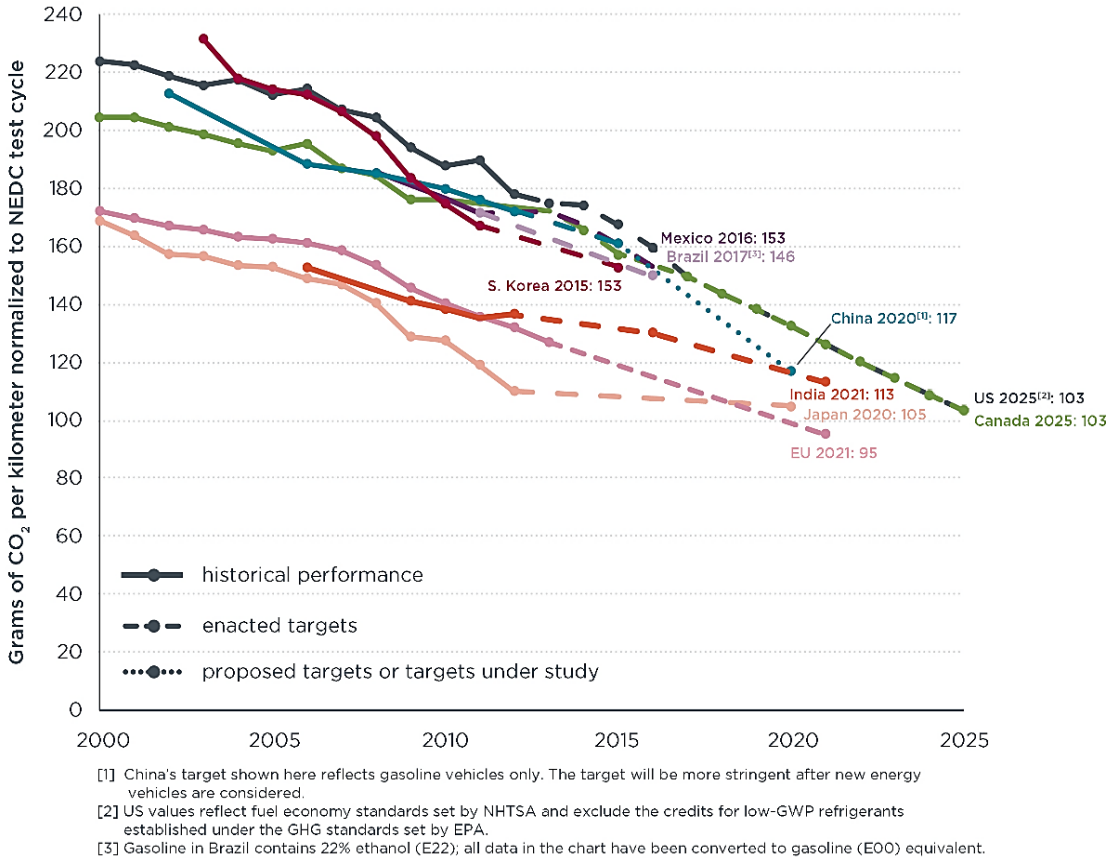

Figure 1-3 Global CO_2 regulations for passenger cars [3]

The European Road Transport Research Advisory Council (ERTRAC) has recently publicised the European Roadmap on future light-duty powertrain technologies and fuel. The main objective is the decarbonisation of road transport by improving energy efficiency predominantly by way of achieving better fuel efficiency in the case of engines, powertrains, and vehicles. ERTRAC's Strategic Research Agenda 2010 indicated that over half of the new light-duty vehicles in 2050 will still be powered by ICE using advanced concepts and technologies.

Figure 1.4 below summarises the variation of energy pathways for a future transport fuels roadmap, starting from the primary energy until the powertrain technology. Renewable energy, such as wind, water, solar, geothermal and biomass energy, is expected to constitute the primary source to power up the electric motor. This will decrease the dependency on fossil energy, which is not sustainable in the long-term. An increasing trend in the case of electric motor options is anticipated in the future, but the combustion engine will be expected to maintain its dominant position for the short- and medium-term based on cost and performance [4].

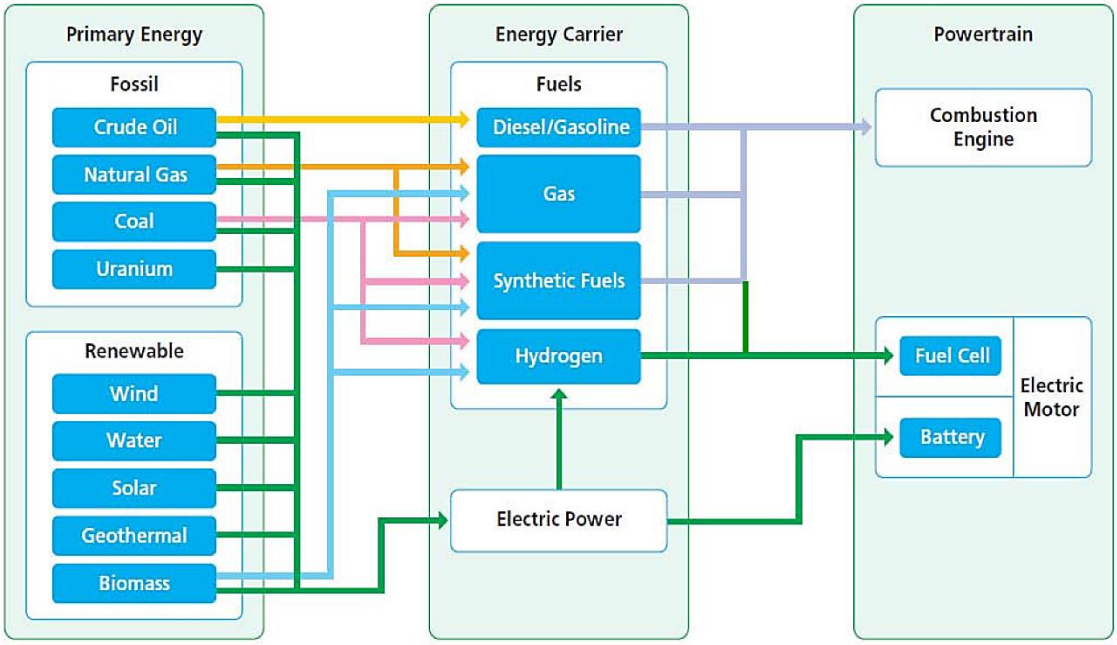

Figure 1-4 Energy pathways for liquid, gaseous, and electric energies [4]

The future demands of advanced internal combustion engines in gaining better energy efficiency and fewer emissions will require more flexibility in the engine operating system. The engine is expected to be able to run at different speed-load conditions with optimised combustion efficiency. The conventional ICE is tuned based on the high-performance requirement, but most of the time, it is operated in the low to medium range. The anticipated flexibility can be achieved by implementing innovative technologies into the engine environment. Downsizing, turbocharging, fully variable valve trains, gasoline direct injection, advanced combustion strategies, and exhaust gas recirculation are some of the technology trends that can be found in most new commercial engines nowadays.

Figure 1.5 indicates the trends for light-duty powertrains up to year 2030. Fully flexible injection and valve train systems, downsizing, downspeeding and also high pressure charging are the technologies to be found in both gasoline and diesel engines starting with 2010 in anticipating the enhancement of fuel efficiency and a reduction in emissions. By having these technologies installed in the engine, advancements in the case of combustion strategies, such as lean stratified SIDI, waste heat recovery, and controlled auto-ignition, can be achieved sooner.

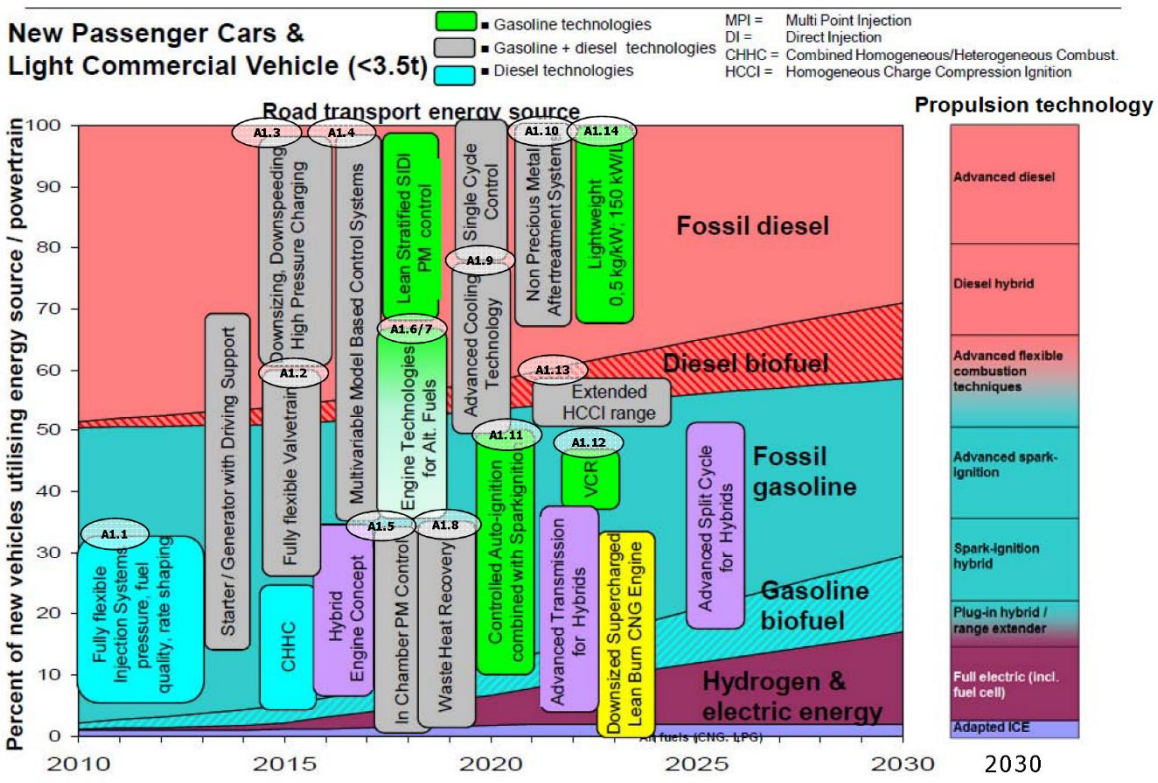

Figure 1-5 Technology trends and the vision engines share in Europe [4]

Fully flexible injection system: A very good fuel system is vital to an engine nowadays, particularly when considering the uncertainty of fossil fuel resources. Thus, any effort to improve the fuel economy of an engine is a serious concern in the automotive industry since fossil fuel is still a preferred energy source as opposed to other alternative fuels due to its high-energy content. The fuel system of ICE has undergone a few stages of development in terms of its mechanism. From carburettor to port fuel injection (PFI), and nowadays direct injection (DI), it is considered to be one of the advanced technologies in the fuel injection system. It has the potential of leaner combustion, constant air-fuel cylinder-to-cylinder ratio, and lower BSFC values. The fuel atomisation is much better

since the fuel is injected under very high pressure, which will subsequently improve the fuel vaporisation rates.

Fully flexible valve trains: Load control by valve train instead of throttle is possible through variable lift and variable opening duration. The response time for load jumps can be decreased. Fully flexible valve trains can also maintain the turbulence level inside the combustion chamber as required by the combustion process through multiple opening events provided that it is decoupled from the crankshaft. By having this technology in the engine, it is thus possible to enable the advanced low temperature combustion strategy.

In the operation of modern internal combustion engines, valve timing plays an important role in the intake and exhaust process. The manner in which it is operated will significantly affect the efficiency of the engine and emissions level. Conventionally, the valve timing is controlled based on camshaft and crankshaft synchronisation, thus the values are fixed. Nowadays, in order to have an independent control of the valve lifting and timing, variable valve timing technology (VVT) is used. The timing can be varied and modified based on the performance needed. The fully variable valve timing (FVVT) strategy is used in order to control the gas exchange process at different speed and load values, but it requires a more advanced VVT system.

Downsizing, downspeeding, high pressure charging: Downsized gasoline engines are no longer a novel concept in the industry. The current maximum brake mean effective pressure (BMEP) reaches up to 25 bar.

For a downsized engine to retain the power capacity of a larger engine, a forced induction system is required in order to increase the amount of air in the cylinder. This is done on the basis of supercharging technology where the charge will be pre-compressed and thus the increased density of the mixture will increase the power output density of the engine. The main difference between a mechanically driven charger (supercharger) and exhaust gas turbocharger is constituted by the power supply required in order to run the compressor. A mechanically driven charger is attached to the engine itself using a belt, while the exhaust gas turbocharger is driven by the exhaust power. The turbocharger is more efficient as it utilises exhaust energy, while the mechanically driven charger wastes some of the power generated from the engine in order to run the compressor itself. The

benefit it brings to the engine is enabling the engine to produce a higher power output at a lighter engine weight.

This project is paying great attention to this trend, particularly in the case of the downsized gasoline engine with the availability of fully flexible valve train and high pressure charging systems. By utilising these technologies, the combustion strategy can be enhanced to achieve more efficiency than the conventional Otto cycle.

1.3 Motivation of Study

The topic of downsizing is currently one of the main drivers in the development of internal combustion engine technology, as discussed in the previous subsection. The objective is to achieve higher engine efficiency, while maintaining the power performance and to fulfil the stringent emission law. Downsizing means that the engines' capacity is declining, while at the same time maintaining the full load performance or maintaining the same capacity but being able to achieve a higher power output.

Common related technologies with downsized engines: turbocharging, fuel injection system, variable valve trains, advanced combustion, cylinder deactivation. A better understanding regarding the interaction between those technologies and the gas exchange process will then make it possible to manipulate the combustion strategy to gain better efficiency.

Problems of interest:

1. With all advanced technologies added to the engine, the capability of the downsized engine is still not fully utilised. The knocking issue becomes severe at high load operations due to the high intake boosting pressure in the downsized engine. Thus, the reduction of the geometric compression ratio is usually selected as the solution to avoid knock, which means that the fuel economy benefit is reduced.
2. The gas exchange process during the part load condition requires additional work to draw in air into the cylinder due to the decreased pressure in the intake manifold coming from the restriction of the throttle plate. This pumping loss affects the engine fuel economy. This situation is a longstanding issue in the case of the naturally aspirated engine and is also encountered in the downsized engine.

3. The conventional Otto cycle is affected by low efficiency and high thermal losses. An alternative cycle is required in order to increase the engine efficiency and perform better under the downsized engine environment. On average, only about ~30 % of energy efficiency is utilised. Thermal losses can go as high up as ~50 – 60 %. Therefore, it is important to recover those losses in order to obtain better engine efficiency.

1.4 Knowledge Gap

1. Extensive works have been undertaken in order to examine the performance improvement using the Miller cycle, but few discussions have been held on how it can influence the knock suppression. One aspect to consider is the potential of combining the Miller cycle with the ignition strategy in order to control the engine knock. Thus, this makes it possible to eliminate the compromise of reducing the compression ratio in the current downsized engine in order to prevent the knock.
2. Previous research studies focused on utilising the fully variable valve train as a load control strategy in a naturally-aspirated engine environment. Nowadays, modern downsized engines are equipped with boosting systems to achieve higher power output. Therefore, the Miller cycle potentials in controlling the load under boosted environments need to be investigated.

1.5 Research Objectives

The thesis aims to establish a structured scientific understanding for the combustion strategy of the Miller cycle in downsized gasoline engines in controlling engine knock and engine load. The objectives of this research are listed as below:

- To compare the efficiency of the Miller cycle with other engine cycles of the Otto, Diesel, Dual, and Atkinson cycles under naturally-aspirated and boosted conditions on the basis of the ideal gas cycle modelling.
- To investigate the Miller cycle performance through the implementation of early intake valve closing and late intake valve closing valve timings in order to determine how it affects the compression process, thus influencing the knock phenomenon during the combustion process in the downsized engine.
- To study the potentials of the load control strategy by the Miller cycle without throttle by varying the intake valve closing profiles in naturally-aspirated and downsized engines via engine modelling and experimental works.

1.6 Research Contributions

The key contributions arising from the research study are listed below:

1. The supercharged Miller cycle can be utilised in the engine as a more efficient combustion strategy as opposed to other cycles based on the air standard cycles' comparison.
2. The comparison of the Miller cycle behaviours that is achieved either through early intake valve closing or late intake valve closing at different speed-load conditions in a downsized gasoline engine is studied extensively.
3. The measurement of the Miller cycle ability in engine knock suppression is established. An understanding of the chemical process that occurred using the chemical kinetics mechanism is achieved in order to better understand the detailed processes.
4. The application of the unthrottled Miller cycle for engine load control in the downsized gasoline engine is done as an extension to the study completed in the naturally aspirated engine.

1.7 Thesis Outline

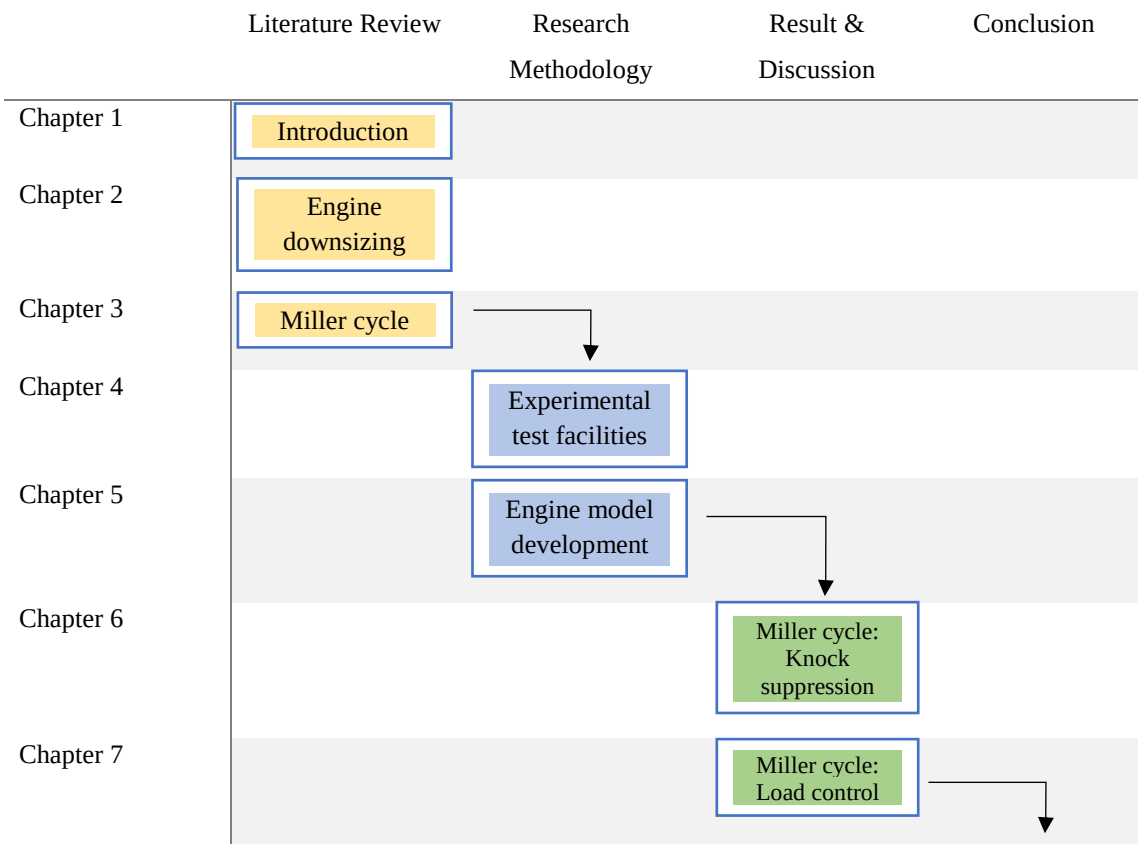

Figure 1-6 Flow of the thesis outline

Chapter Two: Literature Review (Engine downsizing). This chapter reviews the engine downsizing concept and its mechanism. The reasons why downsizing is required for the engine are also discussed. The background is given to the three main technologies related to engine downsizing, namely the boosting system, direct fuel injection system and variable valve train system. The latest downsized engines and research engines available in the market are listed in the chapter. Apart from the benefits, an abnormal combustion at high load is the common issue related to engine downsizing and inefficiency under the part load condition due to the pumping losses, as it will be further elucidated in the chapter.

Chapter Three: Literature Review (Miller Cycle). This chapter reviews the Miller cycle concept as a potential solution to overcome the issues in downsized gasoline engines. It mentioned the history of the Miller cycle. The difference between the Miller cycle and Otto cycle mechanisms are compared. The chapter also lists some recent engine developments that have applied the Miller cycle and their contributions. The benefits and limitations of the Miller cycle are listed below. It also highlights the reason for investigating the Miller cycle in this work.

Chapter Four: Experimental Test Facilities. This chapter describes the experimental test facilities used in the project. There are three engines associated with the project, namely the Lotus SCORE, Lotus OSCAR and Rover K16 engines. The work included in this thesis was conducted on the Lotus SCORE and Rover K16 engines. However, the project involved data transfer from the Lotus OSCAR engine, thus, the description of this engine was also included for reference. There is also supporting data used from the Steady Flow Rig experiment. Thus, the description of the rig set-up is also included in this chapter.

Chapter Five: Development of Engine Model and Model Validation. For this research project, the Ricardo WAVE and MATLAB software applications were used in order to develop a single-cylinder naturally-aspirated engine model and a downsized engine model. MATLAB Simulink was used as a platform for the integration of the combustion model in MATLAB with the engine model developed in the Ricardo WAVE software

application. The combustion model integrated the Cantera software application for problems involving chemical kinetics, thermodynamics and transport processes. The engine models were validated by the experimental results based on their respective characteristics.

Chapter Six: Result & Discussion I (Miller Cycle: Engine Knock Suppression). This chapter discusses the Miller cycle effects in suppressing the engine knocking phenomenon based on the following questions: (1) How does the Miller cycle perform in comparison with other cycles? (2) How does the Miller cycle strategy with the early and late intake valve closing profiles influence the knocking under downsized engine conditions? and (3) Do early and late intake valve closing timings react differently at different engine speeds and different engine loads (low, medium, high)? The results and analysis will be divided into three main parts, namely Part 1: Miller cycle at different speed-load, Part 2: Knock suppression with extreme Miller cycle and Part 3: Knock analysis with combustion kinetics.

Chapter Seven: Result & Discussion II (Miller Cycle: Load Control). This chapter discusses the Miller cycle effects in controlling the load based on the following questions: (1) How does the Miller cycle strategy with the early intake valve closing profiles influence the engine performance for naturally aspirated engines? and (2) What is the performance comparison between naturally aspirated and boosted engines when using the unthrottled Miller cycle strategy to control the load? The focus of this chapter is to demonstrate how the Miller cycle with early IVC affects the gas exchange process and the engine efficiency in both naturally aspirated and downsized engine conditions.

Chapter Eight: Conclusion & Future Work. This research work focused on the application of the Miller cycle combustion strategy in downsized gasoline engines. Two of this study's focal points are the Miller cycle strategy for engine knock suppression and the Miller cycle strategy for load control under a downsized environment. The results presented are summarised and future works to be expanded from the current research are also listed.

Chapter 2

LITERATURE REVIEW: ENGINE DOWNSIZING

2.0 Overview

Downsizing in internal combustion engines has become largely perceived as an effort to attain better engine efficiency and fuel saving in the automotive industry nowadays. This chapter reviews the downsizing concept and its mechanism. An overview of the three main technologies related to engine downsizing, namely the boosting system, direct fuel injection system and variable valve train system, is provided. Current findings and developments particularly related to the downsizing of commercial engines designed by automotive manufacturers are also addressed in this chapter. The benefits and limitations are further discussed in order to determine how this technology brings gains and losses in terms of engine efficiency. Apart from the benefits, an abnormal combustion at a high load is a common issue related to engine downsizing and inefficiency under the part load condition due to pumping losses, as it will be further elucidated in the chapter.

2.1 Downsizing Definition & Mechanism

Downsizing in the SI engine originated from a significant improvement of the CI engine in terms of increasing the power density and mean effective pressure (MEP) in relation to the application of direct injection and supercharging technologies. The benefits of the high torque levels and low fuel consumption gained are favourable to be applied to the SI engine [5]. Based on that, it has enormous potential as an effective way for the SI engine to meet the stringent regulations while maintaining its performance.

Downsizing is defined by having reduced engine capacity with the same or a better power output by means of pressure charging in order to substitute the larger engine [6]. It is therefore sought to maintain the performance by having more air to burn more fuel via the supercharging system. A smaller size means less volume swept by the piston while moving up and down during the cycles. Having a smaller size engine resulted in less friction loss and more fuel being saved. Additionally, the production of CO_2 can be reduced when the engine operates at its optimum.

The current downsized gasoline engines available on market are said to have a 'downsizing factor (*DF*)' of 35 – 40 % which is defined as [7]:

$$DF = \frac{V_{swept,NA} - V_{swept,Downsized}}{V_{swept,NA}} \tag{2.1}$$

Why do we need engine downsizing?

Smaller engines consume less fuel. This is what motivates manufacturers to opt for engine downsizing. Another main drives of the downsizing trend is meeting the future requirement of reducing carbon emissions in passenger vehicles [6]. Car manufacturers have to face the issues of limited fossil fuel reserves and obey the increasingly stringent emission regulations [8]. By reducing the number of cylinders and the engine volumes, it is also possible to reduce the weight of the car since the engine has fewer components and less structure is needed to support the engine.

Downsizing is regarded as a potential solution to overcome the pumping losses in large engines. This is because larger naturally aspirated engines need to throttle more than smaller engines under the part load condition [9]. More pumping work means less mechanical efficiency. High pumping losses predominantly occur during driving in urban conditions. This is because the engine needs throttling in order to reduce the power output as desired. Downsizing should help reduce these losses because the throttle opens wider and it has higher intake pressures [10].

A throttle plate acts as a restrictor in varying the amount of mass of the trapped mixture. The throttle plate lowers the density of the mixture trapped and thus reduces the trapped mass. Nevertheless, this makes the cylinder pressure (P_c) drop below the atmospheric pressure (P_o) level. The piston must then engage in extra unproductive work in order to overcome the flow resistance across the throttle. Urban driving predominantly happens at low loads, and this induction work can account for up to 10 % of the net IMEP. Therefore, if the induction work can be removed completely, the improvement of the ISFC can go up to 9 % [11]. Figure 2.1 shows the induction work (shaded area) that takes place during the intake stroke.

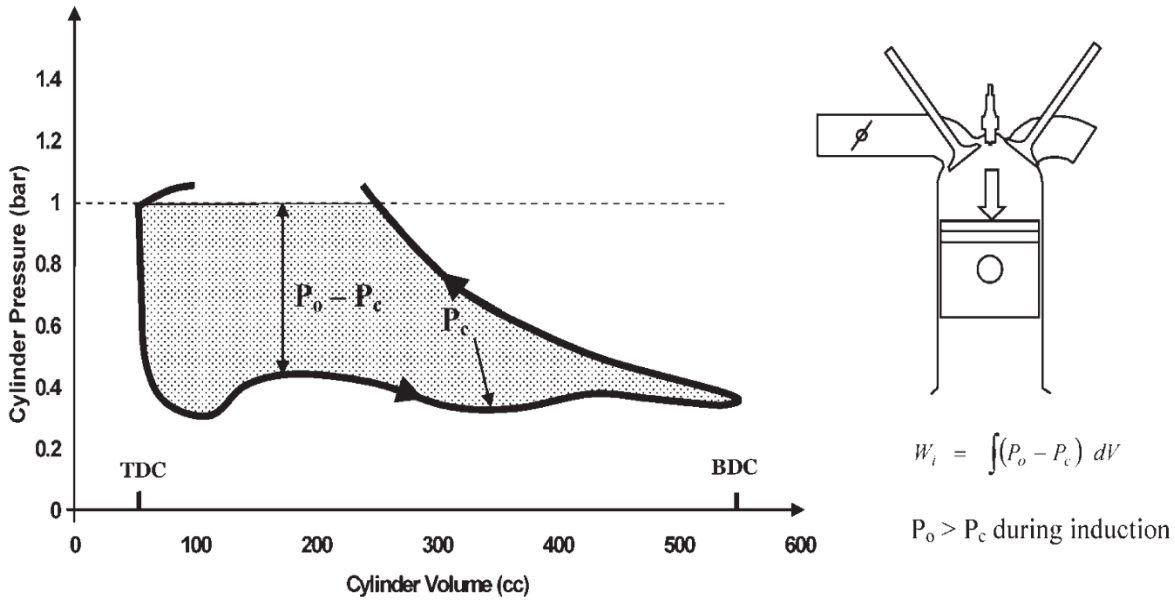

Figure 2-1 Work done during throttled induction in the NA engine [11]

At low loads, the downsized engine operates at higher BMEP with a higher trapped charge density. This results in reduced intake throttling and pumping work [11]. By having a smaller engine through downsizing, the desired power output can be achieved with fewer pumping losses.

2.2 Technologies Related with Engine Downsizing

Further developments of engine downsizing are possible with the advancement of the boosting system, direct injection fuel system and variable valve train system, which are available in the engine. Listed below are the technologies commonly associated with engine downsizing. They are divided into external and internal categories. External is referring to the external modification or system added to the engine, while internal refers to the internal modification of the combustion strategy done inside the cylinder.

External modification:

1) Boosting system (Super/turbo-charging)
2) Direct injection fuel system
3) Variable valve train (VVT)
4) Variable compression ratio (VCR)
5) Cylinder deactivation

Internal modification:

1) Unconventional thermodynamics cycles (Miller, Atkinson, *etc*)
2) Multi-cycles (2, 4, 6-stroke)
3) Control Auto-Ignition (CAI) – Stoichiometric/Lean
4) Homogeneous (Premixed) or Stratified charge, lean burn
5) Waste heat recovery

Boosting System

The steady state low speed torque and transient response are the two main areas which are given more attention in selecting a boosting system for a downsized engine. At present, the single-stage turbocharger has been used in most downsized engines. But in order to address the aforementioned issues, more powerful boosting systems are required. Figure 2.2 shows the different types of boosting system configurations that can be found installed in the engine [12].

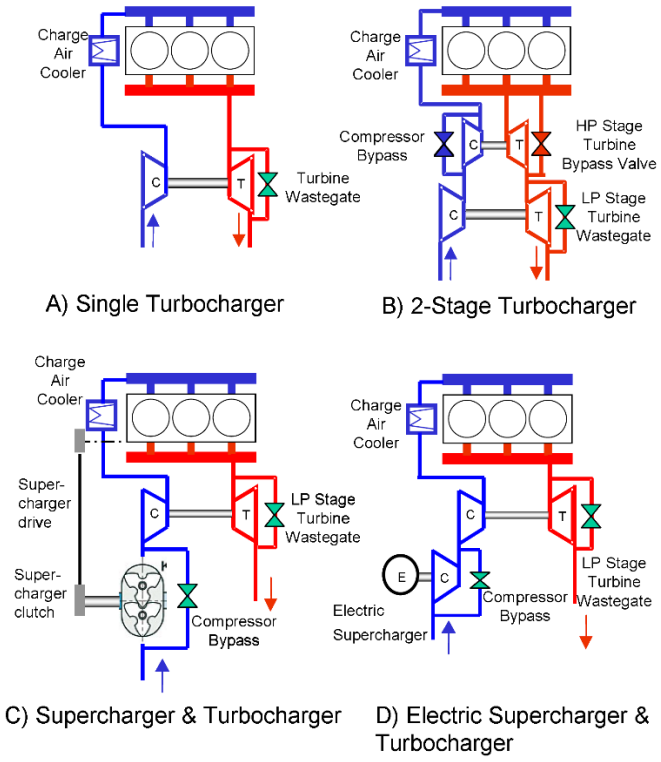

Figure 2-2 Boosting systems [12]

A) Single turbocharger – the standard system with a single compressor and a single turbine. The improved version involves a twin-scroll turbocharger. Variable flow turbines, variable geometry turbines.

B) 2-stage turbocharger – consisting of a small high pressure turbine for low speed and a large low pressure turbine for high-speed operations.

C) Supercharger & turbocharger – the supercharger is utilised at low engine speed and then bypassed by a larger turbocharger as the speed increases.

D) Electric supercharger & turbocharger – an electric supercharger, which is installed up- or downstream of a large turbocharger. The supercharger is used at low engine speed in series with the turbocharger. Then, the turbocharger will take charge once it has spooled up.

Figure 2.3 illustrates the cost and benefit estimation of turbocharging, as well as the downsizing technologies of the cooled EGR, Miller cycle and 48 V electrical system. The reduction in fuel consumption expressed as a percentage is increasing in line with the combination of advanced technologies, but this also indicates an increment in the manufacturing cost. The combination of e-boosting and 48 V is said to be one of the most significant developments in downsized engines. It can directly boost the engine or reduce the turbo lag by spinning the turbocharger faster. The engines can be downsized more and run at lower speeds.

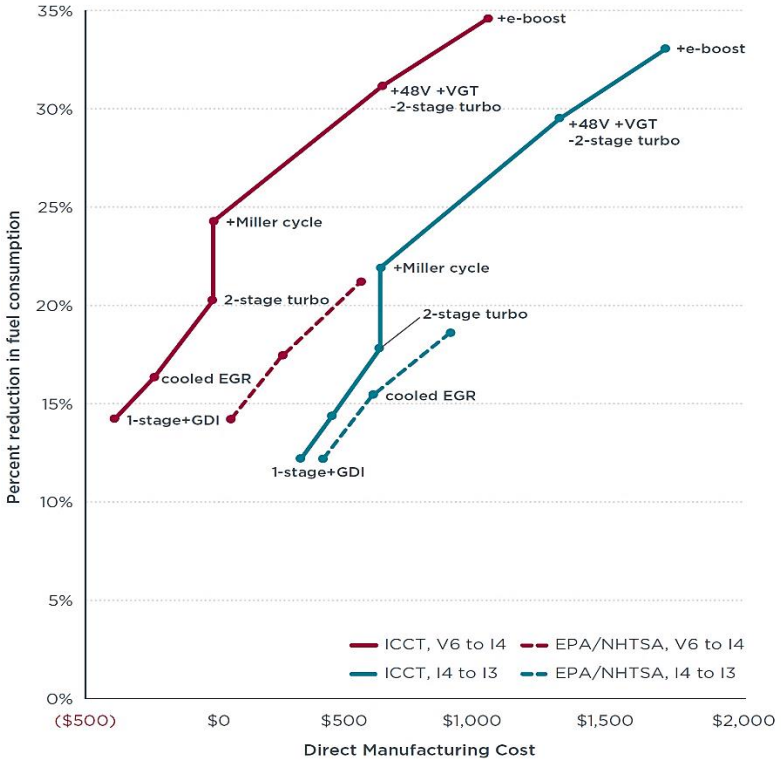

Figure 2-3 Comparison of the 2012 costs and benefits of turbocharging and downsizing technologies [13]

Honeywell and BorgWarner project that 40 % of the market share for turbocharged engines can be achieved by 2020, while the US government projected that 64 % of sales in 2021 should be coming from turbocharged engines [13].

Direct Fuel Injection System

In the case of multiple injections with stratified charge, the lean burn has the advantage of extending the operating mode to a higher load and speed. A series of injections are administered during the compression stroke, which allows for a better mixture and combustion efficiency [14].

Figure 2.4 illustrates the GDI operating modes based on different speed-load regions. A double injection is suggested for the high load, low speed region. The GDI operating mode is divided into two main types of operating modes:

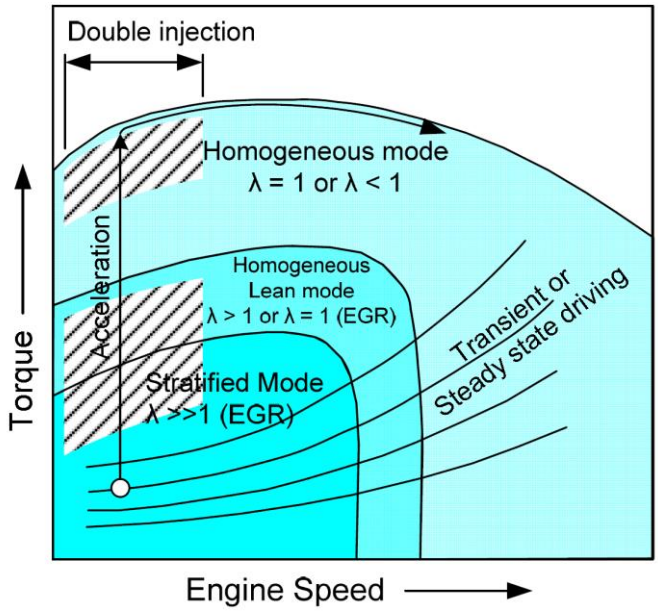

Figure 2-4 GDI operating modes at different operating points [14]

1. *Stratified Charge*: The stratified charge is usually applied at the part load. The injection timing is retarded towards the end of the compression stroke. The engine has a leaner air fuel ratio and unthrottled operation in this condition, with the introduction of the exhaust gas recirculation (EGR). The engine load is adjusted by the fuel/air equivalence ratio.
2. *Homogeneous Charge*: The homogeneous charge is more favourable at a higher load and under higher speed operation. Fuel is injected during the intake stroke to give ample time for the mixture to mix properly. The engine is usually at the

stoichiometric air-fuel ratio or under a slightly rich condition. The engine load is controlled by throttling.

Variable Valve Train

The valve train system plays an important role in implementing greater combustion strategies to fulfil the emission requirements. The gas exchange processes executed by the valve train system directly influence the combustion process during the mixture preparation and compression phase. The system needs to be flexible enough to have a variation of valve timings so that it can avoid losses and prepare the desired mixture.

Figure 2.5 illustrates an example of the valve train adjustment based on the optimum engine performance at different engine speed-load regions for the UniAir system. UniAir is the first fully variable, electro-hydraulic valve system used commercially produced by Schaeffler. In the low speed-load region, dethrottling is a good option to avoid pumping losses and then just a short opening and low lift are able to regulate the load control. Conversely, in the high speed-load region, a longer opening duration and high lift are needed to keep up with the high demand of air for the combustion process.

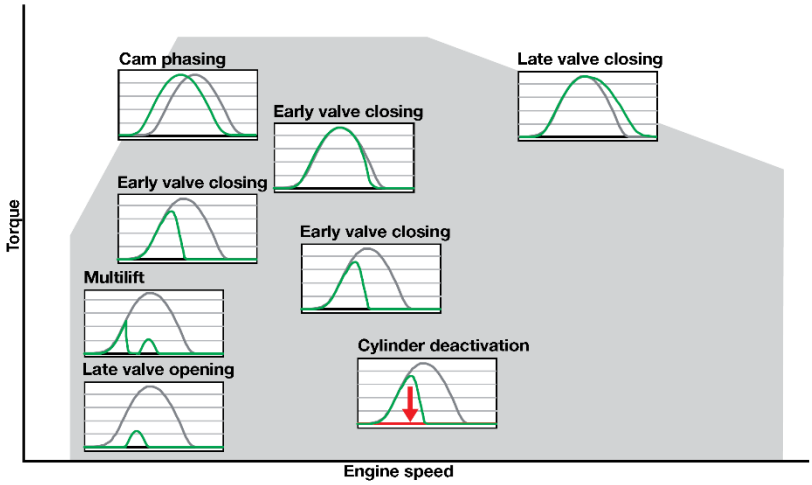

Figure 2-5 Valve lift curves within the engine map [15]

2.3 Downsizing Recent Developments

These last few years have seen an outbreak of gasoline powered vehicles downsized from their usual six cylinders to just four, three and even two cylinders. The displacement volume as example, has shrunk from 2.5 L, naturally-aspirated engines into 1.8 to 2.0 L, turbocharged engines. The industry's trend already reflected this through the production

of smaller engine displacements or with fewer cylinders. A few examples are as described below:

- Mahle designed a 1.2 L, 3-cylinder demonstrator engine and it is equipped with the new Bosch-Mahle modern turbocharger (Figure 2.6). It achieved 50 % downsizing to replace the 2.4 L engine with 25 – 30 % fuel saving. A significant benefit is achieved from the incorporation of the central gasoline direct injection (GDI) piezo injectors, boosting system with the intercooler, dual VVT, and good cooling mechanism. It can produce 160 hp and 286 Nm with fuel economy of 49 mpg after being tested on a Volkswagen Passat. More impressively, the maximum BMEP can reach up to 30 bar. The power output is 144 kW [16], [17].

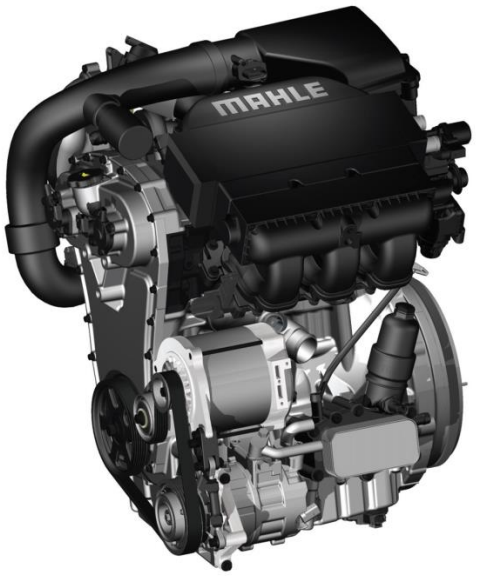

Figure 2-6 MAHLE twin turbocharged engine [17]

- Ford has introduced the 1.0 L, 3-cylinder EcoBoost as part of the 'Fox' engine family, which can produce 125 hp with an ultra-low CO_2 emission of 114 g/km. It also features a new turbocharger with a high performance of 170 Nm from 1300-4500 rpm with no turbo-lag. It recorded 48 mpg for the fuel economy with 15-20 % better fuel saving as compared to 1.6 L, in the case of the NA engine [18]. The key technologies involved are the new turbocharger system, the centrally mounted injectors, the split cooling system and dual cam phasing [19]. This engine won the 'International Engine of the Year' title from 2012 to 2014, and the 'Sub 1-litre' award from 2012 to 2015 [20]. It had already been launched in the

production line of Ford Focus by 2012 and it is now also integrated in the C-MAX and Fiesta models.

- Fiat manufactured a 0.9 L, 2-cylinder, methane/petrol fuelled Twin-Air turbocharger engine, as one of the smallest downsized commercial versions. The integration of the Multi-Air system, which controls the air intake accurately through VVT made it possible to achieve fuel economy of approximately 3.1 kg/100 km, power output of 80 hp and 86 g/km of CO_2 [21], [22].

- Lotus, in partnership with Continental Automotive, also designed the 'Project Sabre - Spark-ignition Advanced Baseline Research Engine' (Figure 2.7). It is a mild downsizing engine with 3 cylinders, turbocharged, and a capacity of 1.5 L, equipped with four valves per cylinder and twin overhead camshafts, designed to serve as an alternative for the 2.2 L 4-cylinder naturally-aspirated engine [23], [24]. This mild downsizing project sought to reduce throttling losses at part load and the high load fuel consumption, instead of the high BMEP value.

Figure 2-7 Lotus Sabre 3-cylinder engine [23]

- One research engine designed in collaboration with Weber Motor and Bosch [25] is a turbocharged 2-cylinder SI-engine with direct gasoline injection (GDI). Figure 2.8 illustrates the fuel economy potential for about 25 % of a 4-cylinder 1.6 L engine with port injection after an extreme downsizing to a 2-cylinder 0.8 L engine, which serves as the motivation for this project. The NA version has been tested and it met the target of fast burn durations, which is about 20 °CA even at high EGR rates (20 %) as a result of the high tumble level. The fuel

consumption and emission levels are considered to be satisfactory enough for use in a hybrid powertrain. Further investigations on the turbocharged version will focus on achieving the target performance of maximum BMEP at 1,500 rpm and on fulfilling the emission target of EU6.

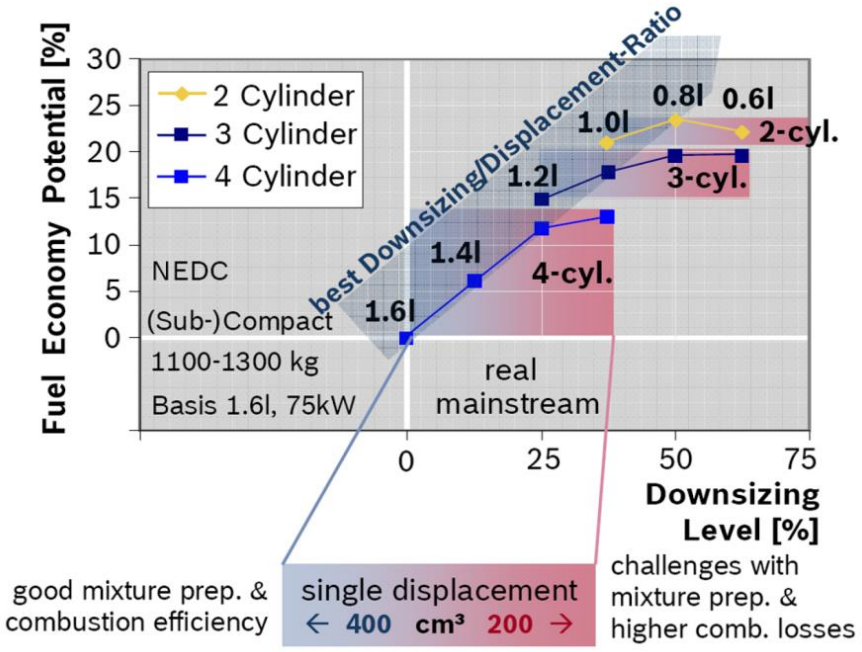

Figure 2-8 2-cylinder engine downsizing concept [25]

- One collaborative project entitled 'Ultra Boost for Economy' aims to demonstrate that it is possible to achieve 60 % reduction in engine capacity, while maintaining the required torque curve. The project has been recognised industry- and academia-wide[1] and is part-funded by the Technology Strategy Board[2]. Based on the chosen baseline engine, namely the JLR AJ133 5.0 L, V8, the results showed that it is possible to achieve 23 % fuel saving with a 60 % downsizing factor [7].

[1] Jaguar Land Rover, GE Precision Engineering, Lotus Engineering, Shell Global Solutions (UK), CD-adapco, University of Bath, Imperial College London, University of Leeds
[2] UK's innovation agency

Table 2-1 Comparison of downsized engines

	LOTUS [Sabre]	**MAHLE**	**FORD [Fox]**	**FIAT**
Year	2008	2008	2012	2012
Key Technology	• GDI: homogeneous air-fuel mixture by multi-stream solenoid injectors • Single-stage, single entry, fixed geometry turbocharger [1 bar] • CVCP [continuous variable cam phase] • Switchable valve train: deactivate one of the intake valves, while switching the other to low lift	• Two-stage turbocharging [2.8bar] / single-stage turbocharging • Split injection with central GDI piezo injector • Split cooling circuit • Cooled EGR 15 % [reduces exhaust gas to 700 °C, inlet 120 °C] • VVT	• Split cooling system • Twin independent variable camshaft timing [Ti-VCT] • Turbocharger • GDI	• Multi-Air technology [electro-hydraulic control of the inlet valves] • TwinAir Turbocharger • Methane / Petrol fueled
Capacity	1.5L (original: 2.2 L)	1.2 L (original: 2.4 L)	1.0 L (original: NA, 1.6 L)	0.9 L (original: NA, 1.4 L)
Cylinder	3-cylinder	3-cylinder	3-cylinder	2-cylinder
Maximum Power	117 kW / 5000 rpm	120 kW / 5000-6000 rpm	125 hp	63 kW / 5500 rpm
Maximum Torque	240Nm	286 Nm / 1600-3500 rpm	170 Nm / 1300-4500 rpm	145 Nm / 1900 rpm

Fuel Saving	6%	25 – 30 %	15 – 20 %	30 %
Max BMEP	20.1 bar	30.0 bar	-	-
Fuel	-	49 mpg [5.8l/100km]	48 mpg	3.1 kg/ 100km
CO_2	140 g/km	135 g/km	114 g/km	86 g/km

2.4 Downsizing Benefits & Challenges

The downsizing benefits have been discussed previously while explaining the concept and technologies associated with it. Listed below are the general benefits gained from downsizing:

- Fuel economy improvement (10 – 30 % potential of reduction in fuel consumption) in comparison with the conventional, naturally aspirated SI engines [5]
- Shifting of operating points to the higher MEP and reducing the specific fuel consumption without sacrificing torque reserves [5]
- Reducing friction, thermal losses, and cutting carbon dioxide emissions [6]
- Beneficial in reducing throttling losses [7]
- Manufacturing and bill of materials (BOM) cost savings for the case of a V-configuration engine to the in-line configuration [7]
- Able to recover some of the thermal energy wasted in the exhaust by using turbocharging for the extra intake pressure [7]

The challenges associated with engine downsizing are discussed below [5]:

- Extra engine packaging and higher cost due to the addition of a complex charging system or additional components
- The full load of the mean effective pressure for spark-ignited engines is limited in order to avoid knocking combustion
- The increasing demand on the different subsystems added, such as the fuel injection system and boosting system to reach the targeted power and torque, may lead to a decrease in engine efficiency gains
- An insufficient amount of exhaust gas enthalpy at low engine speed may affect the low-end torque
- A higher demand from the fuel injection system regarding the difference of fuel mass injection between the idle and full load may affect the quality of the mixture formation.

The combustion limitations are listed in [12] as a technical challenge to overcome in order to further improve the downsized engine. The engine knocking forced the engine to reduce the compression ratio and retarded spark timing, thus leading to lower efficiency.

Another technical challenge associated with downsized engines is the part load fuel economy. The engine needs to have a lower compression ratio in order to avoid the engine knock at high load operation. This will however penalise the part load efficiency that covers 80 – 90 % of the vehicle's operation. As downsizing continues, the fuel economy gains are declining. A high compression ratio under the part load condition will help maximise the fuel economy [9], [12]. The degree of downsizing is still limited, and the desired fuel reduction has not been achieved yet due to the conflict of engine knock at high load and the fuel consumption issue at part load.

2.4.1 Abnormal Combustion

Forced induction, direct fuel injection, and a high compression ratio are the technologies commonly applied in downsized engines to increase the power density. Nevertheless, this combination usually leads to an abnormal combustion, also referred to as Mega Knock, Super Knock, or Low Speed Pre-Ignition (LSPI). This condition is a considerable restriction on increasing the engine's compression ratio and the boosted intake pressure [26]. Figure 2.9 illustrates the comparison between normal combustion, the spark knock and the super knock.

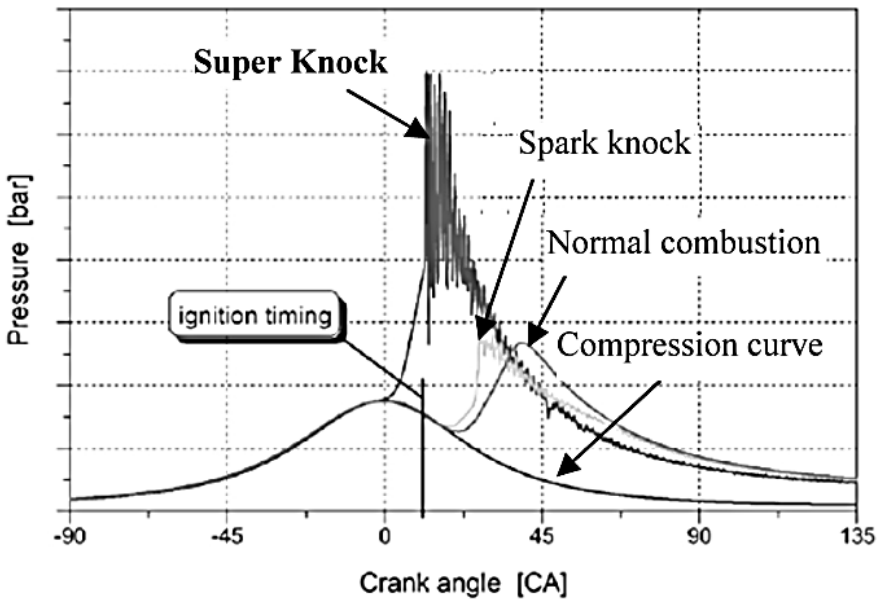

Figure 2-9 In-cylinder pressure curve of Super Knock [26]

Knock phenomenon [27]:

In SI engines, the combustion can progress as a normal or abnormal phenomenon depending on specific operating conditions. The normal combustion is initiated by spark

timing and generates a flame front moving across the cylinder volume in a uniform manner. The abnormal combustion or knock is triggered by the temperature and pressure history of the end-gas, along with the rate of development of the flame.

The causes of knock: two theories of knock, auto-ignition (the commonly accepted theory) and detonation.

- The theory of auto-ignition refers to the ignition of the so-called hot spots in the unburned end gas. Non-uniformities in temperature or concentrations formed the hot spots. The unburned gas is compressed by the expanding burned gas, compressed or expanded by the moving piston, heated by radiation from the flame front, and cooled or heated by the surrounding boundaries after the spark ignition. When the temperature and pressure of the end gas exceed its auto-ignition point, it will ignite spontaneously at a few points. This explosion will cause pressure waves to oscillate in the combustion chamber and trigger the pinging sound.
- Detonation, however, assumes that the knocking occurred due to the propagation of the flame front that accelerates from the spark plug to the other end of the wall. The shock wave would then propagate from one-cylinder wall to another in the combustion chamber. The high magnitude pressure is causing the occurrence of the knock.

Inoue *et al*. [26] recreated the super knock phenomena and examined the potential sources that promote the super knock. The finding has demonstrated that there is no influence of the spark plug to the super knock. On the other hand, the engine parameters have proven the relation to the occurrence of the super knock:

- *Intake pressure*: The higher the intake pressure, the more frequent the occurrence of the super knock. Resultantly, this will increase the maximum combustion pressure.
- *Intake air temperature*: The super knock will occur more frequently at a higher intake temperature.
- *Air-fuel equivalent ratio* (λ): The leaner the mixture, the more common the frequency of the super knock. This is due to the reduced cooling effect provided from the mixture, which then increases the in-cylinder temperature. $\lambda > 1.10$ resulted in poor combustion and low gas temperature, thus lowering the super knock appearance.

- *Ignition timing*: Advancing the ignition will increase the pressure and temperature, thus facilitating the occurrence of the super knock.
- *Fuel injection timing*: A retarded start of injection will result in an increased frequency of the super knock. This is due to a less homogeneous mixture being produced, thus a leaner mixture will increase the temperature.
- *Intake cam phase*: Advancing the cam phase will increase the number of super knocks. This is because the compression ratio is increased, and the increasing valve time overlapping will change the residual gas volume. This factor is considered to be favourable to the super knock occurrence.
- *Blow-by oil*: An increased amount of oil entered the cylinder, which is believed to trigger the ignition point and lead to the super knock.

Figure 2.10 below shows the common knock limited region applied for the downsized gasoline engine. However, when compared to the real-world consumer usage in Figure 2.11, it is demonstrated that the real-world consumer usage falls within the high load region, which is also under the knock limited region. Therefore, it is important to solve the knocking issue, while at the same time maintaining high efficiency and improving fuel consumption.

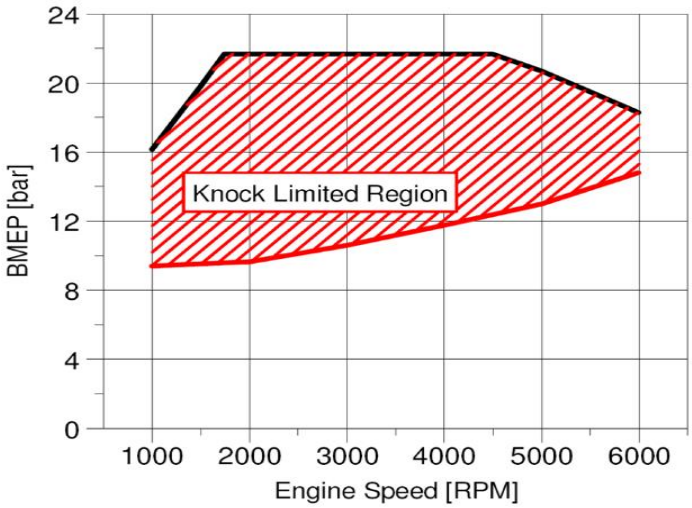

Figure 2-10 Downsized gasoline engine knock limited combustion region [28]

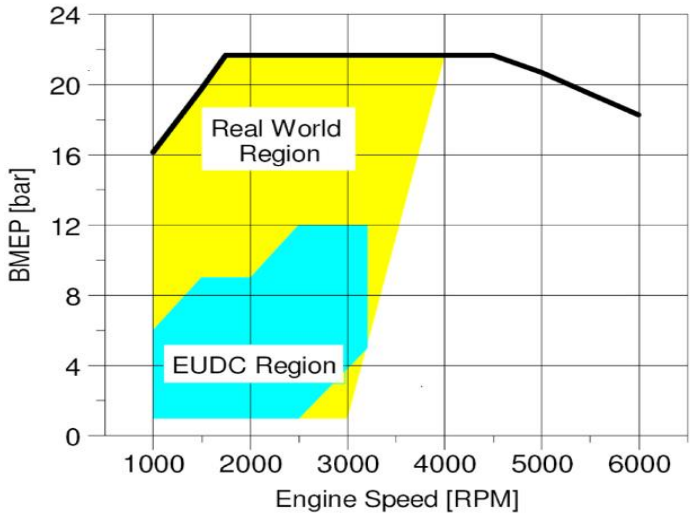

Figure 2-11 Real-world consumer usage region [28]

Effect of knock:

The engine knock phenomenon can potentially exert negative impacts on engines. The mechanical components and the control systems suffer greater strain in order to withstand the effect of the engine knock, and thus consume more fuel at high load condition to suppress the knock. Additionally, the engine knock limits the compression ratio as well as the possibility of extreme downsizing [8].

Table 2-2 Effects on engines if the knock occurs over a long period

	Unfavourable effects of the knock [27]
1	Breakage of piston rings
2	Cylinder head erosion
3	Piston crown and top land erosion
4	Piston melting
5	Limits engine compression ratio
6	Increase air pollution
7	Decrease engine efficiency
8	Considerable rise in engine specific fuel consumption
9	Possibility of structural harms to engine over a long-term period
10	The knock may cause damage and it is a source of noise in engines

Knock control strategy:

Various control strategies can be applied in order to overcome the knocking issue, such as the utilisation of high knock resistant fuels (high octane or alcohol fuels have been proven to resist the knocking impact thanks to their chemical characteristics), of the direct fuel injection, which cooled down the fuel from the vaporisation effects, and variable valve timing (VVT) [29]. Spark ignition timing retardation represents an efficient method to avoid the knock phenomenon, but results in reduced engine performance and poor fuel economy.

Table 2-3 Engine knock control strategy

	Knock control strategy	
1	Increase turbulence	[27]
2	Reduce combustion time	[27]
3	Reduce the end-gas temperature.	[27]
4	Decreasing the intake air temperature	[27]
5	Develop alternative fuel engines	[27]
6	Using the variable-geometry turbocharger (VGT)	[30]
7	Decrease the compression ratio	[31]
8	Increase the fuel octane number	[31], [32]
9	Fuel design and blending	[33]
10	Use of EGR	[30], [34]–[36]
11	Injection of a second fuel, ethanol or methanol	[37], [38]
12	Water injection	[36]
13	Engine cooling and engine thermal control	[39]–[41]

2.5 Summary

Downsizing philosophy is seen as a key in improving internal combustion engines' performance. This is reflected through the industry's trend of producing smaller engines to replace the bigger ones but having the same power output. A comprehensive understanding on downsizing concept has been presented through the current literature

review. On the other hand, the combustion limitation issue at high load regions need to be handled to make sure the capability of the downsized engine is fully utilised. Furthermore, at part load regions, fuel inefficiency due to the pumping losses also affects the downsized engine performance. The research work aims to address the issues with Miller cycle combustion strategy which is explained further in the next chapter.

Chapter 3

LITERATURE REVIEW: MILLER CYCLE

3.0 Overview

The availability of technologies in the downsized engine has enabled the Miller cycle to be implemented as an alternative combustion strategy in order to improve the engine efficiency. This section reviews the Miller cycle concept as a potential solution to overcoming the issues in the downsized gasoline engine. The history of the Miller cycle is explained and the differences between the Miller cycle and the Otto cycle mechanisms are addressed. It also lists some recent developments of the engines that have applied the Miller cycle and their contributions. The benefits and limitations of the Miller cycle are listed down. It also highlights the reason for investigating the Miller cycle in this work.

There are many types of engine cycles being used and developed in internal combustion engines (ICE). The Otto cycle is the main cycle, which is usually associated with ICE fuelled by gasoline. The Otto cycle is also known as the spark ignition (SI) engine where a spark ignition is needed to combust the mixture in the cylinder. Nikolaus Otto (1832 – 1891) is the person behind the four-stroke engine invention, who is regarded as the founder of the modern ICE industry.

The four-stroke Otto cycle mechanism is described as below (please refer to Figure 3.1):

1. *Intake stroke*: A mixture of air and fuel is being induced in the cylinder.
2. *Compression stroke*: The valves are closed, and the piston is going upward, which increases the mixture temperature. Combustion will happen at the end of the compression stroke after being ignited by a spark.
3. *Expansion stroke*: The power stroke will push the piston downward at high pressure and temperature resulting from the combustion.
4. *Exhaust stroke*: The burned gases are being pushed out via the exhaust valves.

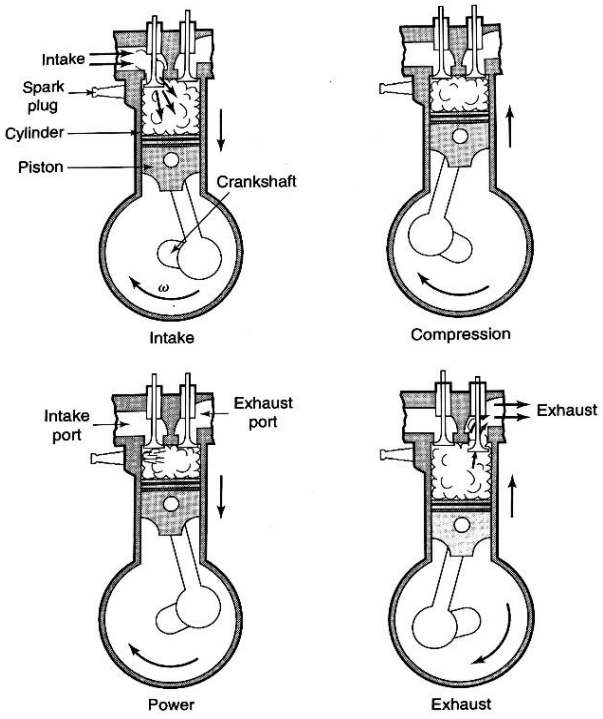

Figure 3-1 A four-stroke spark ignition engine [42]

The Otto cycle is assumed to have a combustion process at constant volume. The simple gas cycle assumes the heat rejection process to happen at the same volume. This is without consideration of the gas flow from the opening and closing of the intake and exhaust valves. The four-stroke Otto cycle can have exhaust and intake strokes with different conditions either through the unthrottled cycle, throttled cycle or supercharged cycle, as indicated in Figure 3.2 [42].

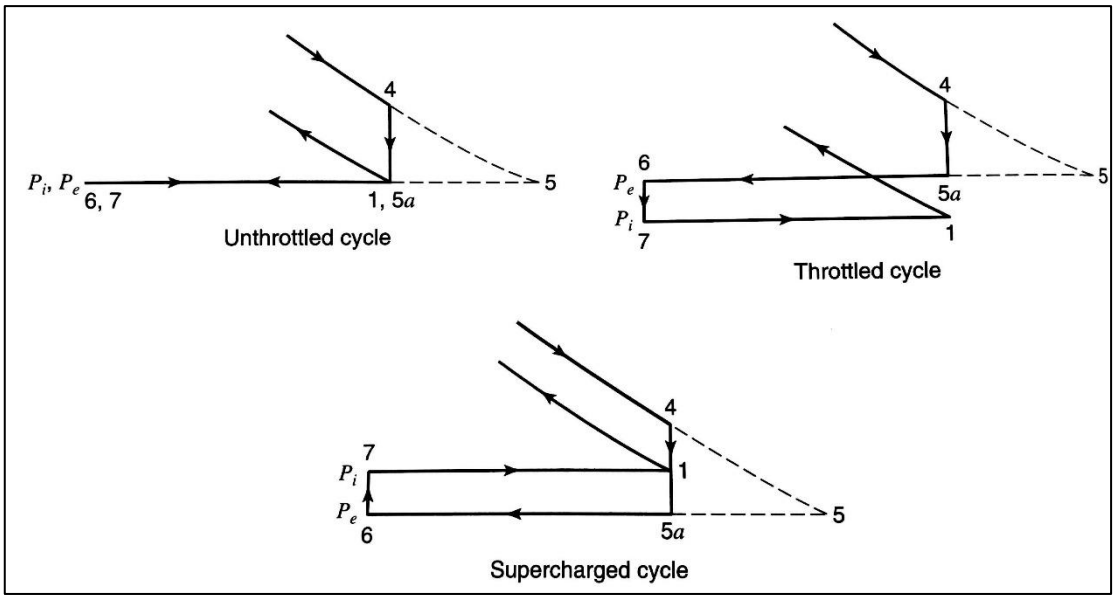

Figure 3-2 The four-stroke inlet and exhaust flow [42]

Below is the computation of the four-stroke Otto gas cycle analysis that includes the exhaust and intake strokes. When the residual gas fraction f is considered, the heat addition Q_{in} is calculated as:

$$Q_{in} = m_i q_{in} = m(1-f)q_{in} \tag{3.1}$$

6, i to 1: Intake stroke

$$T_1 = (1-f)T_i + f\left[1-\left(1-\frac{P_i}{P_e}\right)^{\frac{\gamma-1}{\gamma}}\right]T_e \tag{3.2}$$

$$P_1 = P_i \tag{3.3}$$

1 to 2: Isentropic compression stroke

$$T_2 = T_1 R_c^{\gamma-1} \tag{3.4}$$

$$P_2 = P_1\left(\frac{V_1}{V_2}\right)^{\gamma} = P_1 R_c^{\gamma} \tag{3.5}$$

2 to 3: Constant volume heat addition

$$T_3 = T_2 + Q_{in}\frac{(1-f)}{C_v} \tag{3.6}$$

$$P_3 = P_2\left(\frac{T_3}{T_2}\right) \tag{3.7}$$

3 to 4: Isentropic expansion stroke

$$T_4 = T_3\left(\frac{1}{R_c}\right)^{\gamma-1} \tag{3.8}$$

$$P_4 = P_3\left(\frac{1}{R_c}\right)^{\gamma} \tag{3.9}$$

4 to 5: Isentropic blowdown

$$T_5 = T_4\left(\frac{P_4}{P_e}\right)^{\frac{1-\gamma}{\gamma}} \tag{3.10}$$

$$P_5 = P_e \tag{3.11}$$

5 to 6: Constant pressure adiabatic exhaust stroke

$$T_e = T_5 \tag{3.12}$$

$$P_6 = P_5 = P_e \tag{3.13}$$

$$f = \frac{1}{R_c}\left(\frac{P_6}{P_4}\right)^{\frac{1}{\gamma}} \tag{3.14}$$

Where:

T_i = inlet air or mixture temperature

P_e = exhaust pressure

r = compression ratio

P_i = inlet pressure

γ = ideal gas specific heat ratio

q_{in} = heat added per unit mass of gas induced

3.1 Miller Cycle Definition & Mechanism

The Otto cycle was explained in the previous subsection as the main engine cycle in the gasoline engines. It is nevertheless limited in terms of achieving higher efficiency, which is needed in the engines. Therefore, many research studies are conducted in order to find an alternative to the Otto cycle so that higher efficiency can be achieved.

The Miller cycle is a cycle that is now gaining manufacturers' attention and interest due to its potential to render the engine more efficient than the Otto cycle. The Miller cycle is also known as an over-expanded engine cycle. It was patented by Ralph Miller, an American engineer, US patent 2817322 dated December 24, 1957 [43]. Ship diesel engines have been using the Miller cycle since the 1960s and Mazda adapted the cycle in their vehicles during the 1990s.

The key to improving fuel efficiency lies in increasing an engine's thermal efficiency. This can be done by increasing the expansion ratio. The expansion ratio is the amount of work the engine does each time the air-fuel mixture in the cylinders detonates. However, in conventional engines, the expansion ratio is the same as the compression ratio, so increasing the expansion ratio will also raise the compression ratio. This is a problem because a high compression ratio causes abnormal combustion, or engine knocking.

One of the ways to increase the cycle efficiency is by having an expansion ratio greater than the compression ratio, as adopted by the Miller cycle through early and late intake valve closing. The Miller cycle is a promising solution to overcome the issues of knocking

if the boosting pressure is too high, as well as to regain the thermodynamic efficiency and have a better fuel consumption.

Mechanism:

The Miller cycle known as the over-expanded engine cycle is achieved through the implementation of early or late intake valve closing to have a larger expansion ratio such that a higher thermal efficiency can be achieved. For the early intake valve closing (EIVC), the intake process ended before the stroke finished, namely before it reached the bottom dead centre (BDC). The charge will expand until reaching the BDC and will reach its atmospheric pressure during the compression process. For the late intake valve closing (LIVC), since the valve is still open after the BDC, the charge is pushed back into the manifold. Either way, less charge is trapped compared to the conventional IVC timing [44]. Figure 3.3 shows an example of Miller cycle implementation through early and late intake valve timings, as explained above.

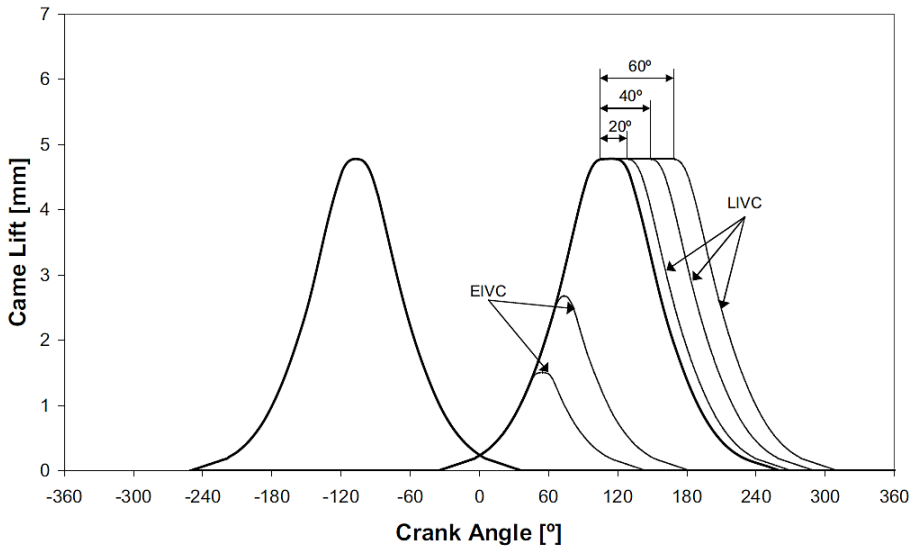

Figure 3-3 Miller cycle valve timing profiles by EIVC or LIVC [45]

Referring to Figure 3.4, the key characteristic of the Miller cycle is that the compression stroke 1 – 2 is shorter than the expansion stroke 4 – 3. In this cycle, as the piston moves downward on the intake stroke, the cylinder pressure follows the constant pressure line from point 6 to point 1.

For the EIVC, the intake valve is closed at point 1 and the cylinder pressure decreases during the expansion to point 7. As the piston moves upward on the compression stroke,

the cylinder pressure retraces the path from point 7 through point 1 to point 2. The net work done along the two paths 1 – 7 and 7 – 1 is cancelled, which results in a lower effective compression ratio ($r_c = V_1/V_2$) than the expansion ratio ($r_e = V_4/V_3$). For the LIVC, some of the intake air is pushed back into the intake manifold before the intake valve closes at point 1. There will be a lower amount of mixture to compress in the cylinder once the intake valve is closed, which means less compression work.

Figure 3.5 shows the T-S diagram for the Miller cycle. The compression stroke 1 – 2 is isentropic. The heat addition, Qin, 2 – 3 is an isochoric process. The expansion stroke, 3 – 4 is an isentropic process. The heat rejection of 4 – 5 is an isochoric process, while the heat rejection of 5 – 1 is an isobaric process. The exhaust process from 1 – 6, which is not illustrated in the T-S diagram, is also an isobaric process.

Below is the formula to obtain the ratio of expansion to the compression ratio and the thermal efficiency of the Miller cycle:

Effective compression ratio, r_c

$$r_c = \frac{V_1}{V_2} \tag{3.15}$$

Expansion ratio, r_e

$$r_e = \frac{V_4}{V_3} \tag{3.16}$$

Ratio of the expansion ratio to the compression ratio, λ

$$\lambda = \frac{r_e}{r_c} \tag{3.17}$$

4 to 5 & 5 to 1: Heat rejection

$$Q_{out} = mc_v\left(T_4 - T_5\right) + mc_p\left(T_5 + T_1\right) \tag{3.18}$$

Indicated efficiency

$$\eta_{Miller} = 1 - \left(\lambda r_c\right)^{1-\gamma} - \frac{\lambda^{1-\gamma} - \lambda\left(1-\gamma\right) - \gamma}{\gamma - 1} \cdot \frac{P_1 V_1}{Q_{in}} \tag{3.19}$$

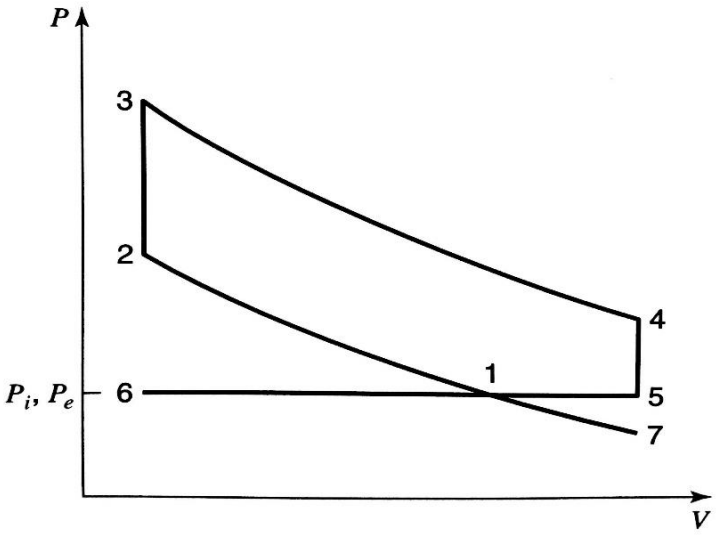

Figure 3-4 P-V diagram for the Miller cycle [42]

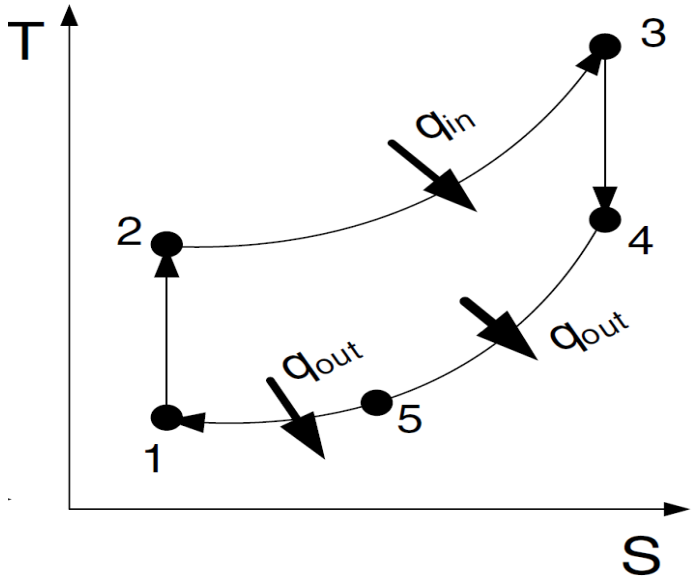

Figure 3-5 T-S diagram for Miller cycle [46]

3.1.1 Comparison between the Otto, Miller and Atkinson Cycles

The main difference between the Miller cycle and the conventional ideal Otto cycle is that the Otto cycle has the same compression stroke 1 – 2 and expansion stroke 3 – 4O, as illustrated in Figure 3.6. The Miller cycle expansion stroke is from 3 – 4M. Another related cycle is the Miller cycle with a full expansion stroke 3 – 4A to the exhaust pressure, also known as the Atkinson cycle [47].

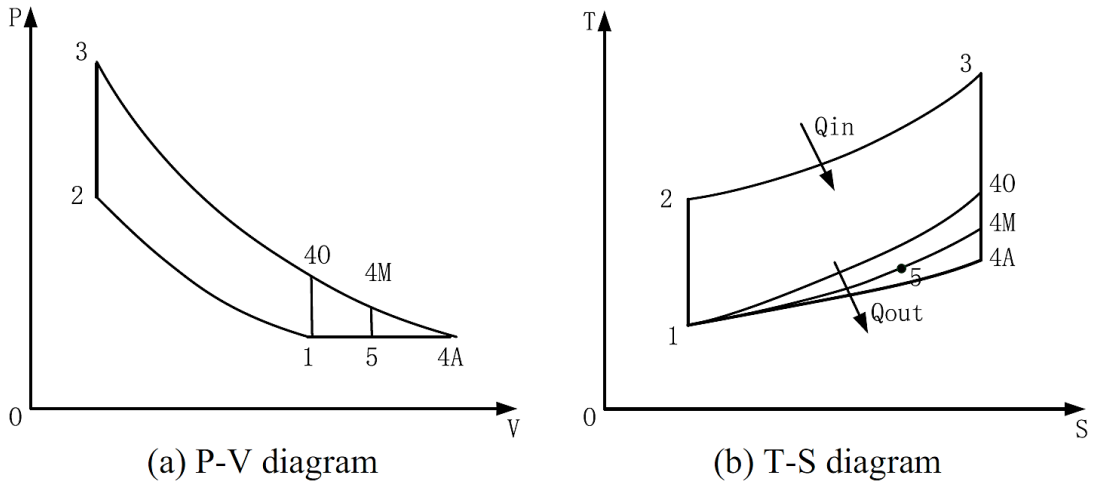

Figure 3-6 P-V and T-S diagrams for the Otto, Miller and Atkinson cycles [48]

The Atkinson cycle is named after James Atkinson (1846 – 1914), an English engineer, who invented an engine known as the 'cycle' engine in 1889. He added a two-bar linkage between the connecting rod and the crankshaft, which made it possible for the engine piston to travel through four unequal strokes in every crankshaft revolution. The engine has 1.78:1 as the expansion to the intake stroke ratio [42].

Higher thermal efficiency can be achieved with the Atkinson cycle because more thermal energy can be converted into mechanical work. However, the thermal efficiency gained by the Atkinson cycle is discounted by the fact that a long expansion stroke extends the cylinder body, increasing the piston friction loss and engine weight. A higher exhaust pumping loss will occur as a result of the low in-cylinder pressure at the end of the expansion stroke.

Therefore, the ideal Miller cycle reflects the practical Atkinson cycle in the engine and they are fundamentally the same. One main difference is that usually the Atkinson cycle is naturally aspirated while the Miller cycle is equipped with a boosting system [48]. It is based on that reasoning that the Miller cycle was chosen to be investigated in this research project because the downsized gasoline engines come with an incorporated boosting system.

The compression ratio is one of the important parameters in evaluating the Miller cycle performance. Figure 3.7 shows the comparison of the cycles in terms of the compression ratio r_c, equivalence ratio ϕ and expansion-to-compression ratio r. The Atkinson cycle

has the highest cycle efficiency in comparison with other cycles, but as the r_c increases, the gap decreases. The Atkinson and Miller cycles have an optimum compression ratio, r_c = 20. Beyond that value, the effective power, power density and effective efficiency start to decrease [49].

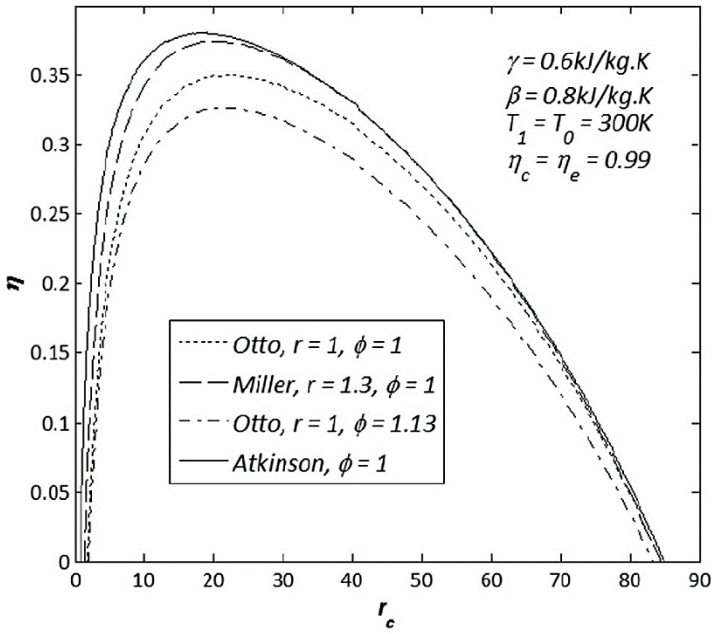

Figure 3-7 Effects of r_c, r and ϕ on cycle efficiency [48]

3.2 Miller Cycle Recent Development

In the long term, the conventional ICE still has the potential for energy savings and emissions reduction. Having an ICE in a hybrid vehicle is regarded as the best transition scheme from the conventional ICE to electric vehicles. Although electric vehicles can greatly reduce the GHG emissions, for countries where electricity is mainly produced from coal, the total well-to-wheel emissions of ICE are lower than in electric vehicles. Some examples of hybrid vehicles include Toyota Prius, which was launched to the market in 1997, Honda Insight by Honda Motor Co., Ltd. in 1999, and Fusion Hybrid by the Ford Company in 2012 [50]–[52].

The gasoline engine is considered to be a better solution for a hybrid vehicle as opposed to the diesel engine in terms of its complexity, cost and weight. However, the Otto cycle in the SI engine cannot have a high GCR due to the engine knocking limit, which then imposes a boundary for the thermal efficiency improvement of the engine. It is for this reason that Toyota Prius is adopting the over-expansion cycle in its engine in order to reach higher thermal efficiency [48]. Therefore, applying the Miller cycle strategy for the

downsized gasoline engine in a hybrid vehicle will help improve the engine performance while at the same time suppressing the engine knocking.

A reduced geometric compression ratio (GCR) is usually taken as a trade-off in order to mitigate engine knocking in downsized gasoline engines. Nevertheless, this method worsens the fuel consumption especially at the part load region. Thus, the Miller cycle is seen as an alternative implemented in order to solve engine knocking with its ability to decouple the compression ratio and expansion ratio. Fuel consumption is improved by having a full expansion stroke to retain efficiency, and engine knocking is also reduced with the lower geometric effective compression ratio. The Miller cycle has great potential in improving the part load BSFC through variation of the geometric effective compression ratio. The engine can have a high geometric compression ratio and variable valve timing is used in order to obtain the longer expansion stroke [12].

One example of engine developments, which implement the Miller cycle is the 1.4 MAHLE gasoline engine. It has a direct injection fuel system and it applies the Miller cycle using its Intake CamInCam® technology, as illustrated in Figure 3.8. It uses the asymmetric intake valve timing control in order to adopt the LIVC strategy. The combination of fixed cam (IV1) and adjustable cam (IV2) was used to control the intake valve lift events.

The output showed improvement at high load due to the lowered geometric effective compression ratio (GECR) and the better performance at low load contributed by reducing the pumping loss. It has been proven to be more efficient than the Otto cycle with 20 % better specific fuel consumption for the Miller cycle at low load. Engine knocking was also lessening by moving the limit to a higher load region. Lower GECR has led to lower in-cylinder pressure and temperature and this entailed the benefit of reduced NO_x production [28].

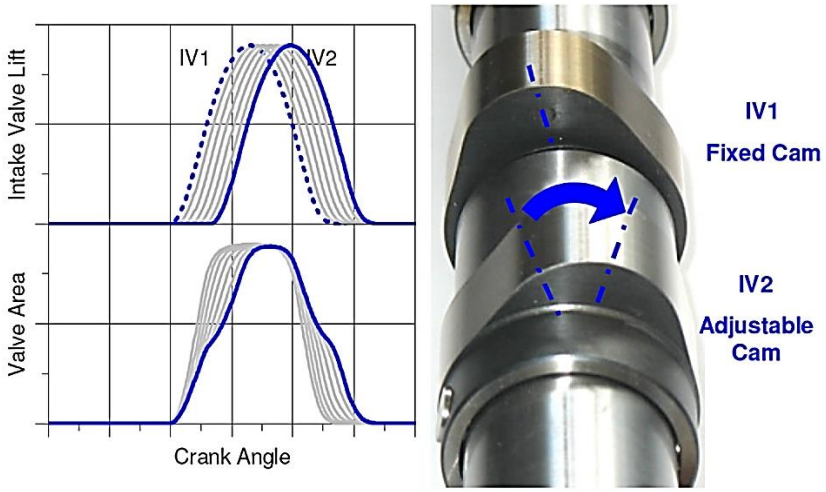

Figure 3-8 Intake CamInCam® technology [28]

IAV GmbH investigated a rapidly variable Miller cycle strategy effect on the engine knocking behaviour based on an early intake valve closing using Schaeffler 'UniAir' VVT in a turbocharged DISI test engine with a GCR value of 13. The results showed a good potential of the Miller cycle as a steady-state anti-knock intervention based on the improvement in the BSFC, exhaust gas temperature and cyclic variation. They also suggested the combination of the Miller cycle with the ignition timing strategy in order to maintain the BMEP value despite the decreasing effective cylinder displacement if the engine parameters are kept constant [53].

Nissan also developed a 1.2 L inline 3-cylinder supercharged gasoline engine with Miller cycle and direct fuel injection system in an effort to reduce the engine knocking occurrence due to its high compression ratio of 13. Nissan's variable valve event and lift technology apply the concept of a valve-throttling system in order to regulate the air flow that enters the cylinders. It reduces the pumping losses at part load, thus improving the fuel efficiency and transient performance. The intake port geometry was designed for the tumble flow to assist the downward fuel injection strategy, which needed a stronger gas flow to mix the fuel and air into a homogeneous mixture so that the combustion is completed faster. The increased turbulence intensity from the design has resulted in a shorter combustion period and is able to suppress the knock because the combustion finished early prior to the occurrence of the knock [54].

BMW introduced the Valvetronic technology, which is a fully variable valve train, to control the load by regulating the valve lift and the closing time of the intake valve. The

concept is similar to the Miller cycle through the early and late intake valve closing to achieve the improvement of the part load efficiency. The camshaft driven mechanical system is based on the infinitely-variable 'Double VANOS' camshaft control system. It has a function of an infinitely adjustable inlet valve lift, which allows for the effective opening period to be shortened. The electromechanical valve train can control the individual valve timing separately. The benefit is gained from de-throttling, which reduced the pumping losses during the gas exchange process, which then translated into a 10 % of fuel consumption reduction and an additional 5 % additional peak torque gained [55].

Ricardo developed a Miller cycle engine, referred to as the Magma engine concept, which was then evaluated on a single cylinder research engine. It is a downsized direct injection gasoline engine equipped with a central injector system and a high compression ratio. The Miller cycle combustion strategy with early intake valve closing combined with an advanced boosting system are used for knock mitigation, while maintaining the desired performance. Based on WLTC and FTP – 75, the downsized Magma engine is able to save 12.5 % and 16.4 % fuel consumption respectively, compared to the baseline engine. Figure 3.9 shows the overall combustion characteristics and strategies for the different speed-load points tested. At full load, a two-stage boost system was used to maintain the BMEP while EIVC was implemented in order to reduce engine knocking [56].

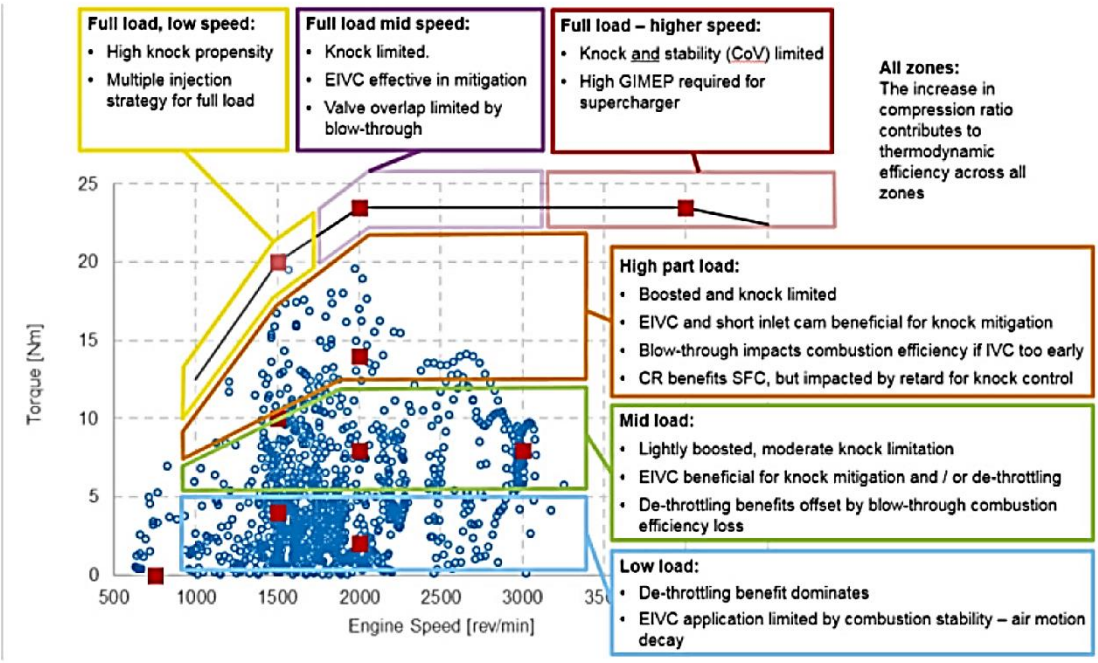

Figure 3-9 Combustion characteristics observed across the speed-load operating zones [56]

The automotive industry players described above have already done works on the Miller cycle, which has proven that it can act not only in order to enhance the engine performance, but also serve as an alternative in controlling the engine knock.

3.3 Miller Cycle Benefits & Challenges

The main contributions of the Miller cycle are to serve as a load control mechanism, reduce the emission of NO_x and to suppress engine knocking [48]. Below are some points explaining the benefits gained from the Miller cycle based on the main contributions mentioned above:

- The Miller cycle with a variable compression ratio (VCR) engine is proven to be more efficient than the Otto cycle engine. It has a better specific fuel consumption at low load than the Otto cycle. Figure 3.10 shows the comparison of the specific fuel consumption achieved by the cycles on the basis of the simulation analysis. By implementing the Miller cycle, the fuel consumption has shown some reduction. Furthermore, by adding the feature of VCR, the engine showed much better fuel saving. The Miller cycle with EIVC reduced pumping losses to a greater extent than the LIVC. This is because the mixture is blown-back into the manifold for the LIVC as a result of the longer IVC delays thereof [45].

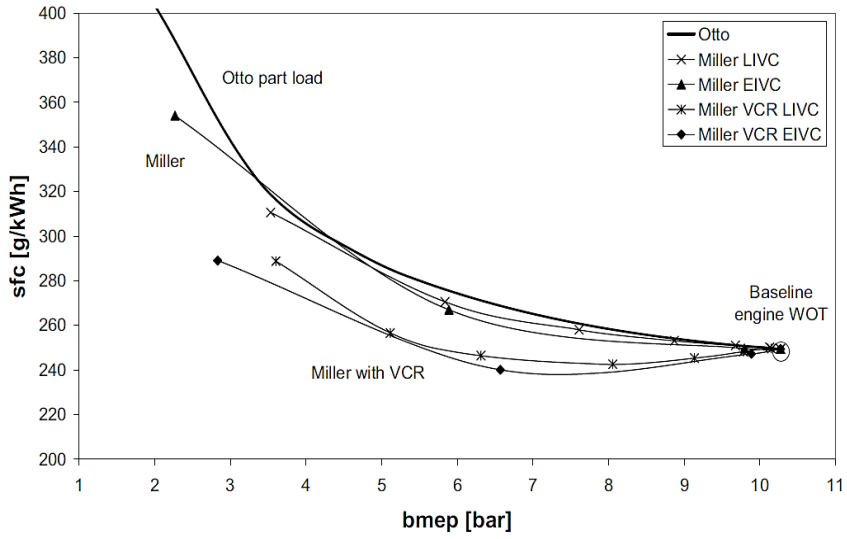

Figure 3-10 Specific fuel consumption comparison for Otto and Miller cycles [45]

- Lower pumping losses from the Miller cycle give higher efficiency compared to the throttle load control. By eliminating the throttle, the intake pressure is higher and experiences reduced irreversibility due to free expansion [44]. Figure 3.11 below

shows the comparison of the P-V diagram between the conventional throttle and VVT methods in load controlling. Both EIVC and LIVC have the same effect of reducing the pumping loop area.

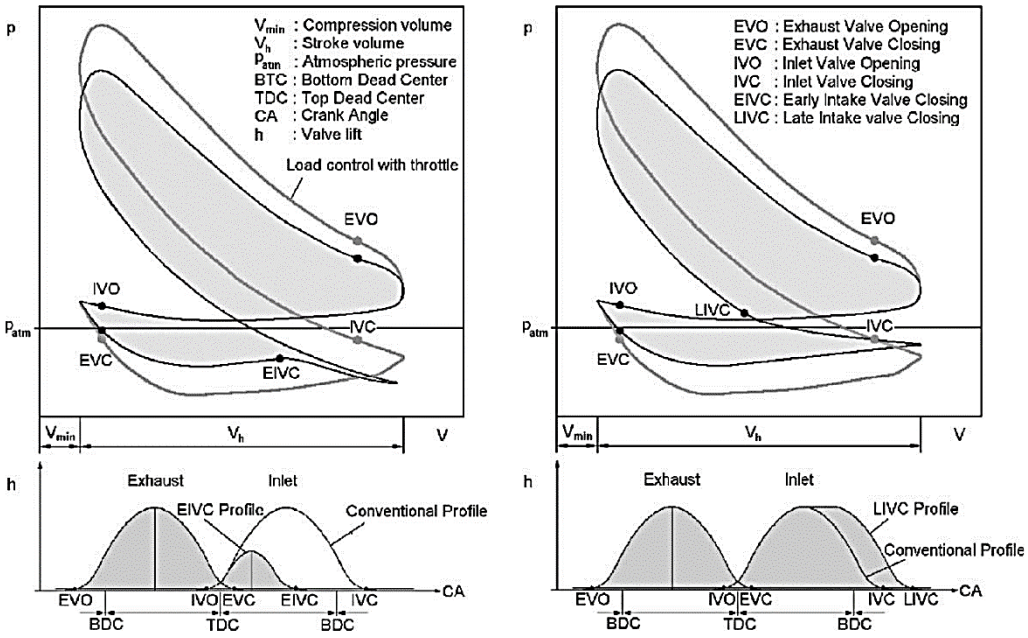

Figure 3-11 P-V diagrams for load control (throttle and VVT methods) [57]

- When applying the Miller cycle by EIVC or LIVC in SI engines, the reduced ECR decreases the mixture temperature and pressure at the end of the compression stroke. Thus, the peak flame temperature is also reduced, which translated to a reduced NO_x formation since the formation of NO_x is temperature-dependent. The reactions hardly occur if the temperature is below 2000 K [58].
- Knocking is lessened by moving the limit to a higher load region and by saving fuel up to 3.2 % in the 1.4 L MAHLE gasoline direct-injection engine. This is achieved with the application of asymmetric intake valve timing control via the MAHLE Intake CamInCam, which is the technology enabler for the Miller/Atkinson cycle combined with a 0.5 increment of compression ratio. Pumping work reduction and 15 g/kWh fuel saving are obtained from the LIVC. A lower temperature at the ignition point is complemented by VCR in order to allow for more decoupling of the compression ratio and expansion ratio [28].
- Figure 3.12 shows the effect of intake valve closing on the knock index. In order to suppress the knock occurrence, the IVC timing or spark timing must be retarded but

this will affect the fuel economy. The LIVC strategy is preferably to be used in order to suppress the engine knocking.

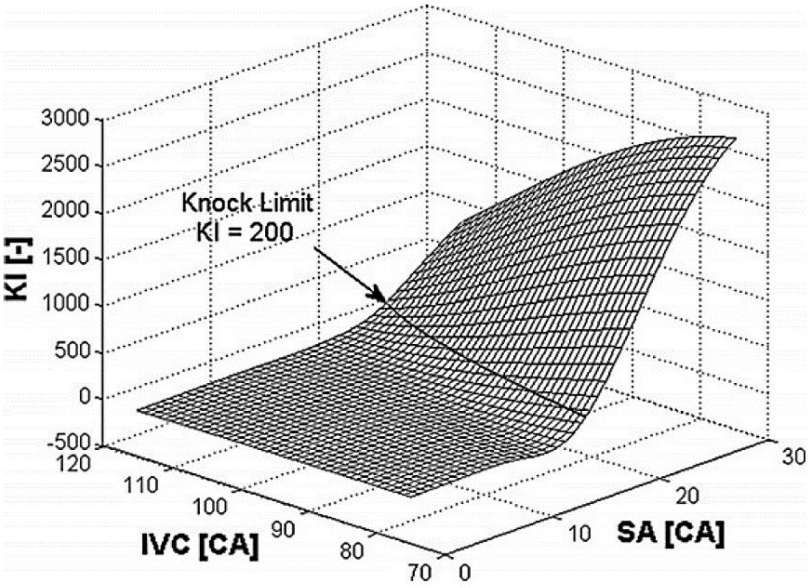

Figure 3-12 IVC effects on knock index [59]

The challenges associated with Miller cycle are listed as below:

- *Problem*: Apart from the benefit of pumping losses via dethrottling means that are no longer controlled by a restriction in the intake duct, there is a limitation to the geometric effective compression ratio (GECR) reduction when applying EIVC or LIVC.

  Solution: Variation of the geometric compression ratio (GCR) to increase the expansion using the variable compression ratio (VCR) technique, keeping the GECR constant. Then, the efficiency becomes better [44].

- *Problem*: The tumble ratio of the Miller cycle (IVC timing = 100 °CA) is weaker near the ignition timing (-50 ~ -30 °CA) as compared with the standard cycle (IVC timing = 59 °CA) resulted from the late IVC, which influenced the flow on the intake side of the piston to go out via the intake port, as illustrated in Figure 3.13.

  Solution: To preserve the turbulence intensity and to have better fuel efficiency, a swirl control valve is used in the case of a high compression ratio. It has been installed in Nissan Pure Drive, a new 1.2 L inline 3-cylinder supercharged gasoline engine [54].

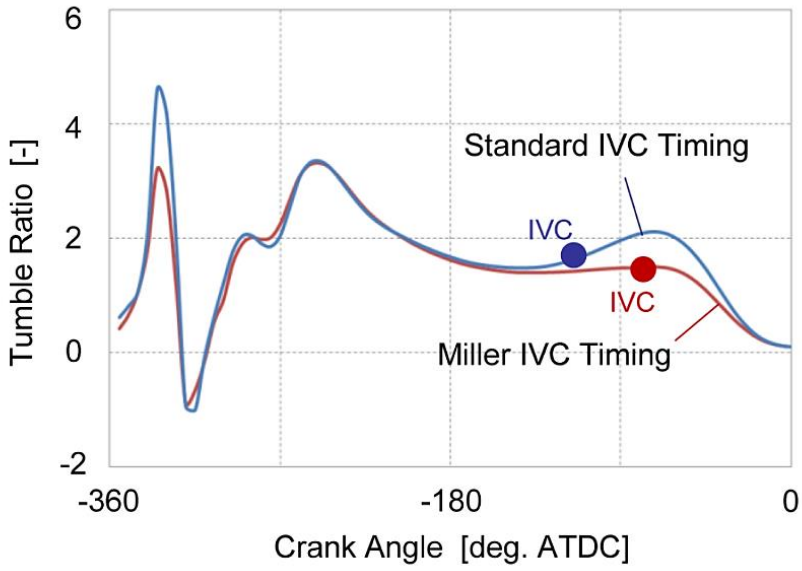

Figure 3-13 Comparison of tumble ratio between Miller cycle and conventional IVC [54]

- *Problem*: The Miller cycle, also known as the over-expanded engine cycle, is usually achieved by implementing the LIVC to have a larger expansion ratio so that a higher thermal efficiency can be achieved. Due to the LIVC, the Miller cycle then reduces its charging efficiency. The charge is expelled back into the intake manifold because the intake valve is still open. The loss of air will then lead to a loss of power.
  Solution: This limitation is compensated using a supercharger to compress more air into the cylinder [54].

- *Problem*: Due to extreme EIVC, the in-cylinder temperature at the beginning of the combustion is decreased compared to the Otto cycle, thus affecting the combustion efficiency.
  Solution: Mixture heating [sucked air heating using the heat of the exhaust gas or cooling water] up to 120 °C is chosen in order to compensate for the lower temperature as compared to the complicated VCR technique. The combustion rate is still decreased with mixture heating, and thus more advanced ignition timing is used [60].

3.4 Summary

Based on the evaluations that have been done regarding the application of the Miller cycle, it has been reviewed that the Miller cycle has great potential to be applied as a combustion strategy in downsized gasoline engines. It has the benefits of improving

thermal efficiency, thus reducing the fuel consumption and exhaust emissions. The next chapter will explain the experimental test facilities that have been used in this research project in order to investigate the performance of the Miller cycle.

Chapter 4

EXPERIMENTAL TEST FACILITIES

4.0 Overview

This chapter describes the experimental test facilities used in the project. There are three engines associated with the project, namely the Lotus SCORE, Lotus OSCAR and Rover K16 engines. The work included in this thesis has been conducted on the Lotus SCORE and Rover K16 engines. However, the project involved data transfer from the Lotus OSCAR engine, thus, the description of that engine has also been included for reference. There is also supporting data gathered from the Steady Flow Rig experiment for the valve flow coefficients. Therefore, the description of the rig set-up is also included in this chapter.

4.1 Lotus SCORE Engine

4.1.1 Cylinder Liner and Piston

Lotus SCORE stands for Lotus Single Cylinder Optical Research Engine, as illustrated in Figure 4.1. The engine has an optical cylinder liner, which can be used for optical access inside the cylinder. Nevertheless, for this project, the optical cylinder was replaced with the cast iron cylinder liner, as no optical access was required for the testing. Table 4.1 lists the engine specifications. The dimensions of the engine components are provided in Appendix A.

The cylinder represents one cylinder from the Lotus 3.0 L supercharged PFI V6 engine. A water-cooled Kistler 6043A60 pressure transducer was installed in the cylinder head in order to measure the in-cylinder pressure. The liner bore was bonded onto a stainless-steel ring and the top was secured up into the head on a silicon gasket by means of a hydraulic ram applying 10 bar pressure. An extended bifurcated piston, featuring a sapphire window in the upper piston crown ran inside the cylinder liner. The sapphire window was 15 mm thick and had a diameter of 60 mm. This window was pressed into the titanium piston crown and sealed with a rubber O-ring. The titanium and sapphire

have similar thermal expansion coefficients. By having this window, the allowable maximum safe operating pressure of the engine is up to 60 bar.

Carbon piston rings were used in order to maintain the correct compression pressure values and prevent abrasion between the upper piston and the liner. In the lower piston, two compression rings and one oil control ring prevented oil from escaping the crankcase. The crankcase is equipped with primary and secondary balance shafts capable of speeding up to 5000 rpm. The engine was driven by a 15 kW Brook Hansen 'Type 160' 3-phase induction motor. Two Leine & Linde rotary encoders, one connected to the crankshaft and one connected to a 2:1 drive representing a cam shaft, provided 360 and 3600 pulses per revolution for the engine timing data [61].

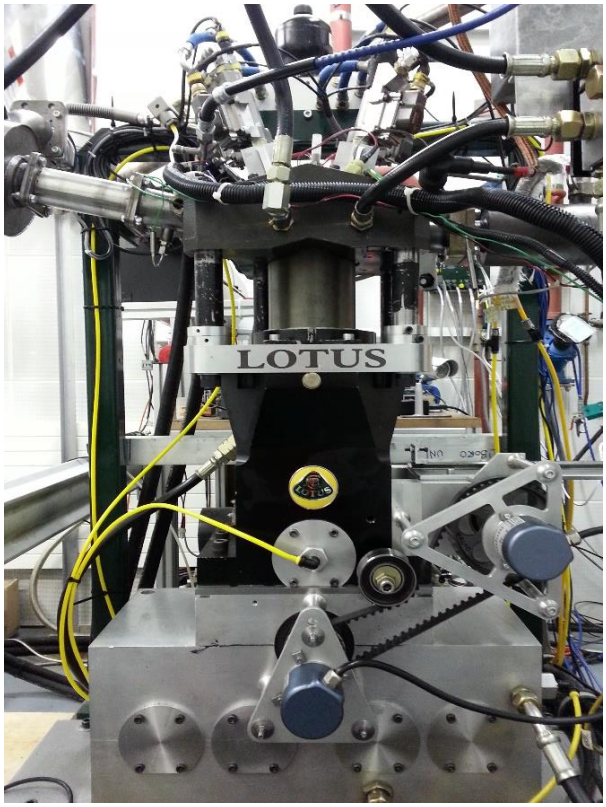

Figure 4-1 Lotus research engine

Table 4-1 Lotus engine specifications

Displaced volume	500 cc
Stroke	82.1 mm
Bore	88.0 mm
Connecting rod	142.0 mm
Number of valves	4

Exhaust valve open	45 °BBDC, 9.35 mm lift
Exhaust valve close	15 °ATDC
Inlet valve open	15 °BTDC, 9.35 mm lift
Inlet valve close	45 °ABDC

4.1.2 Inlet and Exhaust Systems

Figure 4.2 illustrates the inlet system for SCORE, which was designed based on the supercharged V6 parent engine. Two plena were added to the inlet part in order to replicate the pressure wave interactions found in the multi-cylinder engine. An air filter was mounted onto a Romet G65 positive displacement meter (PDM), the PDM provided one pulse every 6 L and gave mean airflow consumptions during the pulsating engine operation. Next to the PDM, a 60 L plenum was mounted in order to minimise the bulk airflow structures entering the inlet port.

A Siemens VDO Hot film integrated Mass Air Flow (MAF) sensor was installed next to the 60 L plenum with the purpose of measuring the instantaneous air flow values. Next to the MAF sensor, there is a 740 mm length pipe followed by a 40 mm diameter butterfly throttle. The second small 2.53 L plenum was configured to have a diameter measuring 150 mm, which was approximately three times that of the runner (49 mm diameter) to the engine in order to give a large expansion for any pressure waves returning from the intake valves.

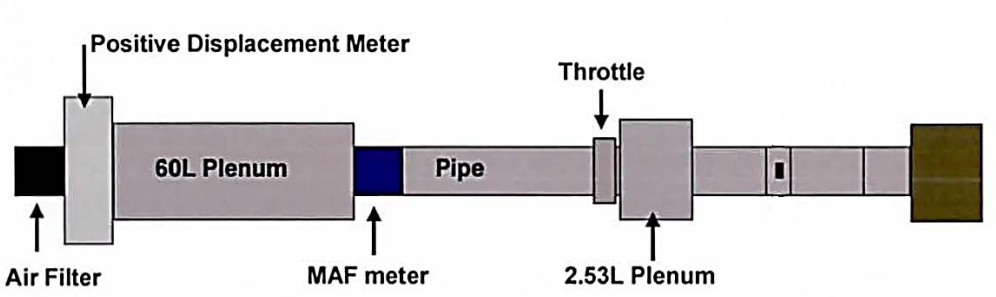

Figure 4-2 SCORE intake system [61]

For the exhaust system, the exhaust port led to an exhaust plenum of 1.1 L in volume. An ECM air-fuel ratio recorder or lambda sensor and a thermocouple were mounted to the plenum. The exhaust plenum was connected to 3.1 m of steel pipe with a 49 mm internal diameter, which led to a standard automotive silencer and an extraction system.

4.1.3 Valve Train System

The Lotus SCORE was equipped with a Lotus Active Valve Train, AVT^{TM} system (Figure 4.3). There were four overhead poppet valves mounted in the pent roof of the cast iron cylinder head actuated by the AVT system. The system has an electrohydraulic valve actuation system, which enabled operation with fully variable valve timing, lift, and velocity for each valve independently.

The valve actuation system consisted of a piston running inside a hydraulic cylinder. The movement of this piston and thus of the poppet valve, was controlled by the flow of hydraulic fluid to each piston. The movement of the hydraulic fluid was controlled by a high speed electromagnetic servo valve. The switching mechanism inside these valves facilitated valve operation at frequencies up to 400 Hz (equivalent 6000 rpm).

The servo valves were connected to a computer based Lotus controller, which serves as an interface for the user. A linear displacement transducer was mounted on each actuator for the instantaneous valve position monitoring. The maximum operating speed of the system was determined by the maximum flow rate of the hydraulic fluid and this was limited by the valve velocity to 4.5 ms^{-1}. The maximum speed varied based on the demanded valve profile [62]. The flexibility of the valve train serves as an excellent tool to test various strategies capable of improving engine performance.

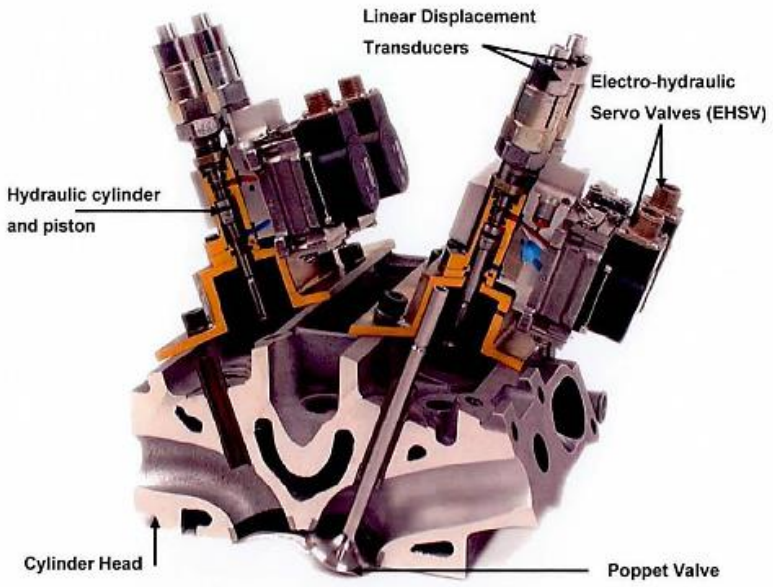

Figure 4-3 Lotus AVT system [61]

4.1.4 Fuel and Ignition Systems

A GDI fuelling system with a central injector (Siemens VDO 6-hole multi-stream GDI injector) was vertically mounted at 10° between valve 3 (intake) and valve 4 (exhaust). Further details of the fuel system can be found in Table 4.2. The injector tip was mounted at the same level with the cylinder head. The inwardly opening injector was designed with 6 equally spaced orifices around the injector axis. The six fuel plumes were orientated away from the injector axis by a nominal 40°. The fuelling system used a low pressure automotive fuel pump, which drew fuel from a 10 L tank and passed it through a pressure relief valve (PRV) set to 3.5 bar in order to feed a three-cylinder Siemens Automotive GDI pump. A second PRV set the output pressure in the line at 120 bar, as measured by a pressure transducer in the fuel line.

Table 4-2 Fuel system specifications

Air/Fuel ratio	14.53 (95 RON gasoline)
Injector type	Direct injection using multi-stream solenoid injectors
Spray spread angle	40 °
Start of injection	Based on experiment
Nozzle diameter	0.1 mm
Injection duration	25 °
Injection pressure	120 bar

The ignition system used a 10 mm NGK H53P spark plug. The spark plug position was also mounted close to the central position next to the fuel injector for the spray-guided configuration, as indicated in Figure 4.4. An engine instrument controller (AVL 4210) controlled the ignition timing, injection timing and injection duration.

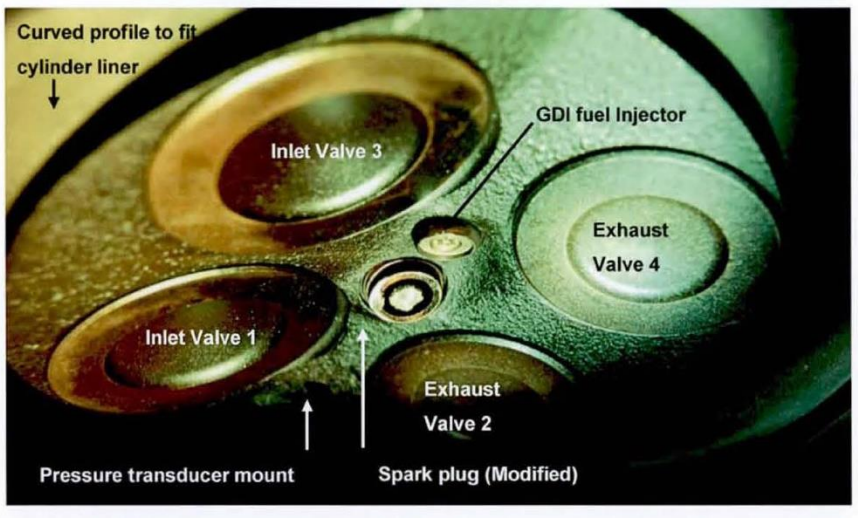

Figure 4-4 GDI fuel injector and spark plug position [61]

4.1.5 Instrumentations

A water-cooled Kistler 6043A60 pressure transducer was positioned in the cylinder head in order to measure the instantaneous in-cylinder pressure. A thermocouple was located on the cylinder head and an Omega OS102 infra-red temperature sensor was aimed at the cylinder liner in order to measure the outer wall temperature. Various operating parameters (oil pressure and temperatures, inlet and exhaust temperatures, in-cylinder pressure, cylinder head temperature) are recorded by the DSP unit and monitored on a computer running LabView software application.

4.2 Lotus OSCAR Engine

The Lotus OSCAR thermodynamic engine (please refer to Figure 4.5) is geometrically identical with Lotus SCORE with the exception of the piston crown, which is accommodating the sapphire window in Lotus SCORE. Since Lotus SCORE has a limited operating range for high speed and high load points, the validation for the wide open throttle (WOT) and high-speed operations was done on the basis of the Lotus OSCAR engine data. The details of the engine's subsystems are listed in Table 4.3.

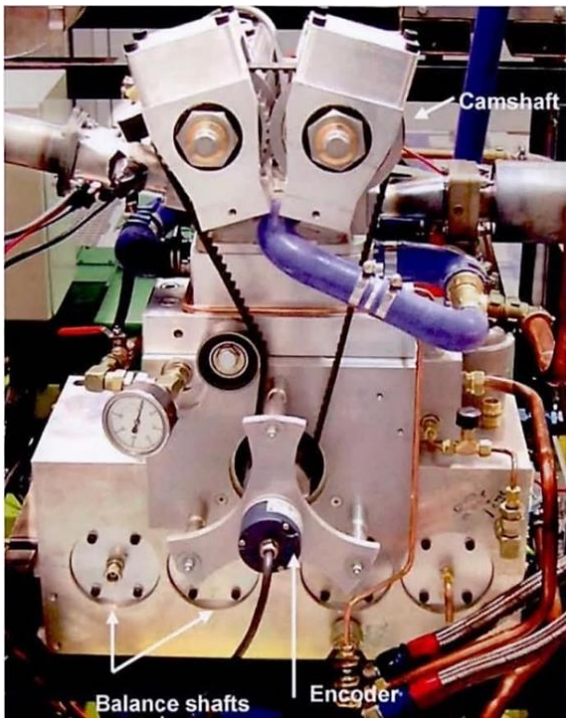

Figure 4-5 Lotus thermodynamic engine [61]

Table 4-3 OSCAR engine subsystems

Inlet and exhaust systems	• The intake manifold pressure was measured using the Druck 7517 absolute pressure transducer. • The ambient pressure was recorded by means of a Prosser Digital Barometer. • Airflow measurements were made using hot-film meters and positive displacement meters. • All temperatures were measured using K-type thermocouples connected to the Nudam microprocessor units.
Valve train system	• The poppet valves were actuated by direct-acting cams driven by a rotating cam. • The intake and exhaust camshafts were installed in separate housings. Therefore, they can be interchanged independently. • The camshaft drive belt pulleys were mounted in outrigger bearings. Thus, the camshaft removal would not disturb the drive belt mechanism.

Fuel and ignition systems	• An AVL 4210 engine timing unit was used to control the injection and spark timing. • The unit took a reference signal from a camshaft mounted encoder with 0.2° CA resolution. • AVL733 dynamic gravimetric fuel balance was used to measure the fuel consumption.
Cylinder liner and piston	• A Kistler 6014A piezo-capacitive pressure transducer was mounted between the intake and exhaust valves at the periphery of the combustion face of the cylinder head and used to measure the in-cylinder pressure. • The pressure was pegged at the BDC of the intake stroke using the Kistler 4075A piezo-resistive transducer, which was mounted towards the bottom of the cylinder liner. • A fast data acquisition system from MTS Systems was used to acquire the cylinder pressure and engine speed data using the crank angle encoder set to a resolution of 0.5° CA.
Crankcase	• The engine featured the primary and secondary balance shafts capable of speeds up to 5000 rpm.
Dynamometer	• The load on the engine was applied by a Borghi & Saveri water-cooled eddy current dynamometer equipped with a load cell to measure the torque.
Emissions	• Standard bench emissions were measured by the Signal Instruments rack: NO_x analyser, a heated THC analyser, an NDIR CO and a CO_2 multi gas analyser. • Exhaust gas was sampled 250 mm downstream of the exhaust manifold in the exhaust plenum. • Particulate samples were collected at the same point and sent to the Combustion DMS500 Fast Particulate Spectrometer. The spectrometer was capable of measuring particulate sizes between 5 and 1000 nm in diameter at a rate of 10 Hz.

4.3 Rover Engine

The Rover K-16 engine (please refer to Figure 4.6) has been used to validate the combustion kinetics and knock model in this project. An additional engine is needed to be used for this purpose because the Lotus engine is characterised by a limitation of the peak pressure, which can only go up to 60 bar. Thus, engine knock could not be produced in the Lotus engine. The Rover K-16 engine has been chosen based on its robust capability. Thus, the engine knock can be produced in order to obtain the data. Details of the engine specifications and its systems can be found in Table 4.4 below.

Figure 4-6 Rover K-16 engine

Table 4-4 Rover K-16 specifications

Arrangement	Straight 4-cylinder transverse
Firing order	1 – 3 – 4 – 2
Max power output	70 kW at 6250 rpm
Max torque	123 Nm at 4000 rpm
CR	10.0:1
Bore	75 mm
Stroke	79 mm
Connecting rod	131.5 mm
Capacity	1397 cm^3 / 1.4 L
Fuel system	Indirect multi-point injection with ECU control
Injection pressure	3.0 ± 0.2 bar

Valve timing	Inlet: opens at 15 °BTDC closes at 45 °ABDC Exhaust: opens at 55 °BBDC closes at 5 °ATDC
Inlet and exhaust systems	• The mass air flow was measured using a manometer tube from Airflow Development Ltd. • The values of the inlet temperature and coolant temperature are measured using K-type thermocouple sensors. • PT100 sensors are used for the exhaust temperature, cell temperature, ambient temperature, and fuel rail temperature.
Fuelling system	• The fuel flow rate was measured by the volumetric fuel measurement system. • The air/fuel ratio was recorded by ECM AFRecorder 2000.
Cylinder liner	• The cylinder pressure was pegged using the piezoelectric pressure sensor [Kistler type 5011 charge amplifier].
ECU	• MEMS 1.3E Type MNE 10020 was used to read data from several sensors and compute an appropriate fuelling rate and ignition advance or retard. • The ECU sampled the engine speed, manifold absolute pressure, coolant temperature, intake air temperature, throttle position, and battery voltage. • The base values for the fuelling and ignition timing are retrieved from a three-dimensional map.
Dynamometer	• The engine torque was produced by the eddy current dynamometer (Froude Cousine AG150-HS). Dynamometer controller: Froude Cousine Texcel V4. • An optical encoder was used to convert the angular position to give a crank angle position.

4.4 Steady Flow Rig

The steady flow rig, as illustrated in Figure 4.7 below, was used to collect data on the valve flow. The discharge coefficient calculation was computed based on the valve flow measurement at different valve lifts. The steady flow rig consists of vacuum pumps below a settling chamber and it was set to create a constant pressure drop. Manometers were used to display the pressure drop values and the volume flow rate. The SuperFlow SF600E flow rig equipped with six orifice plates for varying sizes, as well as throttle for the vacuum pumps to create a flow rate up to 600 cubic feet per minute (0.28 m^3s^{-1}) at a pressure drop of 20" (508 mm) H_20 was used. The rig could work in both intake and exhaust modes.

Figure 4-7 Steady Flow rig

The study of the intake and exhaust valves efficiency was conducted at two pressure drops and 10 valve lifts. Dial gauges were fitted to the valves in order to measure displacement. The holes for the injector and spark plug were covered with modelling clay in order to avoid air leakage. The valves were opened to 10 mm each and the steady flow rig was run at a 250 mm H_20 pressure drop. The pressure is then increased to 635 mm H20 and the same data is noted. The valve lift was then raised by 1 mm to 9 mm, and the process repeated until a 1 mm lift. After this lift, the machine was left to rest for a minute before retaking that measurement and progressing back up until 10 mm, so every lift measurement was taken twice for comparison purposes. The rig was then changed to the

exhaust mode, the head was rotated 180º, and the dial gauges were repositioned onto the exhaust valves before the whole process was repeated.

4.5 Summary

The present chapter has presented the experimental test facilities associated with the research project. The Lotus SCORE and OSCAR engines have been used for the main data collection purposes, while the engine knocking data was collected from the Rover engine. The next chapter discusses the development of the engine models, with the baseline model being based on a single cylinder naturally aspirated engine. Then, a boosting system is added to represent the downsized engine. The engine model is integrated with a combustion model with a reduced kinetics mechanism for a more detailed investigation.

Chapter 5

DEVELOPMENT OF ENGINE MODEL & MODEL VALIDATION

5.0 Overview

Computer simulation is one of the major areas in the internal combustion engine development. It has economic value in the reduction of time and costs for the development of new engines. The main factors why this type of simulation has been used widely are because it renders the design process less intricate, able to predict trends, serves as diagnostic tools, can generate more data, and helps to understand the complex processes that happen in the combustion chamber, which is hardly accessible via engine testing [63].

The simulation of the internal combustion engine has become very important in recent years due to the availability of increasing computer power. The engine model is used to test several changeable parameters as a guideline and reference before being tested on the real engine test cell. By doing this, any possibility of incidents related to exceeding the limitation of the real engine can be avoided. The main limitation of computer simulation is the accuracy factor. In order to address this issue, the engine model needs to be properly validated with experimental data within an acceptable range, and the limitations or assumptions made on the model must be addressed accordingly.

For this research project, the Ricardo WAVE, MATLAB and Cantera software applications have been used in order to develop a single-cylinder downsized engine model equipped with the combustion kinetics model and to test the Miller cycle combustion strategy at various speed-load points. The explanation regarding the software is as discussed below:

Ricardo WAVE Software (Version 2015.1)

The WAVE software is a one-dimensional gas dynamics and engine software package developed by Ricardo Software for the engine design process application. The simulation comprises of three main phases as listed in Table 5.1 [64]:

Table 5-1 Simulation phases in Ricardo WAVE

Pre-processor: WAVEBuild	To set up the simulation/analysis. GUI-based, where the user is provided with an input window on the computer screen and prompted for a series of values, inputs, and parameters required describing the simulation and performing the analysis.
Solver: WAVE	WAVE provides a fully integrated treatment of time-dependent fluid dynamics and thermodynamics by means of a one-dimensional formulation. WAVE is a program used to analyse the data provided by the pre-processors.
Post-processor: WAVEPost	The unified graphical post-processor is used for all WAVE simulations and enables the visualisation of results and report generation.

MATLAB (Version 2015a)

MATLAB is well-known among engineers and scientists as a software application used in order to analyse and design systems and products. It uses matric-based MATLAB language to express computational mathematics and has built-in graphics to visualise and gain information from data. The MATLAB code can be integrated with other languages.

In this project, MATLAB Simulink has been used as a platform for the integration of the combustion model in MATLAB with the engine model developed in the Ricardo WAVE software. Simulink is a block diagram environment for multi-domain simulation and Model-Based Design. Simulink provides a graphical editor, customisable block libraries, and solvers for modelling and simulating dynamic systems [65].

CANTERA (Version 2.2.1)

Cantera is another software application used in this project. It is a suite of object-oriented software tools for problems involving chemical kinetics, thermodynamics and transport processes.

Cantera provides types of objects representing phases of matter, interfaces between these phases, reaction managers, time-dependent reactor networks, and steady one-dimensional reacting flows. Cantera is currently used for applications including combustion, detonations, electrochemical energy conversion and storage, fuel cells, batteries, aqueous

electrolyte solutions, plasmas, and thin film deposition. Cantera can be used from Python and MATLAB, or in applications written in C++ and Fortran 90 [66].

The structure of the engine model development

Figure 5.1 below illustrates the development steps of the engine models including the purpose and real engines used to validate the models. It started with the naturally aspirated engine model, followed by the variable valve train model, adding the boosting system to represent the downsized engine model and combustion kinetics and knocking model. Each of the models is validated by different engines, as each engine served to validate a different parameter. It is also due to the operating limitation that the required criteria were not available in one engine.

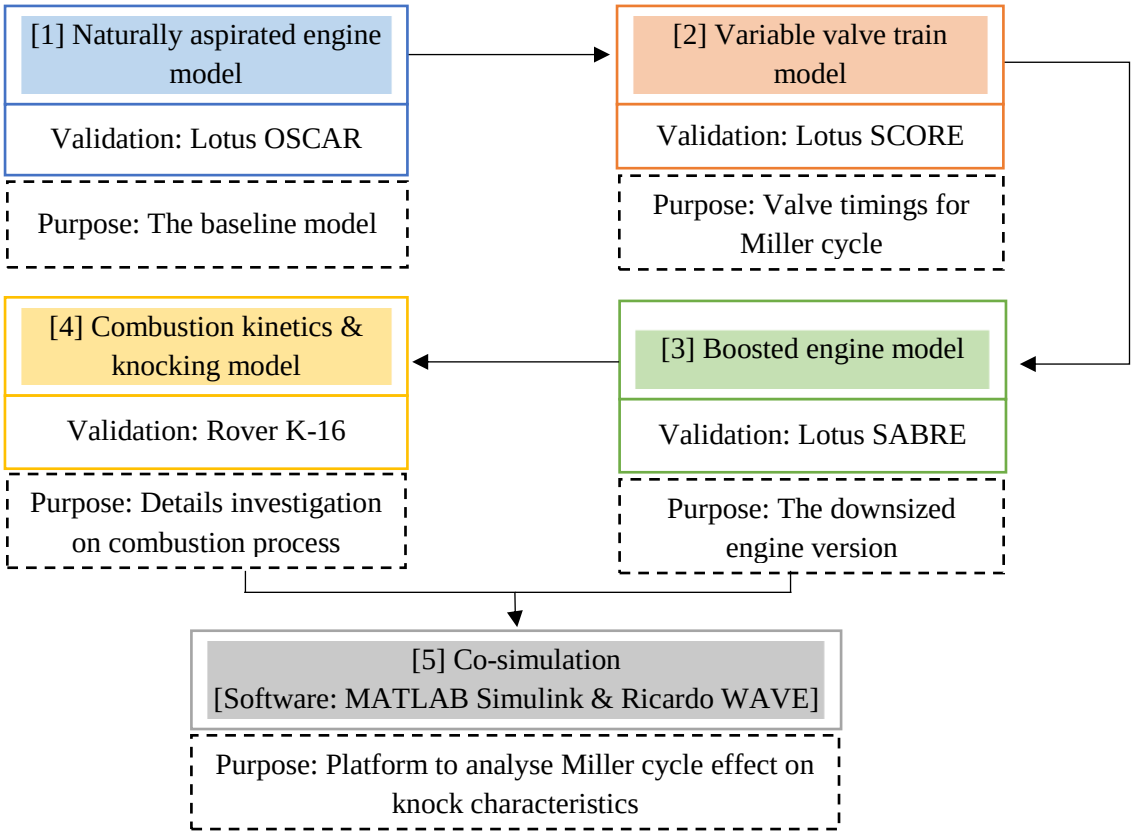

Figure 5-1 Engine models' development chronology

Lotus OSCAR, SCORE and SABRE have the same basic engine specifications. Lotus OSCAR served as the thermodynamics engine, while Lotus SCORE is equipped with the fully variable valve train for the Miller cycle implementation. Lotus SABRE is the downsized version of the engine that has a boosting system added to the engine. Rover K-16 was used for the combustion kinetics and knocking model validation because the

Lotus SCORE engine has a limited maximum peak pressure value of 60 bar. Thus, it cannot be used to produce the knocking data. The boosted engine model and combustion model are integrated together using MATLAB-Simulink as the main platform. Further details referring to each model may be found in the next sections.

5.1 Naturally-aspirated Engine Model

The naturally-aspirated engine model is developed based on the Lotus SCORE engine, as described in Section 4.1. It serves as the baseline engine model. In developing the engine model, there are five main important parts that have been considered, as listed below. The detailed parameters and limitations are discussed in the next subsections.

a) Flow modelling
b) Combustion model
c) Heat transfer
d) Friction model
e) Knock model

The operating parameters of the simulation were gathered in order to ensure that the model was able to replicate the real engine operation as closely as possible, as listed in Table 5.2. The simulation control settings are as described in Table 5.3.

Table 5-2 Engine operating parameters

Inlet and exhaust wall temperatures	a) Plenum and intake runner wall temperatures : 300 – 330 K b) Intake port wall temperatures : 350 – 400 K c) Exhaust port wall temperatures : 450 – 550 K
Initial temperatures & pressures	a) Intake side Initial Temperature : 298.15 K Initial Pressure : 1.0 bar Initial Fluid Composition : 100 % fresh air Initial Wall Temperature : 350 K b) Exhaust side (for a naturally aspirated engine) Initial Temperature : 800 K Initial Pressure : 1.05 bar Initial Wall Temperature : 450 K

Engine operating speed	5000 – 1000 rpm (The cases are set up beginning with the highest rpm because the simulation for lower speed will take longer time)

Table 5-3 Setting for simulation control

Reinitialize model between cases	ON (Turning this on will cause WAVE to start from the user-imposed initial conditions for wall temperatures, gas temperatures, pressures, velocities, and species concentrations in every subsequent case when multiple cases are defined)
Simulation duration	1000 (If the number is higher than required, auto-convergence will stop the simulation)
Fluid properties	RON_95
Convergence	Standard tolerance: 0.01 Consecutive cycles converged: 5 Parameters checked for convergence: All Cell Pressures, Velocities, Conducting Wall Temperatures

5.1.1 Flow Modelling

The engine model diagram of the single-cylinder naturally-aspirated engine is illustrated in Figure 5.2. The detailed specifications of each element in the engine model could be found in Appendix A. It consists of three main parts, namely the intake side, engine block and exhaust side. Each of the pipes is represented by a duct element. An orifice element is used to connect between two ducts. The orifice element has no length or volume and is used to connect two adjoining ducts, which need not have the same diameters.

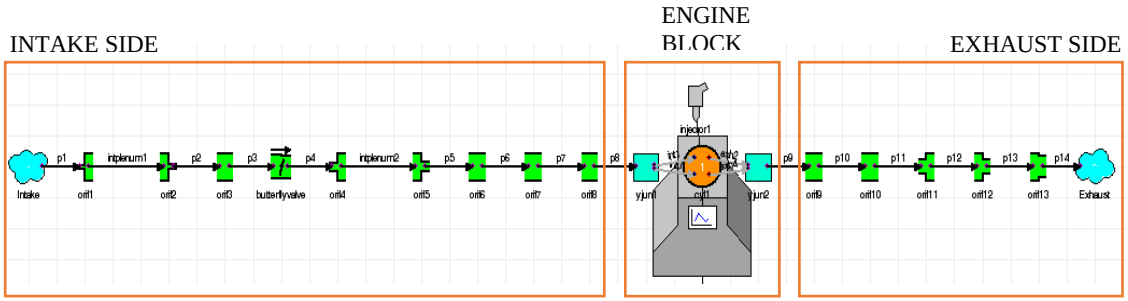

Figure 5-2 Single-cylinder NA engine model

A duct is an element representing a portion of a flow network, which is long creating a one-dimensional flow. The large single volume is being discretised into smaller sub-volumes. The equation for the conservation of energy and mass will be solved in each of the sub-volumes and the scalar quantities of pressure and temperature will be stored at the cell centre, while the equation for the conservation of momentum is solved at the boundaries of the cell, which then stores the vector quantities, such as mass-flow and velocity.

The relationship between the discretization length (dx) and the engine bore diameter (B) based on Ricardo's experience in one-dimensional modelling is given as:

- Intake:

$$dx = 0.45 \times B = 0.45 \times 88 = 39.6 \tag{5.1}$$

- Exhaust:

$$dx = 0.55 \times B = 0.55 \times 88 = 48.4 \tag{5.2}$$

A duct must be connected at each end to one ambient, cylinder, orifice, turbo, valve, or Y-junction element.

a) The ambient element represents a connection to an infinite reservoir at a specified pressure, temperature, and composition. The input fields include the description of the ambient conditions as well as the specification of the opening at the end of the attached duct element.
b) The cylinder element represents a basic piston engine cylinder of an internal combustion engine, as illustrated in Figure 5.3. Each connection point in the cylinder element represents an engine valve, which must be specified on the input panel. When a duct is attached to a connection point, the connection point will change colour to either blue (representing an intake valve) or red (representing an exhaust valve).
c) The compressor is modelled as a planar boundary between adjacent duct sub-volumes and requires at least two connected ducts.
d) Each distinct valve is defined in a list and then used in the flow system at any desired location. WAVE requires valves at all entrances and exits from the cylinder elements.
e) The Y-junction element represents a spherical volume, which may be the junction of multiple ducts.

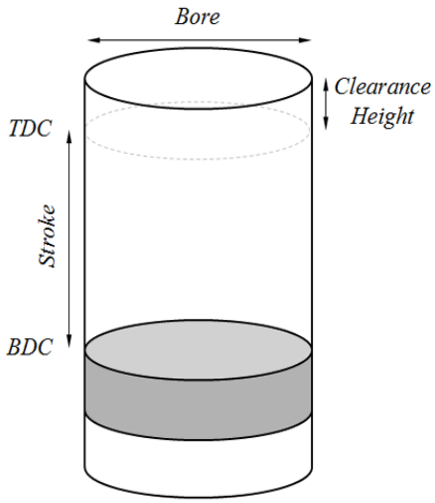

Figure 5-3 Basic geometry model [64]

5.1.2 Combustion Model

The SI Wiebe function is used to describe the rate of fuel mass burned in thermodynamic calculations. This relationship enables the independent input of the function shape parameters and of the burn duration. It is known to represent the experimentally observed trends of the premixed SI combustion fairly accurately. It is a primary combustion model and the most commonly used combustion sub-model in SI engines. The cumulative mass fraction burned as a function of the crank angle is given by the following equation:

$$W = 1.0 - \exp\left(- AWI\left(\frac{\theta}{BDUR} \right)^{(WEXP+1)} \right) \tag{5.3}$$

Where:

AWI = Internally calculated parameter to allow $BDUR$ to cover the range of 10 – 90 %

θ = Degrees past start of combustion

$BDUR$ = User-entered combustion duration (10 – 90 %)

$WEXP$ = User-entered exponent in Wiebe function

The burn profile in the input panel as illustrated in Figure 5.4 is used to observe the effects of varying the input parameters. Varying the 50 % burn point simply shifts the entire curve forward or backward. Varying the 10 % - 90 % duration will extend the total combustion duration, making the profile extend longer or compress shorter. Varying the Wiebe exponent will shift the curve to burn mass earlier or later. 50 % location point and

burn duration inputs were based on the experimental values, which were defined accordingly based on the engine operating speeds.

Typically, in the SI Wiebe function, the 10 – 90 % combustion duration increases steadily as the engine speed increases and the location of the 50 % burn point is affected by the spark timing advance (increases with rpm) but remains almost constant as the engine speed changes [64].

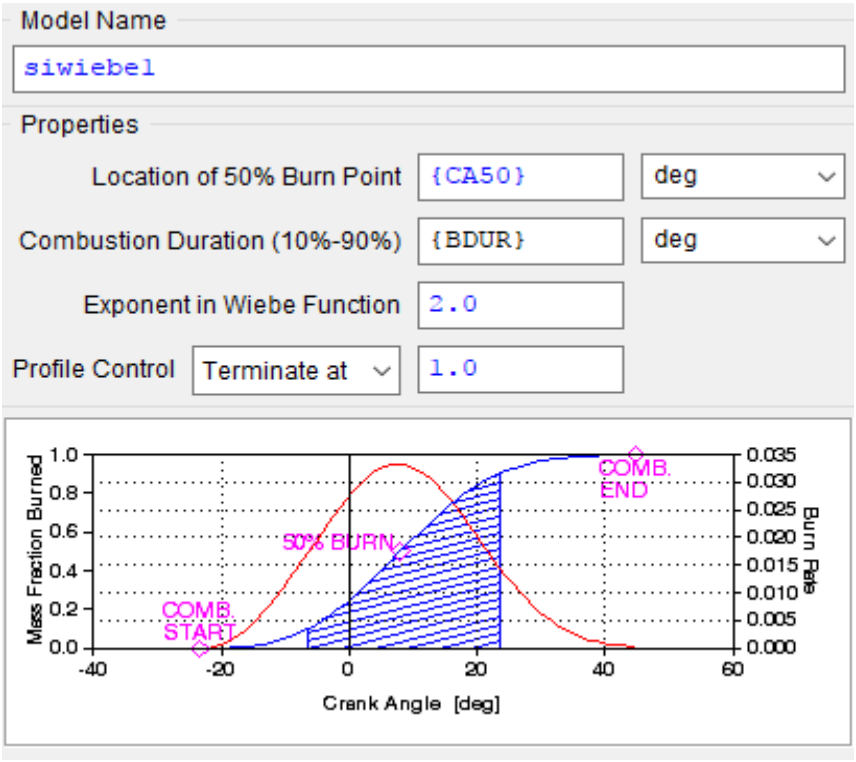

Figure 5-4 Inputs of the SI-Wiebe combustion model

The two-zone combustion model has been adopted to model the cylinder. The two-zone model is used to capture the chemical processes taking place during the combustion period in more detail. This is because it was needed for the engine knock modelling, which will affect both the unburned and burned zones.

- For the two-zone model in the unburned zone:

$$m_{u1}u_{u1} - m_{u0}u_{u0} + P(V_{u1} - V_{u0}) + Q_u - \Delta m_{ui}h_{ui} = 0 \quad (5.4)$$

Using the equation of the state, it becomes:

$$m_{u1}u_{u1} - m_{u0}u_{u0} + m_{u1}R_{u1}T_{u1} - PV_{u0} + Q_u - \Delta m_{ui}h_{ui} = 0 \quad (5.5)$$

- Similarly, for the burned zone:

$$m_{b1}u_{b1} - m_{b0}u_{b0} + m_{b1}R_{b1}T_{b1} - PV_{b0} + Q_b - \Delta m_{bi}h_{bi} = 0 \quad (5.6)$$

- As a constraint, the volumes of the unburned and burned zones are summed up to the total cylinder volume:

$$m_{u1}R_{u1}T_{u1} + m_{b1}R_{b1}T_{b1} - PV_c = 0 \quad (5.7)$$

- The last three equations are a complete set and are solved by using the Newton iteration method.

5.1.3 Heat Transfer Model

The Woschni heat transfer sub-model views the charge as having a uniform heat flow coefficient and velocity on all surfaces of the cylinder. Table 5.4 below lists the inputs that have been set for the heat transfer model.

Table 5-4 Inputs for the Woschni heat transfer model

Model type	Original
Heat transfer multiplier when the intake valves open	1.0
Heat transfer multiplier when the intake valves close	1.0

The Woschni heat transfer coefficient is calculated using the following equation:

$$h_g = 0.0128 D^{-0.20} P^{0.80} T^{-0.53} v_c^{\ 0.8} C^{enht} \quad (5.8)$$

Where:

D = Cylinder bore
P = Cylinder pressure
T = Cylinder temperature
v_c = Characteristic velocity
C^{enht} = User-entered multiplier

The characteristic velocity, v_c is the sum of the mean piston speed and an additional combustion-related velocity that depends on the difference between the cylinder pressure and the pressure that would exist under motoring conditions.

$$v_c = c_1 v_m + c_2 \frac{V_D T_\gamma}{P_\gamma V_\gamma}\left(P - P_{mot}\right) \quad (5.9)$$

5.1.4 Friction Model

A modified form of the Chen-Flynn correlation is used to model friction in the WAVE engine. The correlation has a constant term (for accessory friction), a term which varies with the peak cylinder pressure, a third term linearly dependent on the mean piston velocity (for hydrodynamic friction) and a fourth term quadratic with the mean piston velocity (for windage losses). The Chen-Flynn correlation values are found using the tool provided by WAVE as in Appendix B after putting in the cylinder pressure, engine speed and FMEP values measured from the Lotus OSCAR engine. The values are listed in Table 5.5 below.

Table 5-5 Friction correlation inputs

ACF	0.8009 bar
BCF	0.0050
CCF	544.1776 Pa.min/m
QCF	0.2 Pa.min^2/m^2

The equation used to calculate friction is given below:

$$FMEP = A_{cf} + \frac{1}{ncyl}\sum_{i=1}^{ncyl}\left[B_{cf}\left(P_{cyl}\right)_i + C_{cf} * \left(S_{fact}\right)_i + Q_{cf} * \left(S_{fact}\right)_i^2\right] \quad (5.10)$$

Where:

S_{fact} = RPM * stroke / 2

A_{cf} = ACF user input

B_{cf} = BCF user input

P_{max} = Maximum cylinder pressure

RPM = Cycle-average engine speed

stroke = Cylinder stroke

C_{cf} = CCF user input

Q_{cf} = QCF user input

5.1.5 Knock Model

The knock model in the WAVE software is activated simultaneously with the two-zone combustion in the cylinder. The knock model is based on Douaud and Eyzat's induction

time correlation [67]. The knock model characterises the knocking behaviour of the fuel and engine based on the fuel octane number. From the octane number, the model identifies the parameters of its induction/ignition delay time.

The induction time (ignition delay) in seconds is calculated at every timestep using the equation:

$$\tau = 0.01869 / A_p * \left(\frac{ON}{100}\right)^{3.4107} * P^{-1.7} \exp\left(\frac{3800/A_T}{T}\right) \quad (5.11)$$

Where:

A_p	=	User-entered pre-exponential multiplier
ON	=	User-entered fuel octane number
P	=	Cylinder pressure [kgf/cm^2]
A_T	=	User-entered activation temperature multiplier
T	=	Unburned gas temperature

Normally, as the combustion process is developing, the unburned zone temperature is rising, and the induction time is decreasing. The end-gas will auto-ignite or knock if the induction time falls below the flame arrival time. The model assumes that auto-ignition occurs when:

$$\int_{t0}^{ti} \frac{d\tau}{\tau} = 1 \quad (5.12)$$

Where:

$t0$	=	Start of end-gas compression
ti	=	Time of auto-ignition
τ	=	Induction time, defined above

When this situation occurs, a spontaneous mass burning rate due to knock is defined. The information is sent to the cylinder, which leads to a rapid rate of increase in cylinder pressure and temperature. During knocking, the heat transfer coefficient is also increased. The combustion is then governed by the post-knock burn time scale as indicated below:

$$\tau = f_c \left[\frac{0.8573}{B_0 (1 + A/F)} \exp\left(\frac{T_a}{T_f}\right) \right] \quad (5.13)$$

Where:

f_c = Post-knock burn scale multiplier
B_0 = Frequency factor, hard-coded as 2233e3 1/s
A/F = Air/fuel ratio of unburned end gas
T_a = Activation temperature, hard-coded as 15150 K
T_f = Adiabatic flame temperature

The fuel burn rate in the post-knock period is assumed to be constant and is calculated as:

$$m_{dot,\,fuel} = \frac{m_{fvapor} + m_{fliquid}}{\tau_{postknock}} \tag{5.14}$$

Air is burned proportionally at a rate given by:

$$m_{dot,air} = m_{dot,\,fuel} * (A/F) \tag{5.15}$$

Where:

m_{fvapor} = Unburned fuel vapour mass at the time of knock
$m_{fliquid}$ = Unburned fuel liquid mass at the time of knock

When WAVE detects knock while the simulation is running, it will issue a warning to the output file. It will report back the cylinder number, time of the knock occurrence, total mass fraction burned at the time of the knock occurrence, and the knock intensity as the amount of unburned mass divided by the total mass (normalised mass fraction), which is consumed during the knock event [64].

The knock model used in WAVE by Douaud and Eyzat was validated by experimental work. About one thousand measurements of octane requirements made at WOT and various constant speeds on about 60 European and Japanese passenger cars have been considered. The method has an average accuracy of 0.5 octane points in predicting the behaviour of the fuels from the one thousand samples collected via experiments [67]. Thus, this method is valid to be used to characterise the knocking behaviour of fuels and engines. Moreover, it is easy to be applied as it only requires the octane number of fuel, thus making it possible to identify the autoignition delay parameters with an error estimate.

Table 5.6 below lists the settings required to activate the knock model in the engine. The fuel octane number is the same as what was used in the experimental works. The other

data are the values from the WAVE simulation setting. The main reason we decided to use the default values is due to the constraints imposed by the current available engines in the lab. The Lotus research engine has a fully variable valve timing system to accommodate the Miller cycle valve timing variations and gasoline direct injection system. However, this cannot be applied in the case of a peak cylinder pressure value higher than 60 bar as the maximum safe operating pressure to generate the knocking due to the sapphire window mounted in the piston crown. Additionally, it does not have a boosting system to represent the downsized engine. The other available engines can generate engine knock, but they do not have the freedom to vary the valve timings for the Miller cycle operation.

Table 5-6 Knock model settings

Fuel octane number	95
Pre-exponential multiplier	1.0
Activation temperature multiplier	1.0
Post-knock burn timescale multiplier	1.0

5.1.6 NA Engine Model Validation

The experiment values for the location of θ_{50} and $\theta_{10\text{-}90}$ burn duration from the Lotus OSCAR engine were used to define the Wiebe curve of the combustion model. Additional explanations regarding the engine can be found in Section 4.2. The simulations were performed with the experiment start of injection (SOI) timing and the throttle position at WOT.

The operating points used for the validation are given in Table 5.7. The results of the engine model in the WAVE software are validated against those values.

Table 5-7 Operating points for the engine model validation

No	Speed (rpm)	θ_{50} (°CA)	$\theta_{10\text{-}90}$ (°CA)	Fuel mass flow (kg/hr)	Peak pressure (bar)	BMEP (bar)
1	5000	6.42	24.15	4.972	57.21	8.88
2	4000	6.57	22.86	3.875	56.60	9.14
3	4000	5.67	22.77	3.859	57.83	9.13

4	4000	6.03	23.12	3.897	57.18	9.07
5	3000	5.09	20.72	2.988	62.05	9.84
6	3000	3.87	20.27	2.992	63.71	9.76
7	3000	4.45	20.97	2.851	62.58	9.68
8	3000	4.47	21.59	3.070	62.06	9.60
9	2000	1.39	17.47	2.106	71.10	10.17
10	2000	0.92	17.56	2.124	71.01	10.20

Figure 5.5 compares the simulated and experimental values for brake power and brake torque, with ± 1.9 % errors respectively. The simulated fuel mass flow is within ± 3.8 % of the experiment data. The BMEP prediction is within ± 2 % of the measured values. The peak pressures predicted by the model are within ± 3.1 % of the measured values while the peak pressure locations are ± 1.7 % compared to the experiment results. The R-squared values were computed as a statistical measure in order to determine how close the data are to the fitted regression line. Based on this comparison, the engine model can replicate the experiment values confidently.

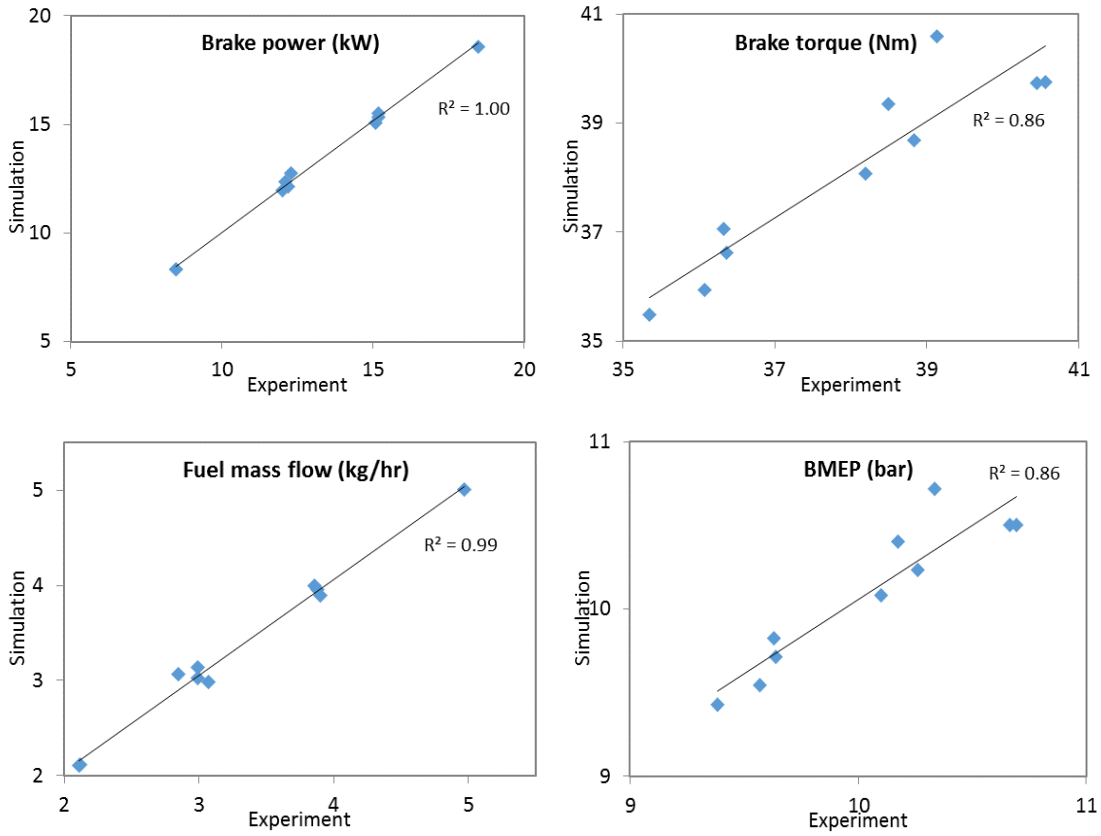

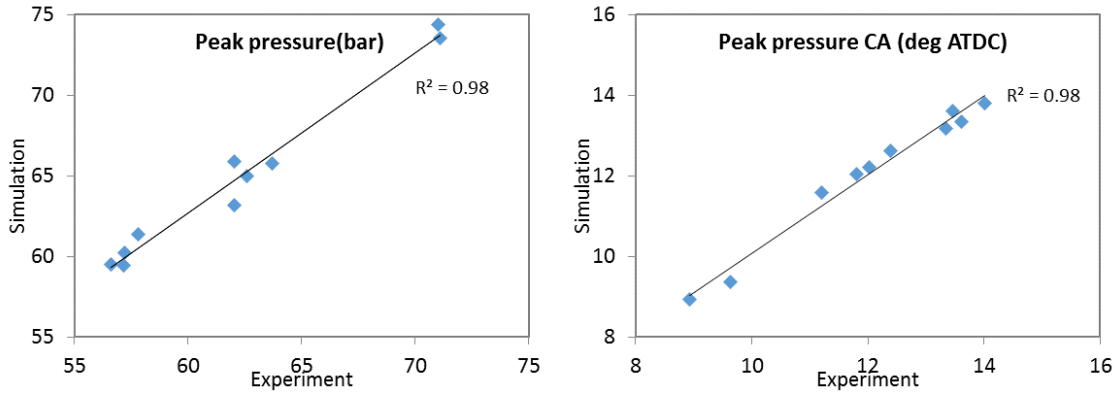

Figure 5-5 Comparison of the experimental and simulation results.

5.2 Variable Valve Train Model

The lift valve sub-model in Ricardo WAVE defines a lift profile with some basic valve train definitions as well as a flow coefficient profile. A lift valve must have either the Forward/Reverse Flow Coefficients or Pressure Ratio Dependent Flow Coefficients defined. The intake and exhaust flow and discharge coefficients were retrieved from the experimental work conducted on a Steady Flow test rig, as described in Section 4.4.

Flow Coefficient and Discharge Coefficient

The forward/reverse flow coefficients are used to describe the complex behaviour of flow through a valve due to a combination of factors, including port geometry and finish, valve seating, valve position, etc. These factors are simplified into a multiplier (0 to 1, reduction factor) of the geometric area to create an effective area through which flow can pass (please refer to Table 5.8 and 5.9).

Table 5-8 Intake valves flow coefficient profile: forward/reverse

L/D	CDF	CDR
0.031	0.07	0.07
0.063	0.16	0.16
0.094	0.25	0.25
0.125	0.33	0.33
0.156	0.4	0.4
0.188	0.47	0.47
0.219	0.53	0.53

0.250	0.59	0.59
0.281	0.63	0.63
0.313	0.65	0.65

Table 5-9 Exhaust valves flow coefficient profile: forward/reverse

L/D	**CDF**	**CDR**
0.031	0.08	0.08
0.063	0.16	0.16
0.094	0.26	0.26
0.125	0.34	0.34
0.156	0.41	0.41
0.188	0.45	0.45
0.219	0.47	0.47
0.250	0.50	0.50
0.281	0.52	0.52
0.313	0.53	0.53
0.360	0.53	0.53

5.2.1 VVT Model Validation

The valve train model is validated in order to ensure that it is operating like the Lotus AVT system installed on the Lotus SCORE engine, as described in Section 4.1. This part is important because the Miller cycle strategy is implemented with variation of valve timings. The testing points employed for load control by the Miller cycle through EIVC timings was used for validation purposes.

Figure 5.6 compares the IMEP values between the experiment and the simulation works. At 2.0 bar IMEP, the throttled one is 2.9 % different from the experiment value, while the unthrottled one exhibits a 5.6 % difference compared to the experiment value. At 2.7 bar IMEP, the percentage difference is 1.8 % for the throttled and the unthrottled conditions. The maximum pressure values and the indicated power percentage difference is within ± 3.4 % between the experiment and the simulation works. The confidence interval error bar has been used to show the correlation between the data.

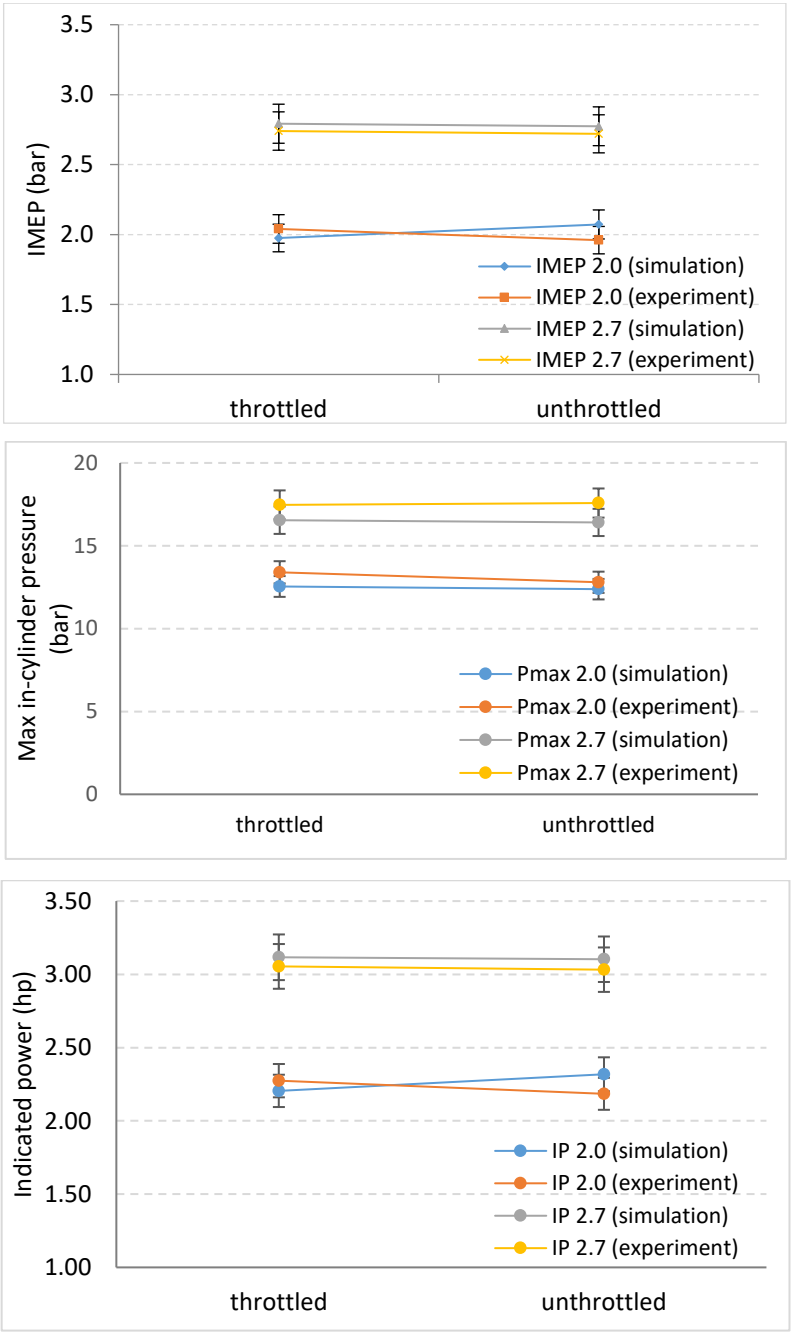

Figure 5-6 Comparison between experiment and simulation results

5.3 Downsized Engine Model

With the completion of the naturally-aspirated engine model validation, a compressor was added to the model to simulate the downsized engine environment. The main purpose of this model is to design an engine capable of delivering a high BMEP performance, which is commonly achieved in today's downsized boosted engines. The model is used as a research tool for the conceptual study of the Miller cycle combustion strategy of the downsized gasoline engine in this project.

The performance of the boosted model in terms of the BMEP value is compared with the Lotus SABRE Phase 1 engine from a literature study [24]. Lotus SABRE is a 1.5 L, 3-cylinder engine with a compression ratio of 10.2:1. It has the same engine cylinder specifications as the Lotus SCORE engine. More details can be found in Table 5.10 below.

Table 5-10 Summary of Lotus SABRE engine specifications

Volume	1.5 L
Arrangement	3-cylinder (in-line)
Firing order	1 – 3 – 2
Max power	117 kW at 5000 rpm
Max torque	240 Nm (from 2000-4000 rpm)
Max BMEP	20.1 bar
Stroke	82.1 mm
Bore	88.0 mm
Connecting rod length	142.0 mm
Compression ratio	10.2:1
Air/Fuel ratio	14.53 (95 RON gasoline)
Injector type	Direct injection using multi-stream solenoid injectors
Injection pressure	200 bar
Supercharger type	Turbocharger
Maximum boosting pressure	1 bar

For the boosting system in the engine model, a mapless compressor was used to represent a compressor. This type of compressor was chosen to assist this conceptual study of investigating the effect of the boosted pressure ratio on the engine performance because the compressor map data used by Lotus SABRE is not available. The compressor is modelled as a planar 'rotor' (where the mass flow and outlet enthalpy are controlled) and as an outlet flow passage (Figure 5.7). The outlet enthalpy of the compressor was calculated based on the user input pressure ratio and isentropic efficiency. The compressor will control the mass flow in order to achieve the targeted outlet pressure. A single turbo shaft is connected to the hub of the compressor.

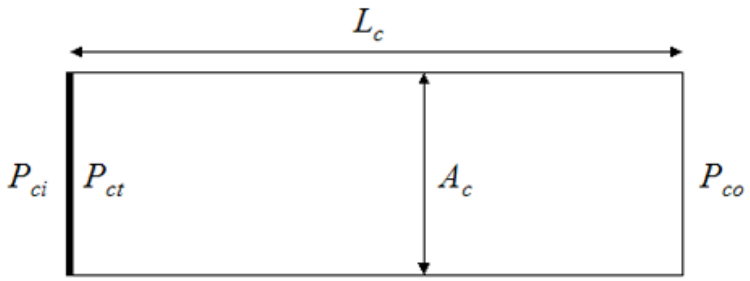

Figure 5-7 Mapless compressor diagram

The inlet static pressure, P_{ci}, is provided by the duct attached at the compressor inlet. On the outlet side of the planar rotor, the target static pressure P_{ct} is imposed. The acceleration of the flow in the outlet duct depends only on the forces exerted by P_{ct} (the user-input target static pressure) and the outlet static pressure, with P_{co}, representing the pressure in the duct attached at the compressor outlet [64]. The change in mass flow ($d\dot{m}/dt$) in the compressor is calculated by the following equation:

$$\frac{d\dot{m}}{dt} = \frac{A_c}{L_c}\left(P_{ct} - P_{co}\right) \tag{5.16}$$

Where:

A_c = Duct area of compressor

L_c = Duct length of compressor

5.3.1 Downsized Engine Model Validation

The compressor model parameters are listed in Table 5.11 below. The performance of the boosted engine model is compared with Lotus SABRE's BMEP and BSFC values (please refer to Figure 5.8).

Table 5-11 Compressor model parameters

Isentropic efficiency	1.0
Gain multiplier	1.0
Maximum pressure ratio	3.0
Initial pressure ratio	1.0

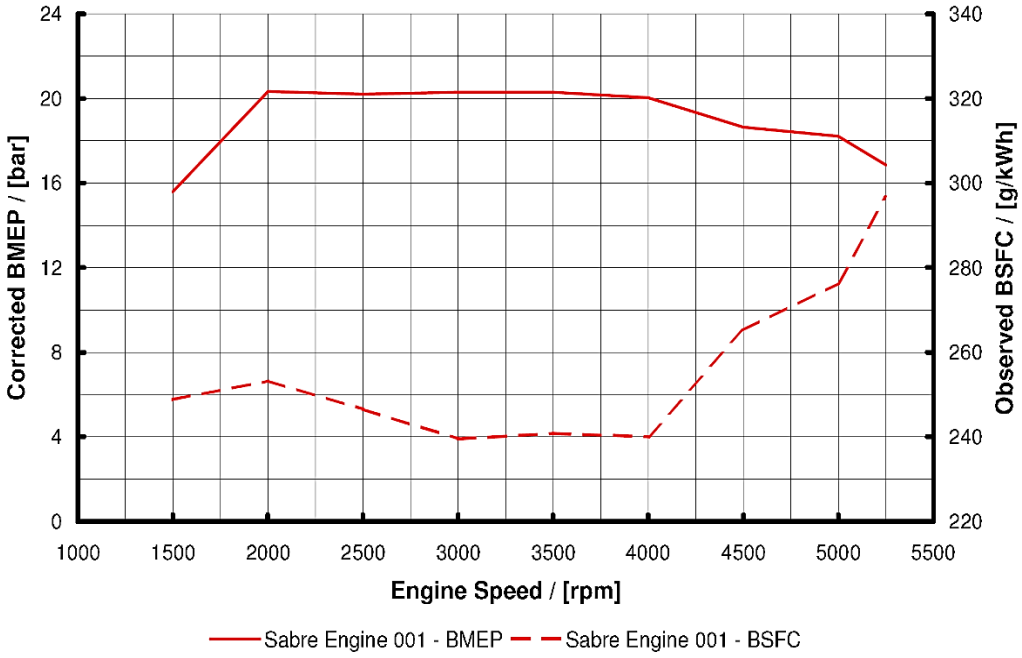

Figure 5-8 Lotus SABRE BMEP and BSFC values [24]

Figure 5.9 and Figure 5.10 indicate that the BMEP comparison is ± 5.0 % between the engine model and Lotus engine, while the engine model BSFC is within ± 6.3 % as compared to the Lotus engine. Although the percentage errors for some of the points are a bit high, the BMEP and BSFC graphs' trends are highly similar to the experimental values.

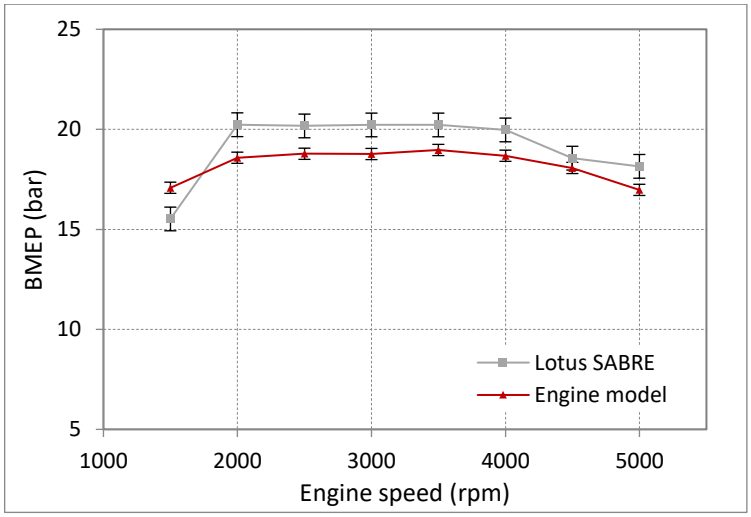

Figure 5-9 BMEP comparison between Lotus SABRE and engine model

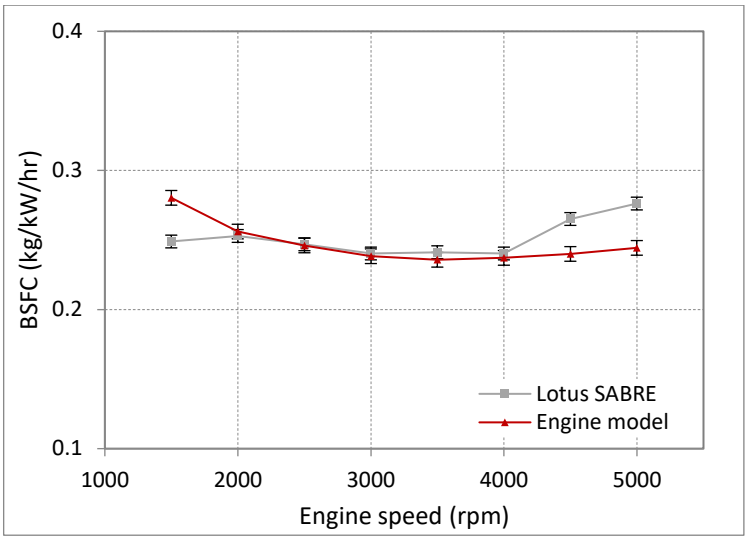

Figure 5-10 BSFC comparison between Lotus SABRE and engine model

5.4 Combustion Model with Reduced Kinetics Mechanism

In order to understand the downsized engine knocking behaviour, a further step to analyse the phenomenon in more detail has been taken by using a combustion model. The investigation of the combustion process was done using the zero-dimensional combustion model with a reduced kinetics mechanism. The downsized engine model from Ricardo WAVE was combined with the combustion and knocking model from the MATLAB software for this purpose.

The chemical kinetics mechanism has been widely used in modelling the engine knocking phenomenon [68]–[71]. Detailed chemical kinetics coupled with computational fluid dynamics (CFD) modelling showed a great potential in simulating the engine knock. It serves as a great fundamental step to predict and solve issues due to experimental limitations [72]. In developing the detailed chemical kinetics mechanisms, the reaction rate parameters and thermal chemical data were adjusted to fit the experimental data. The reduced mechanisms were extracted from the detailed kinetic mechanism by conducting the computerized reaction sensitivity analysis or by simplifying the chemical reaction processes into a few generalised chain branching mechanisms [68].

The zero-dimensional engine model technique provides a better advantage in terms of the computational efficiency in predicting the engine behaviour, as opposed to a complex CFD model. The zero-dimensional model has been incorporated with various combustion chemical kinetics mechanisms, such as the Shell auto ignition model, semi reduced chemical kinetic mechanism, or reduced chemical kinetic mechanism, to enable it to predict the engine knock phenomenon.

In this project, a three-zone zero-dimensional based on an SI engine combustion model combined with the reduced primary reference fuel (PRF) mechanism was used for simulating the combustion of gasoline fuel. The primary reference fuel (PRF) mechanism is one of the established simplified surrogate fuel models to mimic the combustion processes of the complex compositions of diesel and gasoline fuels. Certain advantages are gained through the usage of a multi-zone model to simulate the combustion process in the combustion chamber. First, it specifies the temperatures and compositions for each zone (reflects the inhomogeneous prosperities of the in-cylinder mixture). The model describes the volume and mass change caused by the in-cylinder flow dynamics, and takes

into account the crevices and thermal boundary layer. Furthermore, it is capable of describing the combustion process chemically and predicting the auto-ignition timing and the energy release rate [73].

Figure 5.11 illustrates the combustion chamber, which has been divided into three zones: burned and unburned zones separated by a flame front, which is the burning zone. In each zone, the gas mixture properties are different, and the zone volume varies with the piston motion and mass entrained by the flame front. They are transferred across the flame front from the unburned zone to the burned zone. The three-zone model is the most simplified physical representation of the combustion process in SI engines taking into account the flame propagation, mass transfer and volume change.

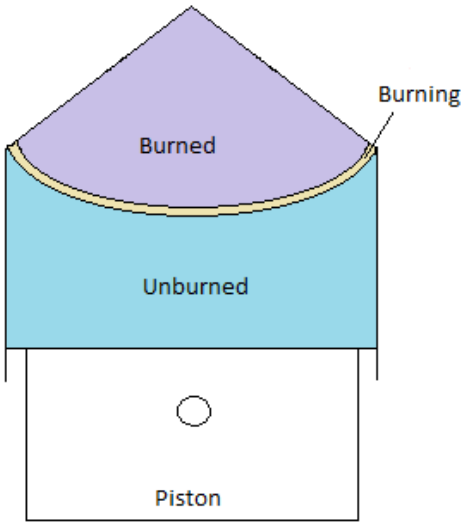

Figure 5-11 Combustion zones inside cylinder.

In-cylinder gas mixtures are divided into three zones based on the thermodynamics states and compositions, as explained in Table 5.12 below [68].

Table 5-12 Three-zone characteristics

Unburned zone	- unburned mixture of fuel and air in front of the propagating flame - no burned residuals are considered
Burning zone	- the reaction zone of the thin flame front - transporting mass and energy from the unburned to the burned gas regions - assume to have no volume and regarded as a transporting process

	- modelled by chemical equilibrium calculations
Burned zone	- the region consisting of burned products

The first law of thermodynamics, equation of state and conservation of mass and volume are applied to the burned and unburned zones. The pressure is assumed to be uniform throughout the cylinder charge. A system of first-order ordinary differential equations (ODEs) is obtained for the pressure, mass, volume, temperature of the burned and unburned zones, heat transfer from the burned and unburned zone, and mass flow into and out of the crevices.

Figure 5.12 illustrates the procedure flowchart for the combustion model processes. Fundamental energy, temperature, pressure and species mass fraction derivative equations are formed within each phase, which are then integrated by the ODE15 solver. Parameters, such as composition, temperature, pressure of the mixture at the IVC point and the Wiebe function parameters were provided by the user. The heat transfer rate constants, cylinder wall temperature and blow-by effects were estimated accordingly.

Here are the assumptions made for the combustion model:

- Chemical kinetics is modelled in both zones during combustion
- The burned and unburned zones are ideal gases, where the ideal gas constant R change rate is legitimately assumed zero in normal combustion
- The air-fuel mixture is spatially homogenous in temperature and in composition within both the unburned and burned zones
- Spatially averaged instantaneous heat transfer rates are adequate to estimate heat transfer to the cylinder walls
- No heat transfer occurs from the burned to the unburned zone and vice versa
- The instantaneous pressure is the same in both zones as the flame is a deflagration combustion wave
- The flame is assumed to be adiabatic and in chemical and thermodynamic equilibrium
- The flame front has negligible volume
- The work required to transfer fluid from the unburned to the burned zone is negligible
- The mass and energy / enthalpy exchange are transported from the unburned zone to the flame front, and instantaneously from the flame front to the unburned zone

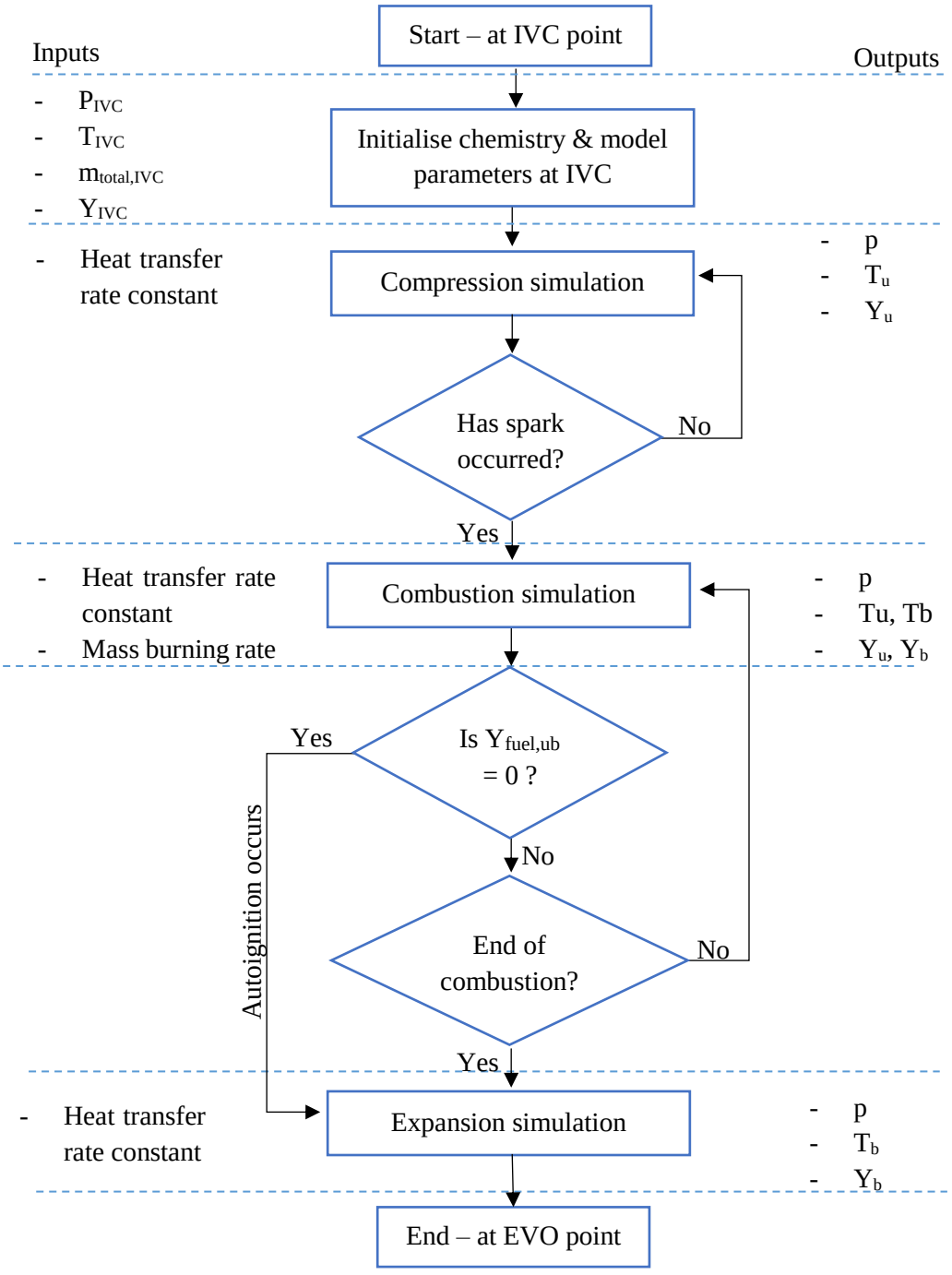

Figure 5-12 Procedure flowchart of combustion modelling

5.4.1 Fundamental theories of the combustion model

1. *Mass conservation*

The model is based on the mass and energy conservation for the burned and unburned zones.

a) In the unburned zone, when the pressure and temperature are sufficiently high, the air-fuel mixture is no longer stable and cool flame reactions start, potentially

leading to auto-ignition if the temperature increases. This leads to the introduction of chemical kinetics within the unburned zone. The change of rate of the mass fraction of a species, *i* in the unburned zone, $X_{i,u}$:

$$\frac{dX_{i,u}}{dt} = \frac{\overline{M}_i \dot{\omega}_i}{\rho_u} \tag{5.17}$$

Where:

$\overline{M}_i$ = molecular mass

$\dot{\omega}_i$ = volume specific molar production rate

ρ_u = density of unburned zone

b) In the burned zone, the mass fraction change of each species is affected by formation of the flame reactions and consumption of the post flame kinetic reactions. Total mass in the burned zone, m_b':

$$m_b' = m_b + \Delta m \tag{5.18}$$

Where:

m_b = burned zone mass before taking the transferred mass

The mass fraction of a species, *i* after mixing with the mass transferred from the burning zone:

$$X'_{i,b} = \frac{\Delta m \cdot X_{i,f} + m_b \cdot X_{i,b}}{m_b'} \tag{5.19}$$

Where:

$X_{i,f}$ = mass fraction of a species, *i* in the transferred mass from the burning zone

$X_{i,b}$ = existing fraction before the transfer

Substituting equation (5.18) into equation (5.19) yields the mass fraction change of a species, *i* due to formation by the flame reaction. The mass fraction change of a species, *i* in the burned zone:

$$\frac{dX_{i,b}}{dt} = \frac{1}{m_b'} \frac{dm_b}{dt} \cdot \left(X_{i,f} - X_{i,b}\right) + \frac{\overline{M}_i \dot{\omega}_i}{\rho_b} \tag{5.20}$$

2. *Energy conservation*

The energy conservation equation is applied to represent the energy change in the unburned and burned zone.

a) For the unburned zone, it relates the temperature change to the heat transfer, $\dot{Q}_{l,u}$ the work due to the volume change, and the energy change due to the chemical kinetic reactions:

$$m_u c_{p,u} \frac{dT_u}{dt} = \dot{Q}_{l,u} + V_u \cdot \frac{dp}{dt} - V_u \cdot \sum_{i=1}^{n} \omega_{i,u} \cdot \overline{M}_i \cdot h_{i,u} \tag{5.21}$$

Where:

h = specific enthalpy

c_p = specific heat capacity

V = zone volume

p = cylinder pressure

T = zone temperature

b) For the burned zone, the effect of the energy transferred from the burning zone, $\dot{m}_b \cdot (h_f - h_b)$ on the temperature change needs to be considered:

$$m_b c_{p,b} \frac{dT_b}{dt} = \dot{Q}_{l,b} + V_b \cdot \frac{dp}{dt} + \dot{m}_b \cdot (h_f - h_b) - V_b \cdot \sum_{i=1}^{N_s} \omega_{i,b} \cdot \overline{M}_{i,b} \cdot h_{i,b} \tag{5.22}$$

3. *Heat transfer*

a) Heat transfer of the unburned zone consists of two parts:

Q_{conv_w} : heat convection between the unburned gas and the cylinder wall

Q_{conv_f} : heat convection between the unburned gas and the flame front

$$\begin{aligned} Q_{l,u} &= Q_{conv\_w} + Q_{conv\_f} \\ &= h_{conv\_w} \cdot A_u \cdot (T_u - T_w) + h_{conv\_f} \cdot A_f \cdot (T_u - T_f) \end{aligned} \tag{5.23}$$

Where:

A_u = contact area between the end gas and the cylinder wall

A_f = contact area between the end gas and the flame front

$A_f = C_A \cdot A_b$

A_b = the area of burned gases in contact with the cylinder wall

C_A = adjustable constant (usually a value over 1)

h_{conv_w}, h_{conv_f} have been simulated using the Woshni correlation:

$$h = C_h B^{-0.2} p^{0.8} w^{0.8} T^{0.53} \tag{5.24}$$

b) Thermal radiation from the burned zone to the cylinder wall is modelled by the Stefan-Boltzmann law:

$$Q_{rad} = A_w \sigma T^4 \tag{5.25}$$

Where:

σ = Stefan-Boltzmann constant (5.67×10^{-8}[w/m^{2}K^4]

4. *Mass fraction burned*

The burned mass in the cylinder consists of two parts:

$$x_b = x_{flame} + x_{autoignition} \tag{5.26}$$

a) The mass transported from the burning zone due to the flame propagation, which is calculated by the Wiebe function:

$$x_b = 1 - e^{\left[-a\left(\frac{\theta-\theta_0}{\Delta\theta_b}\right)^{m+1}\right]} \tag{5.27}$$

b) The mass burned in the unburned zone due to the chemical kinetic reactions of the unburned gas auto ignition:

$$x_{autoignition} = \sum_{i=1}^{a}\sum_{j=1}^{n} m_u \Delta x_{i,u,j} \Delta t \tag{5.28}$$

Where:

Δt = calculation time step

j = step number

i = species number where 1 = fuel, 2 = O_2, 3 = N_2

5.4.2 Chemical kinetics mechanism & numerical solver

A reduced PRF mechanism was used together with the combustion model to represent the chemical kinetics mechanism of the gasoline fuel. The mechanism consists of 73 species and 296 reactions. It is based on the detailed Lawrence Livermore National Laboratory (LLNL) mechanisms. The reaction pathways reduced the n-C_7H_{16} and i-C_8H_{18}

mechanisms and followed the general pathways of Curran *et al.* [74], [75]. In ensuring the predictive capability and the possibility to be used for other fuels, the major reaction pathways of the detailed mechanism were predominantly maintained in the reduced mechanism.

The reduced mechanism can predict the ignition timings, laminar flame speeds, and important species concentrations under different validation conditions and are able to show a reliable performance for different engine validation conditions [76]. Thus, it can provide reliable forecasts for PRF, gasoline or diesel surrogate combustion simulations. By understanding the in-cylinder processes, it assists as a guidance to design better engines.

An in-house MATLAB code referred to as LUCKS2 (Loughborough University Chemical Kinetics Simulation 2) has been used to simulate the combustion systems with chemical kinetics. This code is based on a numerical model [77] and the updated version of the first LUCKS model [73]. The code was designed to solve the first order ODEs describing the combustion processes in engines.

MATLAB provides the core platform of the engine modelling. Cantera supplies the chemical kinetic input data. Explanation about the software could be found in section 5.0. One MATLAB input data file is used to select parameters, such as the geometrical properties of the engine as well as the engine speed, compression ratio, spark timing and valve timing.

5.4.3 Model Validation & Knock Identification

In analysing the combustion model performance, the simulation output was validated against the non-knocking cycle and knocking cycle. The in-cylinder pressure from the experiment work has been compared with the one produced from the simulation. This method of comparing the in-cylinder pressure performance is commonly used to identify knocking via a numerical analysis. Listed below are a few other methods of knocking identification, which are currently being implemented in the industry and research works:

- In-cylinder pressure analysis: Pressure fluctuation and sharp pressure rise [78]
- Engine block vibration analysis [27]

- Exhaust gas temperature: It is observed that there is a clear correlation between engines knocks and the exhaust gas temperature. In knocking combustion conditions, the exhaust gas temperature was shown to be reduced [27]
- Intermediate radicals & species analysis [27]
- Heat release analysis [79]

5.4.1 Non-knocking cycle

The combustion model was validated using the same method as in work done by Zhen Liu [73] since this model used the same principal as in his work. The combustion model was first validated by comparing the simulation and experimental data from Rover K-series engine (refer subsection 4.3 for the engine details) at no knocking condition. If the engine operates without knocking, the combustion kinetics employed in the model will be dominated by the low temperature reactions, and thus no auto-ignition occurs. Figure 5.13 shows the comparison between the simulated and measured in-cylinder pressure at a no engine knocking condition. Figure 5.14 shows the calculated burned mass fraction values without autoignition. The measured in-cylinder pressure was averaged over 50 cycles at wide open throttle condition with a speed of 2500 rpm, a spark timing of 20 °CA BTDC, and AFR of 14.3:1.

The same engine conditions were used in the model to replicate the real engine. The calculated in-cylinder pressure agrees well with the measured result with percentage error of 2 %. It shows that the model has the capability to reflect the non-knocking operation condition very well. However, the compression and combustion phases (please refer to the blue and red lines) were slightly under predicted while the expansion phase (please refer to the orange line) was slightly over predicted. The difference between experimental and simulated data can be due to several reasons. One reason that might contribute to this is the estimation of Wiebe parameters. Despite the difference, it is important to note that the overall trend of the pressure traces is very similar.

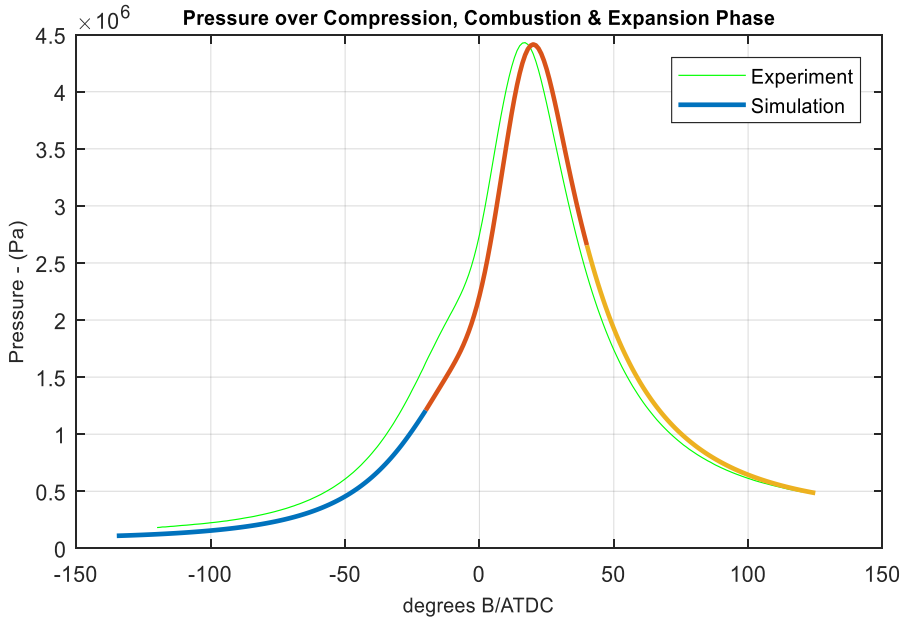

Figure 5-13 Non-knocking cycle. (Speed: 2500rpm, Spark timing: 20° BTDC).

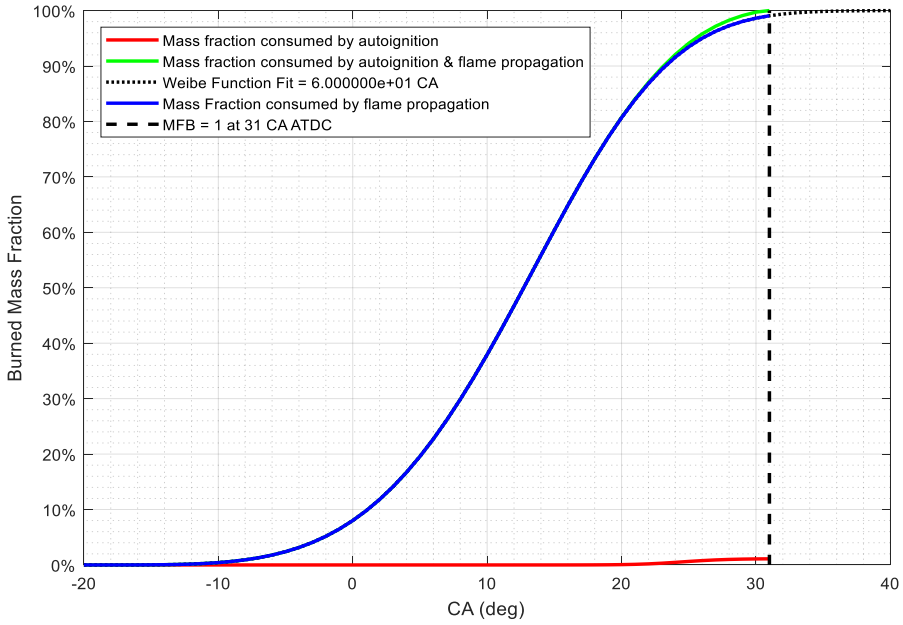

Figure 5-14 Burned mass fraction during no knocking condition

5.4.2 Knocking cycle

In order to validate the model prediction of knock characteristics based on its knock intensity, knock onset, and peak pressure, the simulation results of these characteristics are compared with the average value of the experimental data of the knocking cycles. Figures 5.15 illustrates the comparison between the peak pressure of simulated and average of 50 measured cycles. The engine test condition was set at an engine speed of 3000 rpm, a spark timing of 32 °CA BTDC, and AFR of 14.3:1, at WOT. The model data

agree well with the average experimental data with a percentage error of 7.8 %. The average measured peak pressure is 82.5 bar while the calculated peak pressure is 76.0 bar. Figure 5.16 shows the calculated burned mass fraction with and without autoignition. It can be seen that when autoignition occurs in the unburned region, the burned mass fraction suddenly accelerates due to the autoignition. The mass fraction consumed by flame propagation and autoignition has shorten the overall combustion duration than the one defined by the Weibe function.

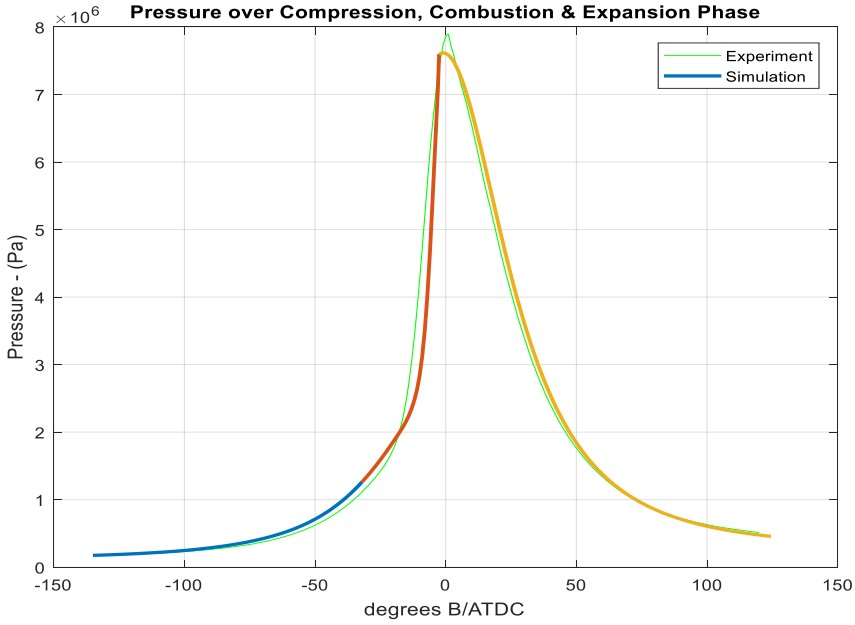

Figure 5-15 Knocking cycle (Speed: 3000 rpm, Spark timing: 32 °BTDC).

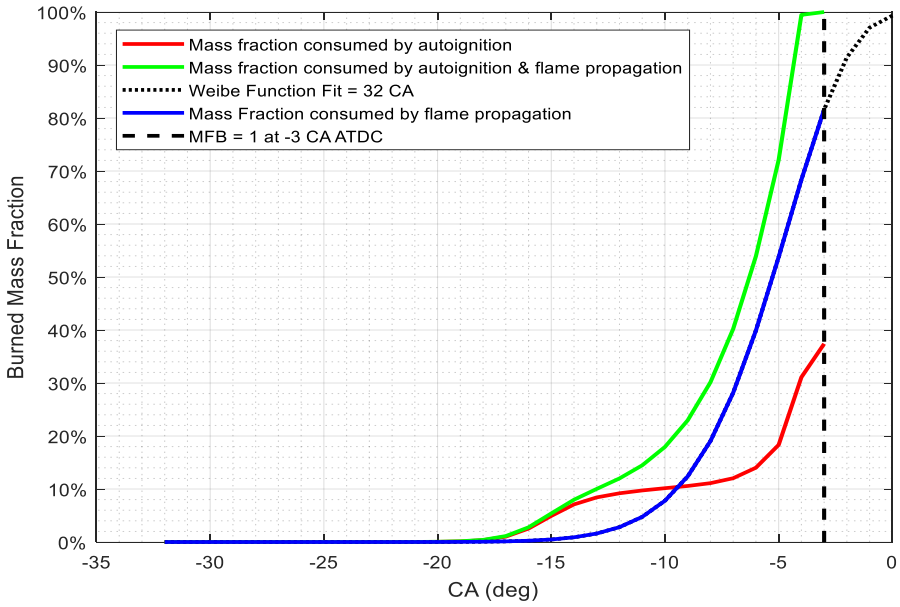

Figure 5-16 Burned mass fraction during knocking condition

Figure 5.17 illustrates the peak pressure of the values measured from 50 cycles. The difference of the measured cycle data is attributed to the significant cycle-to-cycle variation under knocking conditions. The measured values were averaged over the 50 cycles (please refer to Figure 5.18) and compared with the simulation result.

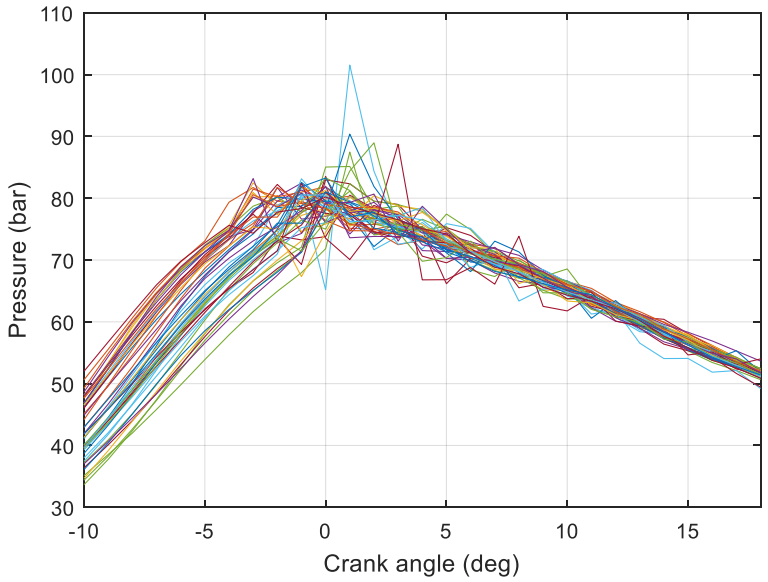

Figure 5-17 Maximum in-cylinder pressure measured from 50 cycles.

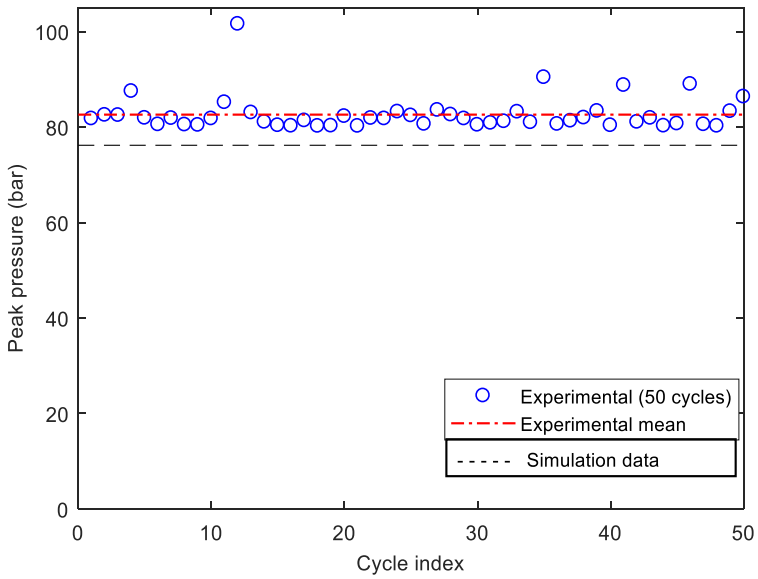

Figure 5-18 Peak pressure comparison between experiment and simulation

The same method as the peak pressure was applied to validate the model prediction of knock characteristics based on its knock intensity and knock onset. The knocking level is evaluated based on its intensity which is defined as the maximum amplitude of pressure increase rate. Figure 5.19 shows the measured knock intensity from 50 cycles while

Figure 5.20 compares the experimental mean with the simulation result. The model knock intensity was at 8.1 bar/CA while experimental knock intensity was recorded at 7.65 bar/CA, so the percentage error is 5.9 %.

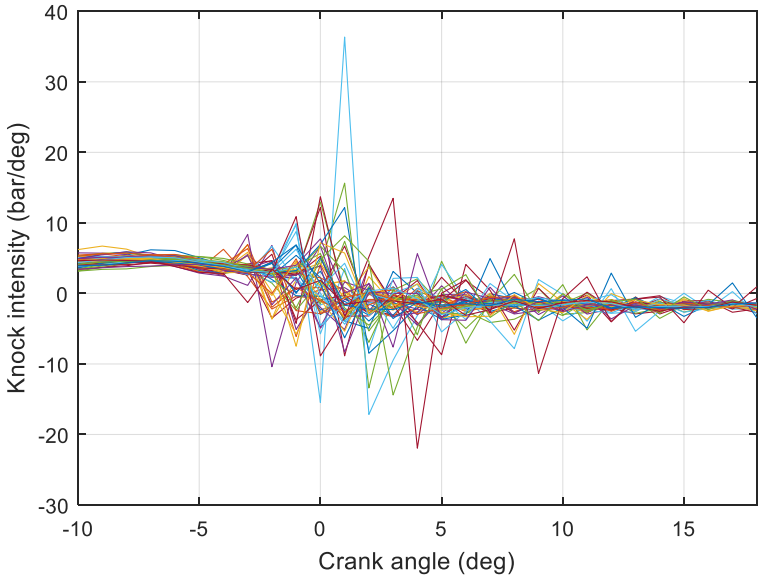

Figure 5-19 Knock intensity measured from 50 cycles

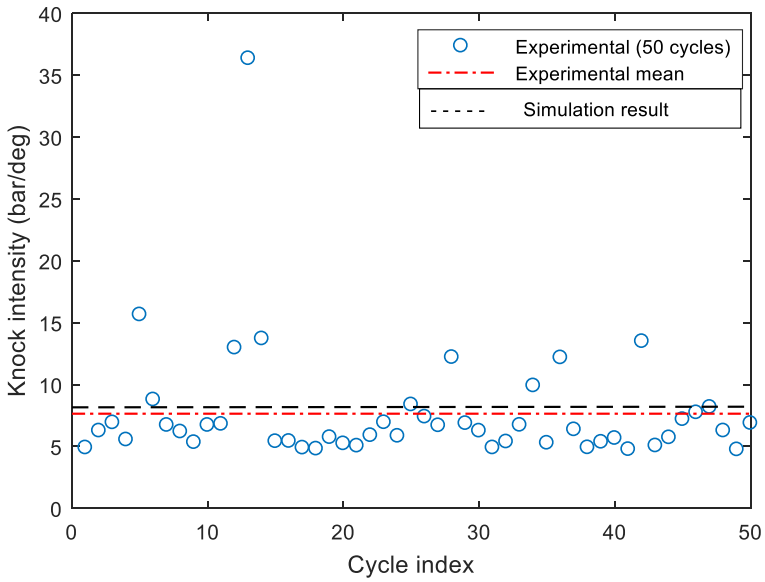

Figure 5-20 Knock intensity comparison between experiment and simulation

One method used for the knock onset detection is known as threshold value exceeded (TVE) method, in which the first crank angle where the band-pass filtered pressure signal exceeds a predetermined threshold is defined as the knock onset. The threshold is set so as to exclude all signals that indicate normal combustion and pass only high amplitude peaks that indicate the presence of detonation in the engine [79]. The knock onset position

is identified by calculating the pressure slope change rate, K across every three adjacent values on the pressure curve [68]. A threshold value of 30 bar/CA^2 corresponds well with the knock occurrence in the experimental work. The cycles with the value of K over than this criterion were counted as knocking cycles. The first crank angle where K is greater than this value is taken as knock onset point. Model knock onset is at -3 CA BTDC while the experimental mean is at - 1.4 CA BTDC with a percentage error of 4 % over one cycle (please refer to Figure 5.21 and Figure 5.22).

$$K = \frac{(p_n - p_{n-1})/\Delta\theta - (p_{n+1} - p_n)/\Delta\theta}{\Delta\theta} \tag{5.29}$$

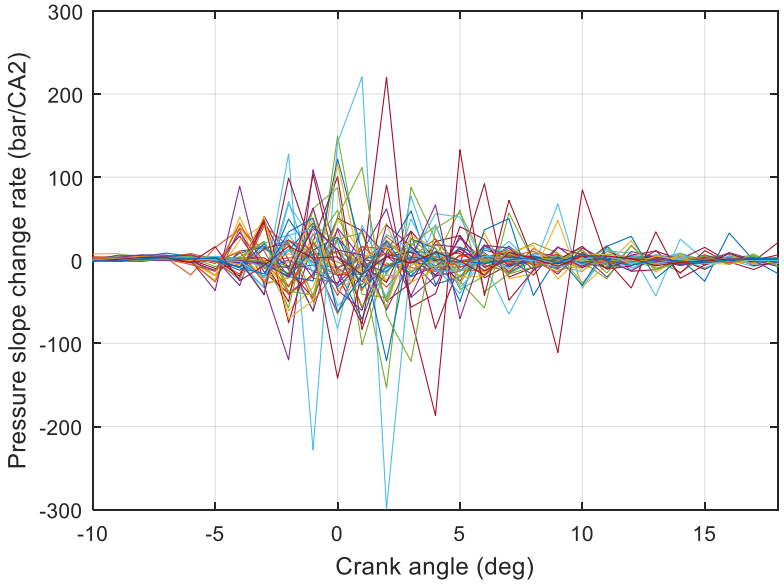

Figure 5-21 Knock onset measured from 50 cycles

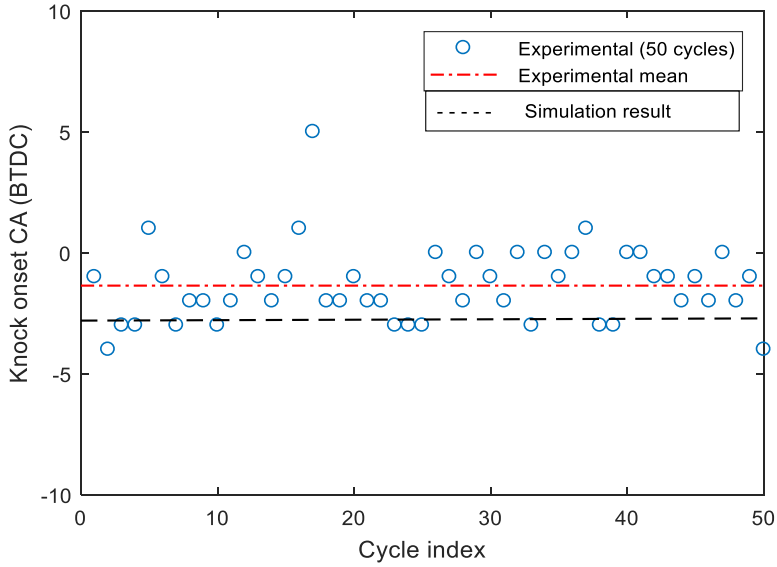

Figure 5-22 Knock onset comparison between experiment and simulation

Knock detection based on radical species

Commonly in experiments, the knock evaluation is conducted on the basis of the in-cylinder pressure analysis. However, for the modelling case with the mathematical model, it is impossible to simulate the pressure oscillating variation with time with a knock. Knock detection based on the radical species analysis has been proven to be convenient and reliable to predict the auto-ignition occurrence because of high sensitivity reaction rates on certain species during the knock process.

The OH species reaction intensity is higher during the knocking combustion, which made it possible for this category to become the major species in the combustion chamber during the knocking phase [80]–[82]. The knock onset and intensity of the model are evaluated based on this OH radical data. The knock intensity can be related to the OH species reaction rate as it will become higher than other species during the knocking combustion [82]. Figure 5.23 shows the model knock onset based on OH species. During the no knocking condition, there is no OH species mass fraction fluctuation at all. For the knocking condition, the OH species mass fraction suddenly shoots up. The OH species crank angle is exactly the same with the knock onset crank angle calculated based on the pressure slope as shown in previous section. This method is used as another way to identify knock characteristics in this work.

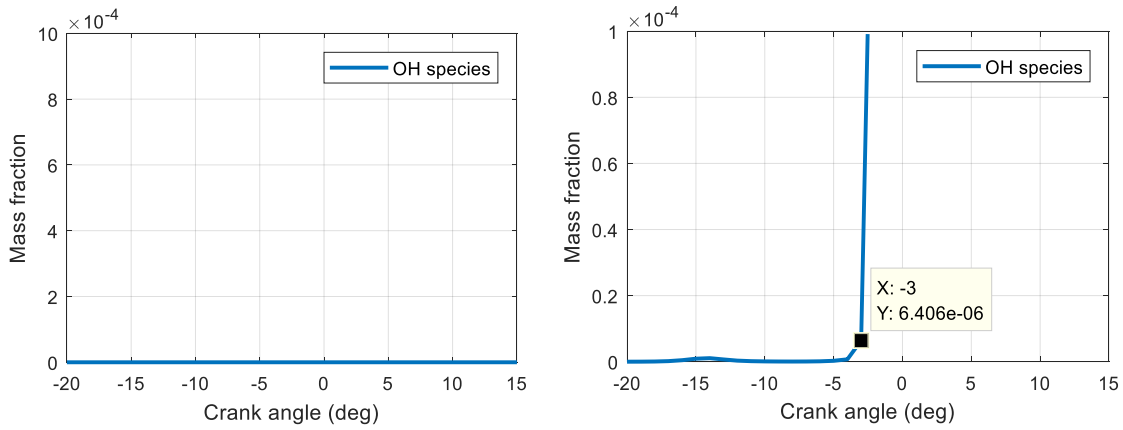

(i) No knocking (ii) Knocking

Figure 5-23 Knock onset detection based on OH radical species

5.5 Co-simulation

Once the validation for the combustion kinetics and knock model had been completed, the combustion model was combined with the downsized engine model. The combustion model in MATLAB was integrated with the single-cylinder engine model in Ricardo-WAVE using Simulink as the common platform. The engine model will provide data during the gas exchange process and then the information will be used in order to simulate the combustion process in the combustion model.

WAVE allows for co-simulation with Simulink models for various purposes, including:

- Engine plant modelling: WAVE is the plant model and the control system resides within Simulink
- Generic system interaction: WAVE is the engine system and other physical systems are modelled in Simulink
- Hub and spoke co-simulation: Simulink acts as a co-simulation hub, allowing data to be passed from WAVE to other modelling tools

Figure 5.24 shows the flow of the co-simulation process used in this study. The simulation starts by setting the valves timing in a single-cylinder downsized engine model in Ricardo-WAVE in order to simulate the gas dynamics process. Temperature, pressure and crank angle values are sent to MATLAB-Simulink at the intake valve closing (IVC) point. A three-zone combustion model with chemical kinetics is used in order to evaluate the combustion process of the SI engine. The temperature, pressure and species reactions from the simulation are used to evaluate the knocking phenomenon.

Figure 5.25 shows the layout of the co-simulation between the two software applications in Ricardo WAVE interface. A Wiring Connector element in Ricardo WAVE was used to enable signals to pass in and out of WAVE to SIMULINK. There are five connecting points in the wiring connector component. Three points are for temperature, pressure and crank angle data from Ricardo WAVE to SIMULINK. Another two are for valve lift and opening duration which are set in SIMULINK then send to Ricardo WAVE. Simulink can only control Case #1 of a WAVE model, so this is a single-case model.

Figure 5.26 illustrates the co-simulation layout in SIMULINK program. There are seven main sections which had been developed to analyse the data from Ricardo WAVE and then send to the combustion model. The chronology of the program is as below:

1. The valve opening duration and lift constants are set in SIMULINK. When the programme is running, the data are send to Ricardo WAVE for the engine model to run accordingly.
2. The intake valve closing (IVC) point in Ricardo WAVE is set to match with IVC set in SIMULINK.
3. Temperature, pressure at the IVC point are acquired from Ricardo WAVE.
4. The temperature and pressure at IVC are summed up from every cycle.
5. The cycle total number is summed up together.
6. Average values of the temperature and pressure are calculated by dividing them with the number of cycle.
7. The average values are then sent to the combustion model with the chemical kinetics.

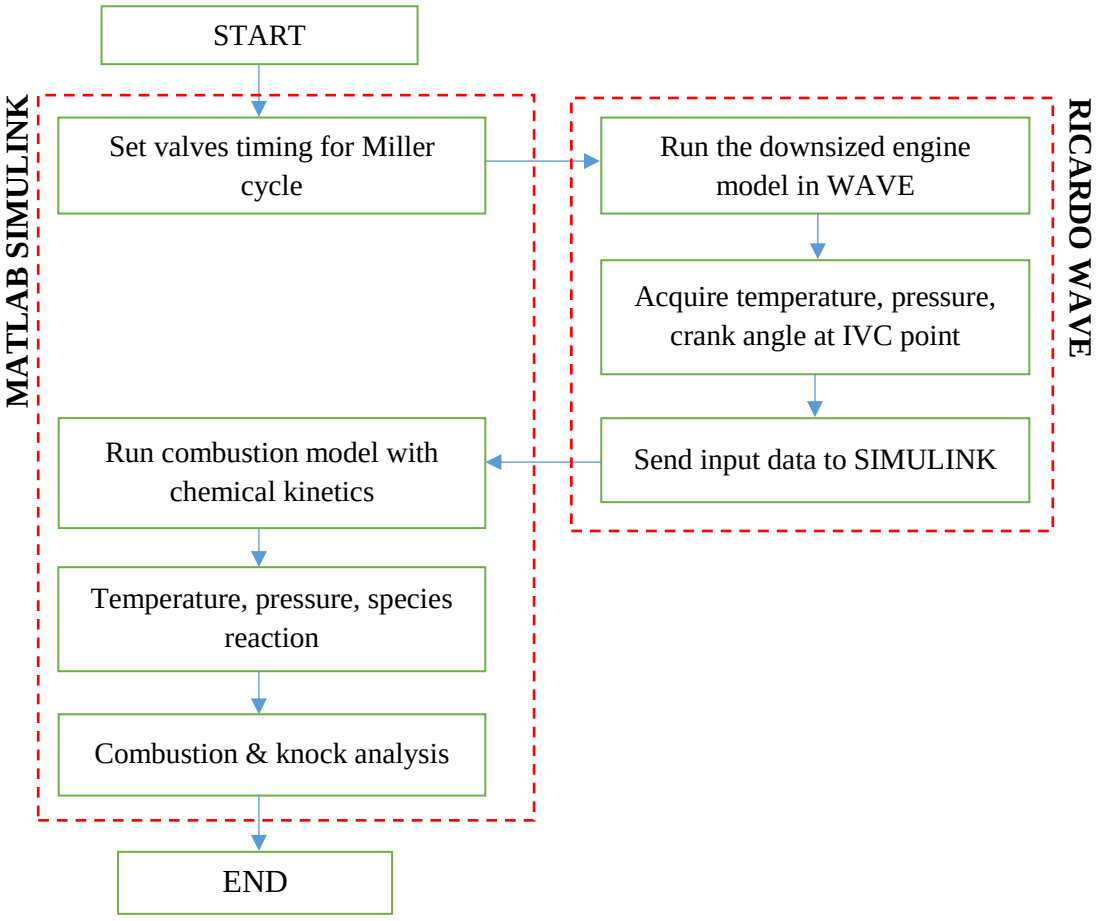

Figure 5-24 Structure of the co-simulation program

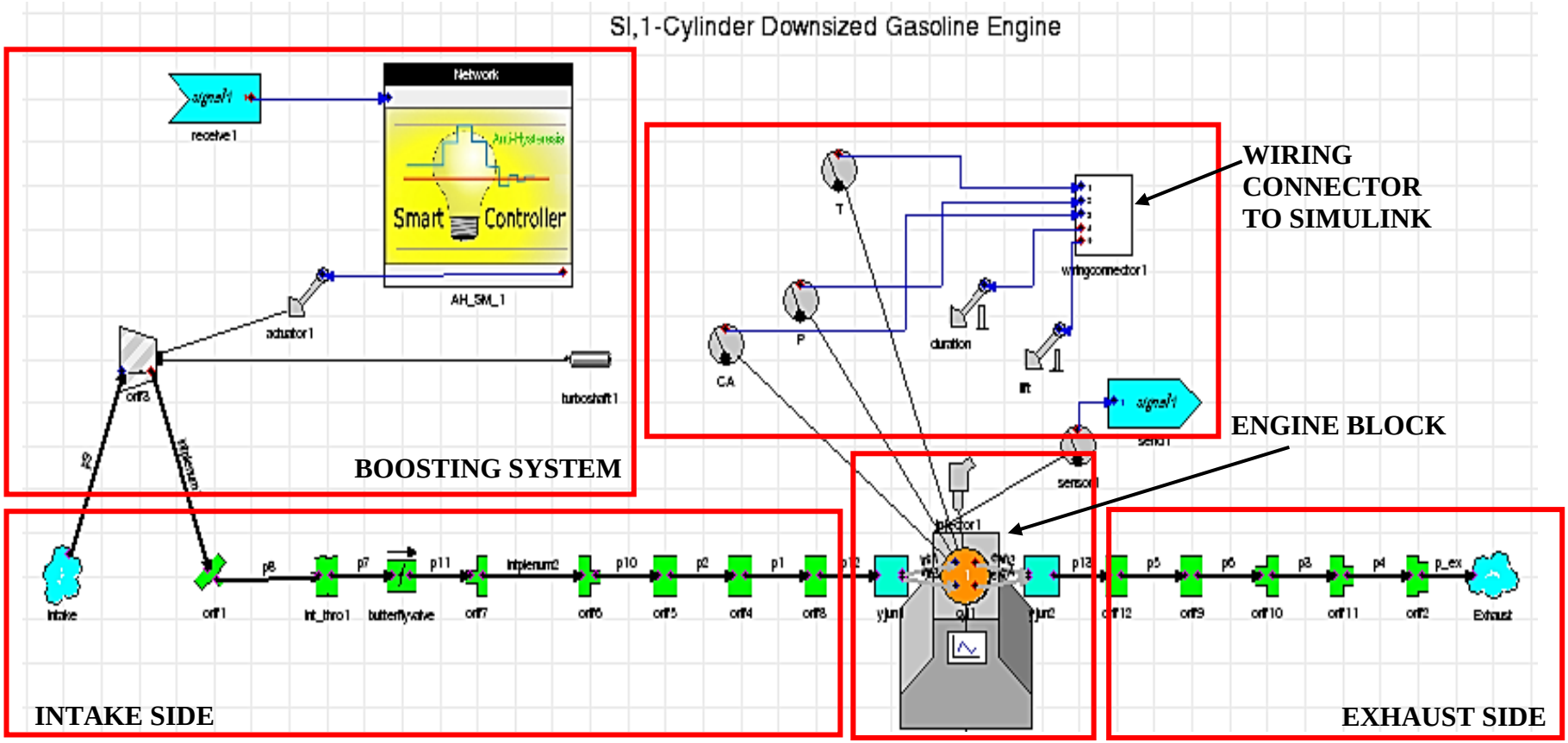

Figure 5-25 Co-simulation of WAVE engine model via wiring connector element

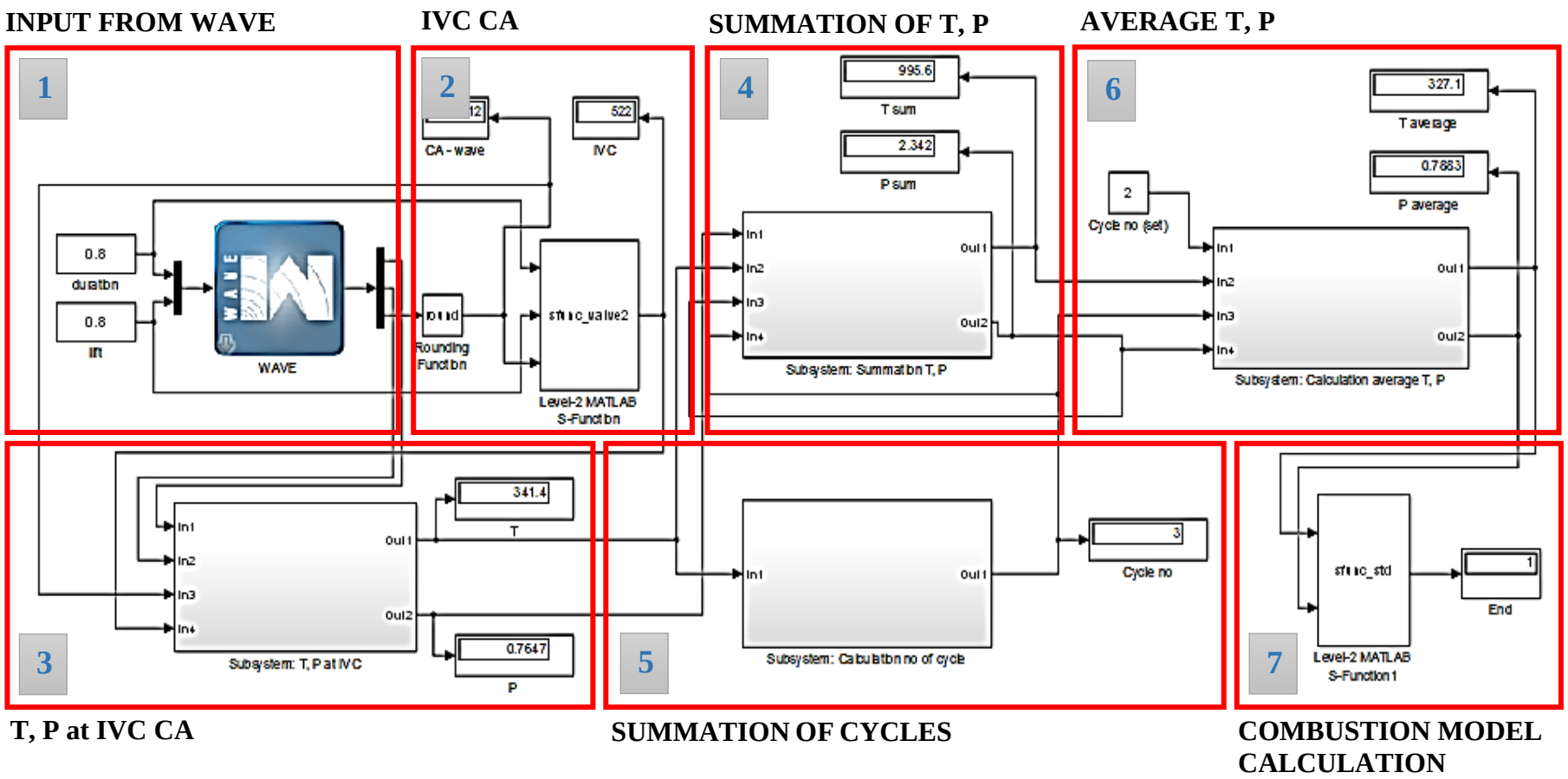

Figure 5-26 Simulink layout for the co-simulation

5.6 Summary

This chapter has presented the engine model and model validation related to the project. A naturally aspirated engine model has been developed to serve as the baseline engine. Then, a boosting system was added to represent a downsized engine model. A combustion kinetics and knock model was used to investigate the knocking behaviour in detail. All models were validated with the experimental results in order to ensure the accuracy of the model. The next chapter will discuss how the Miller cycle is simulated and how the analysis of the results will be conducted.

Chapter 6

RESULT & DISCUSSION I: MILLER CYCLE – KNOCK SUPPRESSION

6.0 Overview

This chapter discusses the Miller cycle effects on suppressing the knocking phenomenon based on the following questions: (1) How does the Miller cycle perform in comparison with other engine cycles? (2) Do the EIVC & LIVC react differently at different engine speeds and different engine loads (low, medium, high)? and (3) How does the Miller cycle strategy with the EIVC & LIVC profiles influence the knocking under downsized engine conditions?

The results and analysis will be divided into 3 main parts:

Part 1: Miller cycle at different speed-load

Part 2: Knock suppression with extreme Miller cycle

Part 3: Knock analysis with combustion kinetic

Miller Cycle VS Otto, Diesel, Dual Cycles

First, the Miller cycle potential has been accessed in comparison with other cycles (Otto, Diesel, Dual, Atkinson). The thermodynamics engine cycles' calculations were developed using the MATLAB software application in order to analyse the theoretical efficiency that can be reached by each cycle. The discussion uses the compression ratio as an indicator to evaluate the effect of the valve profiles on the engine performance. The compression ratio falls under two categories, namely the geometric compression ratio (GCR) and the geometric effective compression ratio (GECR).

The GCR is the ratio of the maximum volume (volume at BDC) to the minimum volume (volume at TDC) in a cylinder, as illustrated in Figure 6.1. The GCR indicates the utmost limit of the engine's capacity. The GECR is the ratio of cylinder volume at the intake valve closing (IVC) point to the minimum volume in the engine's cylinder. The IVC

indicates the end of the intake stroke and the start of the compression stroke. The equations used to evaluate the GCR and GECR are expressed as below [47]:

a. Geometric compression ratio

$$GCR = \frac{V_d + V_c}{V_c} = \frac{V_{BDC}}{V_{TDC}} \tag{6.1}$$

b. Geometric effective compression ratio

$$GECR = \frac{V_{ivc}}{V_c} \tag{6.2}$$

Where:

$$V_{ivc} = V_c + \frac{\pi B^2}{4}(l + a - s) \tag{6.3}$$

$$s = a\cos\theta + \left(l^2 - a^2 \sin^2\theta\right)^{1/2} \tag{6.4}$$

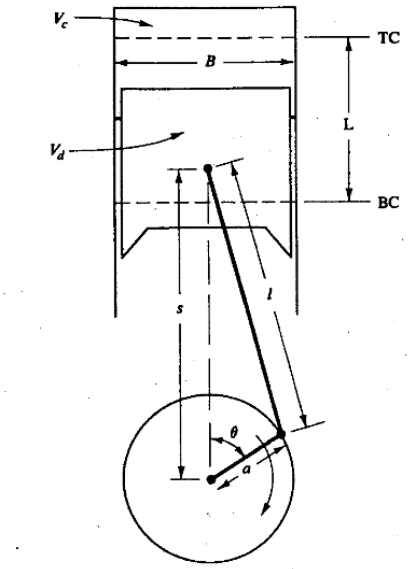

Figure 6-1 Cylinder geometry [47]

In an ideal Otto cycle, the expansion and compression stroke are the same. However, the GCR is limited for the spark-ignition gasoline engine due to the engine knocking phenomenon. Hence, the expansion ratio, which has influenced the thermal efficiency, is limited to the maximum allowable compression ratio. The Miller cycle dissociates the GCR from the expansion ratio by utilising the variable valve train technology. The Miller cycle reduces the compression ratio while maintaining the full expansion ratio through the early or late intake valve closing. It reduces the pressure and temperature at the end

of the compression stroke [83]. This results from the lower GECR and in-cylinder temperature at the intake valve closing.

Therefore, the main advantages derived from this setting are the reduction of the knock tendency and the increase of GCR in order to achieve higher efficiency [84]. Thus, understanding the effects of the GECR on the gas motion during the compression stroke is vital in order to ensure that a perfect combustion process can be achieved afterwards.

The thermal efficiency formula of the Otto cycle illustrated below shows that, theoretically, the compression ratio (R_c) is the main variable that affects the efficiency:

Indicated efficiency:

$$\eta_{Otto} = 1 - R_c^{1-\gamma} \tag{6.5}$$

Thus, raising it to the maximum value will provide extra benefit to the performance, but this is limited by the engine knock. The Miller cycle is based on the Otto cycle, but it has an expansion stroke longer than the compression stroke. The Miller cycle with full expansion stroke until it reaches the atmospheric pressure is known as the Atkinson cycle [45], [85]. A more detailed explanation about the cycles could be found in Chapter Three.

Figure 6.2 shows the comparison of various cycles' efficiency percentage (normalised as a value of 1) calculated across different GCR values. The Otto and Miller cycles are also evaluated with boosted intake pressure in order to represent the downsized engine environment. The boosting system is added to gain more power to achieve the same capability as a bigger size engine. A detailed representation of the formula for the cycles could be found in Appendix C.

The parameters for each cycle are maintained the same at 1000 rpm with an AFR of 14.7:1. The Miller cycle was calculated with a GECR value of 20 % less than the full expansion ratio. The supercharger was calculated with 75 % compressor efficiency and a pressure ratio of 2.5. From the graph, the efficiency increments between different cycles are quite significant for compression ratios from 5 to 15. As the GCR becomes higher, the efficiency gained between different cycles is smaller than the lower GCR values. Thus, utilising the right cycle to get the most efficiency for the desired engine operation based on the compression ratio is important.

The supercharged Miller cycle has shown that it has the highest efficiency across the different compression ratios in comparison with the supercharged Otto, Atkinson, Miller, Dual, Diesel and Otto cycles. The efficiency is increasing as the compression ratio is increasing. A project in [46] also conducted an evaluation on an air-standard Miller cycle model and found that the efficiency of the Miller cycle increases with the increasing compression ratio.

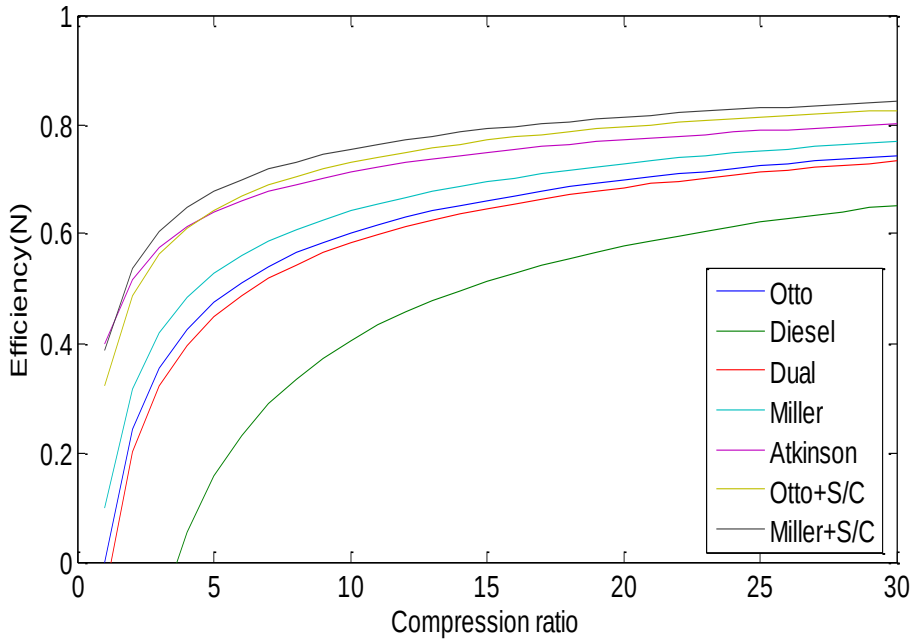

Figure 6-2 Comparison of various cycles' efficiency

Figure 6.3 below illustrates the efficiency percentage (normalised as a value of 1) gained at a compression ratio of 10. The cycles' capability was evaluated in comparison with each other. Diesel and dual cycles are having the lowest efficiency values for the given compression ratio value of 10. The supercharged Miller (Miller+S/C) cycle gained 11.2 % more efficiency in comparison with its naturally-aspirated Miller cycle counterpart and gained 15.3 % more in comparison with the naturally-aspirated Otto cycle. More efficiency can be gained by implementing the Miller cycle strategy if the expansion-compression ratio value and pressure ratio of the boosting system are increased. The analysis from this air-standard Miller cycle demonstrated that the Miller cycle is more efficient than the Otto cycle. For this reason, the Miller cycle has been chosen as the more effective strategy to be used in the engine, as compared to other cycles.

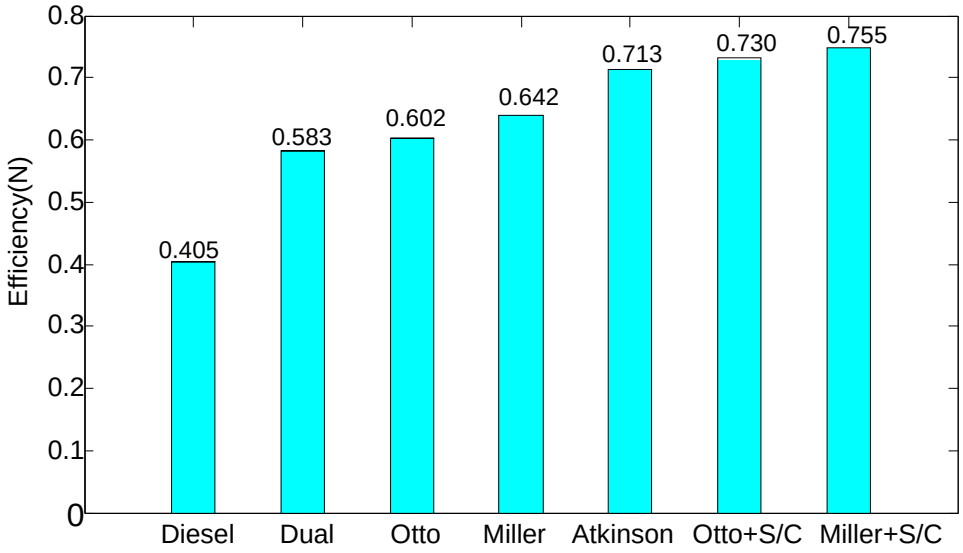

Figure 6-3 Efficiency gained at a compression ratio of 10

6.1 Part 1: Miller Cycle at Different Speed-load

The engine performance has been tested using the Miller cycle based on the test matrix, as illustrated in Figure 6.4. The test points were selected by varying the engine speeds from 1000 to 5000 rpm. The loads were tested under three different conditions: low load (6 bar BMEP), medium load (12 bar BMEP) and high load (18 bar BMEP). The air-fuel ratio is fixed at a stoichiometric value of 14.7:1. All test points were tested using standard valve timing, early intake valve closing (EIVC) and late intake valve closing (LIVC).

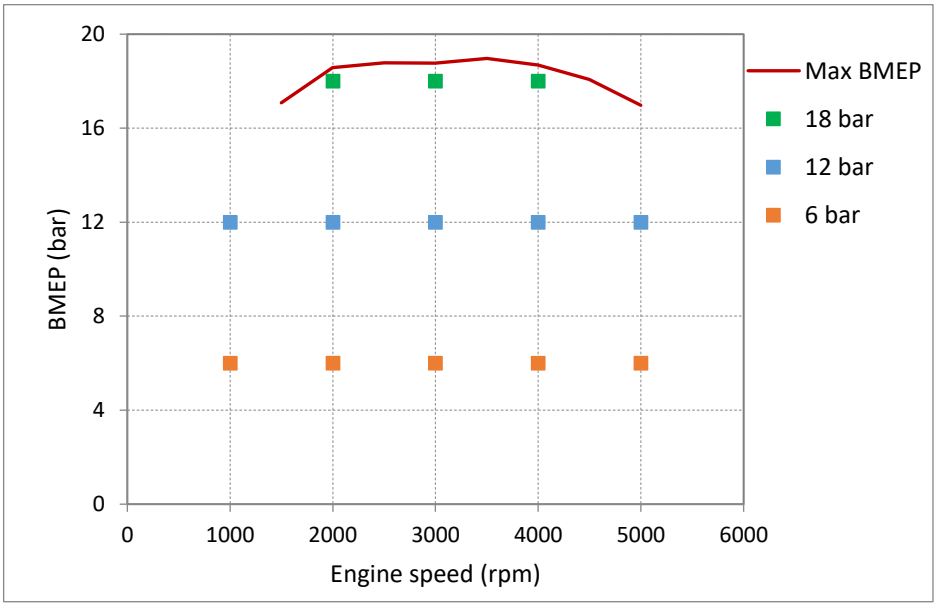

Figure 6-4 Testing points

Figure 6.5 shows the different intake valve closings tested with the EIVC at 10 % less than the standard timing, and LIVC at 10 % more than the standard timing. Only the value of constant IVC was changed, as indicated in Table 6.1, while the other parameters remained constant in order to minimise their influence on the results. Changing the IVC to EIVC means that the duration was shortened, while for the LIVC, the duration was longer than the standard IVC. The difference between each constant is 24 °CA. The lift value for all valve timings is kept constant at 9.35 mm.

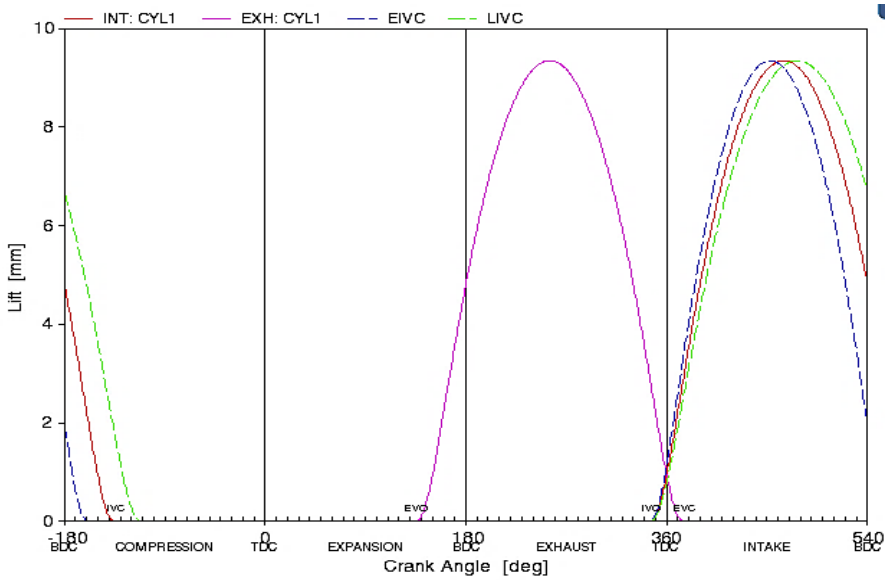

Figure 6-5 Valve profiles

Table 6-1 Variation of IVC timing

No	Profile	IVC (CA)	IVC Constant	Duration (CA)
1	EIVC	21 °ABDC	0.9	216
2	Standard	45 °ABDC	1.0	240
3	LIVC	69 °ABDC	1.1	264

6.1.1 EIVC vs LIVC at low load

The result evaluation commences with the Miller cycle strategy tested at the low load condition. Commonly, the intake valve will remain open until 50 – 70 °ABDC in order to induce more air into the cylinder. In our case, the standard IVC is at 45 °ABDC. Figure

6.6 shows the value of the GECR based on the IVC points that have been tested. From the graph, we can observe that the GECR for the EIVC profiles are almost the same as the GCR. In this case, when the intake duration was shortened by 10 %, as compared to the standard profile, the valves closed near to the maximum cylinder volume at BDC. While for the LIVC profiles, when the intake duration was lengthened, the valves closed when the piston was going upward and the GECR value in this case became smaller than the GCR.

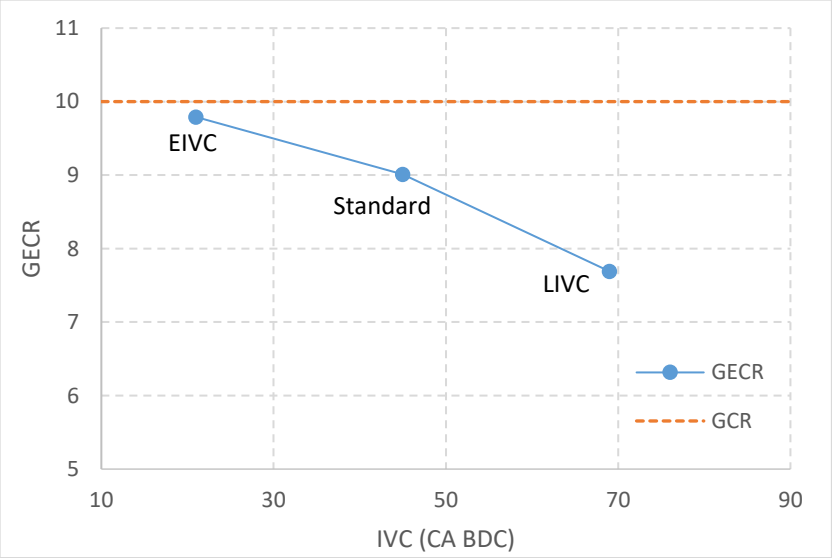

Figure 6-6 The GECR vs. value of constant IVC

The Miller cycle is evaluated in terms of how it suppressed the knock based on the knock intensity, unburned zone temperature and BSFC. The knock intensity is defined as the amount of unburned mass divided by the total mass (normalised mass fraction), which is consumed by the knock event. The knock event is also indicated by the sudden jump in the unburned temperature profile during the final stage of the combustion process [86]. Another simple way to check the engine knock is to ensure that the peak pressure values are not exceeding the typical value of 75 bar for naturally aspirated gasoline engines or 85 bar if the engine is turbocharged [64].

Figure 6.7 and Figure 6.8 show the knock intensity and BSFC for the low load condition (BMEP = 6 bar). It shows that the knocking only exists at the low speed condition. At 1000 rpm, the knock intensity for LIVC is 6.8 % less than the standard profile, with 2 % less in BSFC. It is however suffering 5.7 % more in the BSFC at 2000 rpm with 12.1 % knock suppression compared to the standard profile. The EIVC has no significant

improvement in the knock intensity and the BSFC improvement is observed at all speeds in comparison to the standard profile with the exception of a slight reduction in knock intensity by 1.2 % at 2000 rpm. More fuel is consumed at higher speeds (4000 and 5000 rpm) for all three valve timings. This might be contributed by the combustion instability at the high speed condition [10].

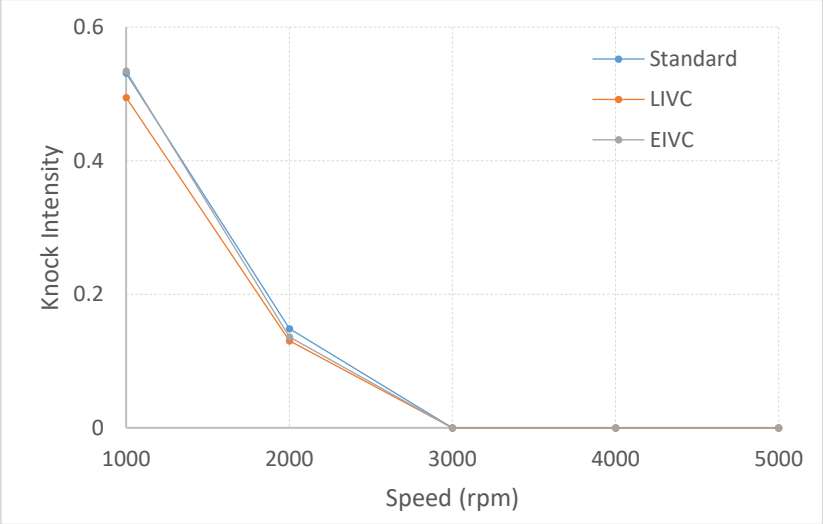

Figure 6-7 Knock intensity at low load condition

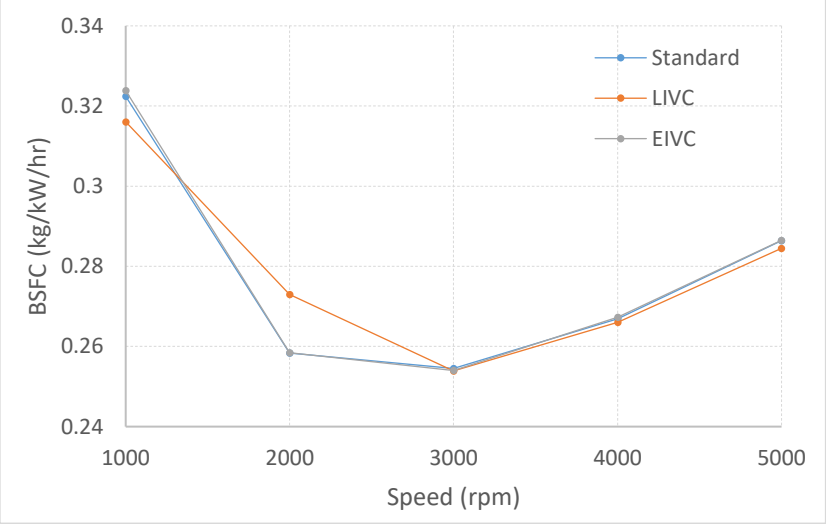

Figure 6-8 BSFC at low load condition

Figure 6.9 shows the cylinder temperature for the unburned zone for the standard profile at different speeds for the low load condition. The low speeds (from 1000 to 2000 rpm) have higher unburned temperatures where the knock occurred. A higher temperature at 1000 rpm leads to an increase in knock intensity by 38.2 % in comparison to the knock

intensity at 2000 rpm (please refer to Figure 6.7). As for higher speeds (from 3000 to 5000 rpm), the unburned zone temperatures are below 2500 K with no knock.

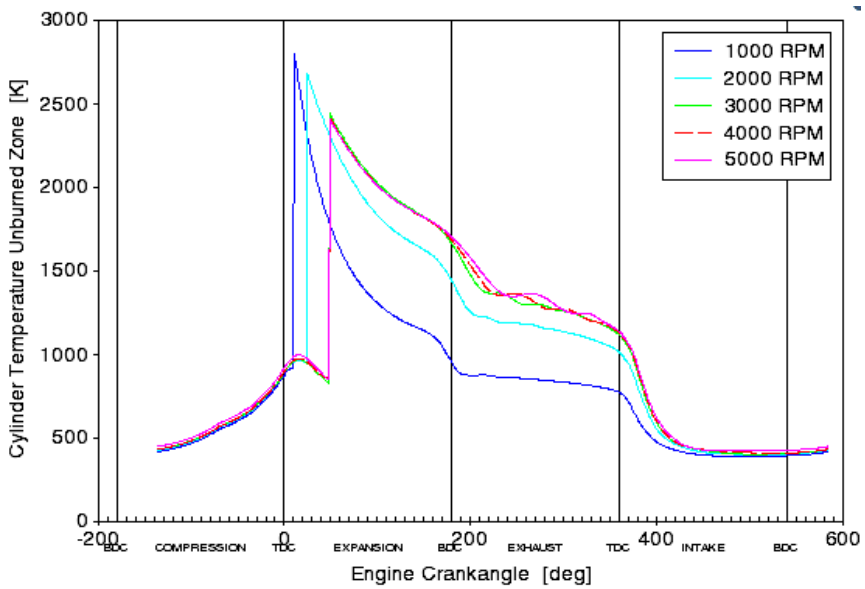

Figure 6-9 Cylinder unburned temperature for standard valve timing

6.1.2 EIVC vs LIVC at medium load

Figure 6.10 and Figure 6.11 show the knock intensity for the medium load condition with a BMEP value of 12 bar. The BSFC at 1000 rpm is significantly high as compared to other speeds. The knock intensity is about 80 % at 1000 rpm. Neither the EIVC nor the LIVC are able to suppress the knock at that speed. For speeds of 2000 – 5000 rpm, the LIVC shows an improvement in suppressing the knock and BSFC, while the EIVC does not contribute to any improvement at any speed.

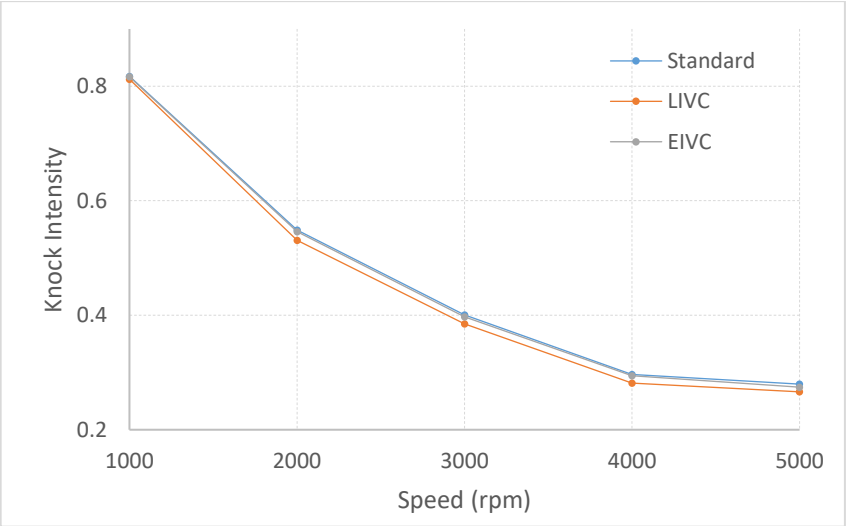

Figure 6-10 Knock intensity at medium load condition

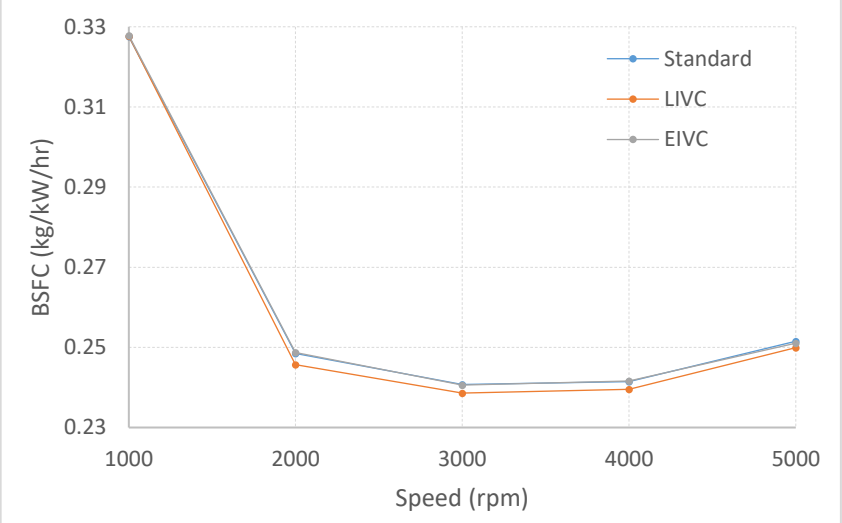

Figure 6-11 BSFC values at medium load condition

6.1.3 EIVC vs LIVC at high load

Due to the boost pressure limitation to reaching high load at lower and high speeds, the testing was performed for engine speeds ranging from 2000 to 4000 rpm only. At low speed, 2000 rpm, the LIVC performed better than the EIVC and standard profiles (Figure 6.12) in suppressing the knock. At high speed, 3000 – 4000 rpm, the EIVC outperformed the LIVC and there is no significant difference between the standard profile and the LIVC. In terms of the BSFC at high load in Figure 6.13, the EIVC has shown a better performance at all speed values compared with the LIVC profile. Figure 6.14 shows that the volumetric efficiency followed the same trend as the BSFC values.

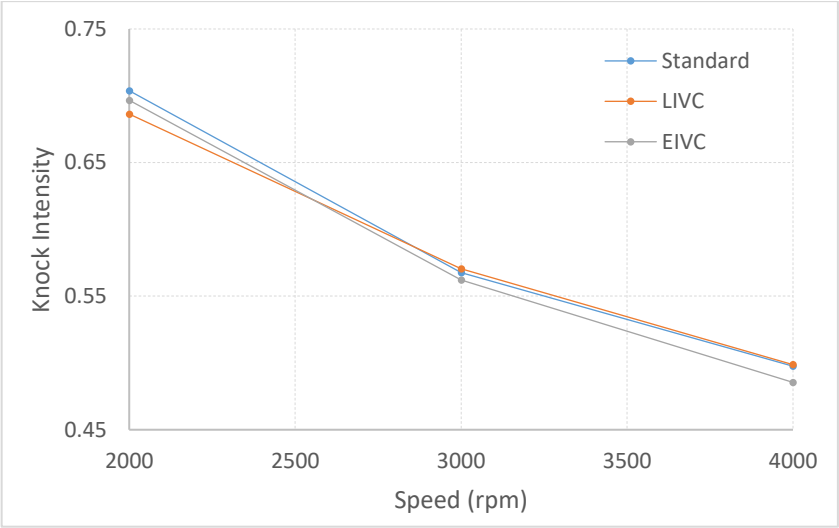

Figure 6-12 Knock intensity at high load condition

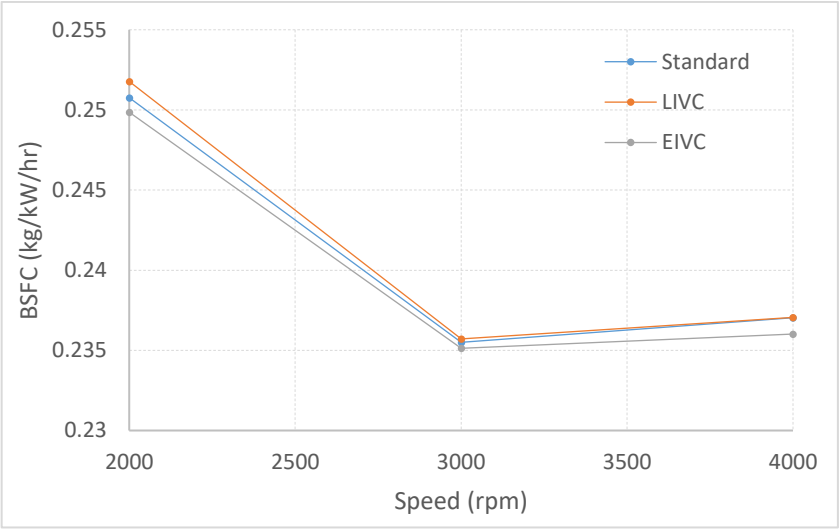

Figure 6-13 BSFC at high load condition

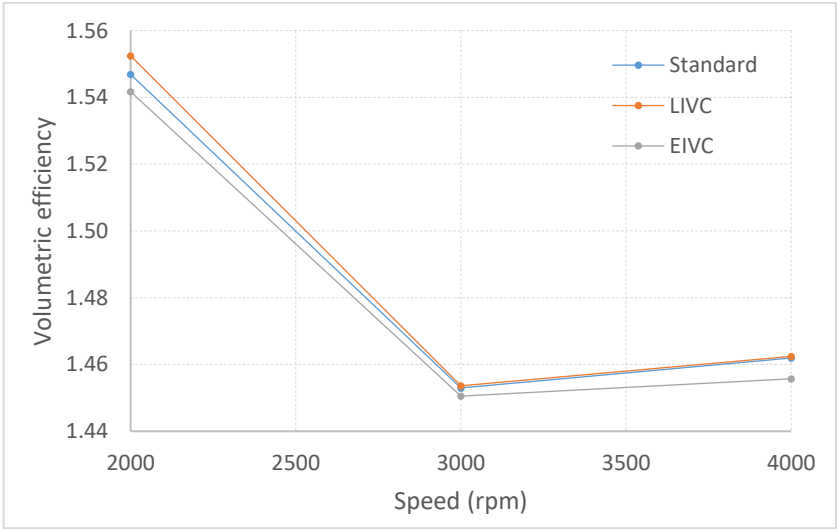

Figure 6-14 Volumetric efficiency at high load

Figure 6.15 shows the in-cylinder temperature for one complete cycle and Figure 6.16 zooms into the temperature during the compression phase near the TDC point. It can be noted that by applying the Miller cycle strategy, it is possible to lower the temperatures during the compression stroke. The LIVC is characterised by a lower temperature compared to the EIVC and standard operations. By having a lower temperature during the compression stroke, it suppresses the engine knock to a greater extent and makes it possible to benefit from better thermodynamic efficiency. The findings of project [86] also report a similar trend with our result, indicating the Miller cycle ability to lower the temperature during the compression stroke.

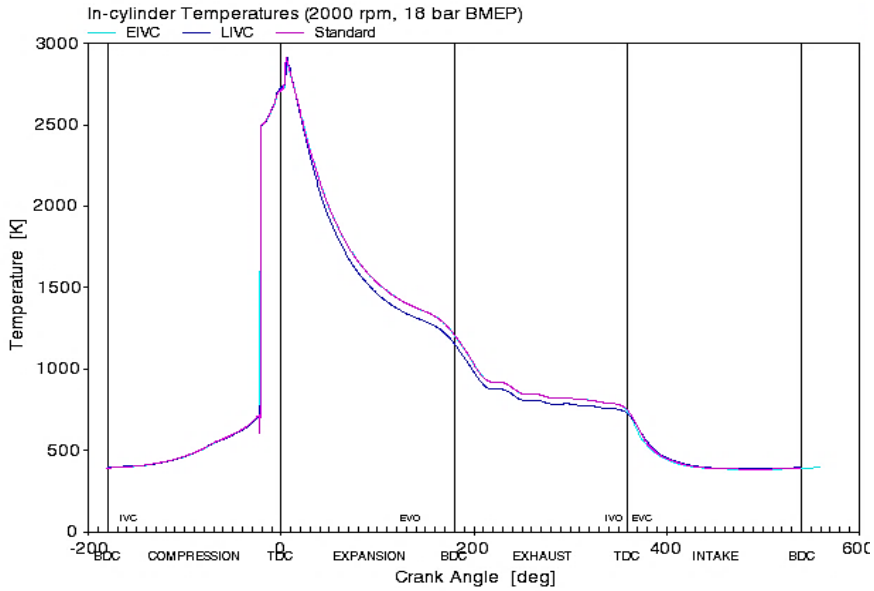

Figure 6-15 In-cylinder temperature (2000 rpm, 18 bar BMEP)

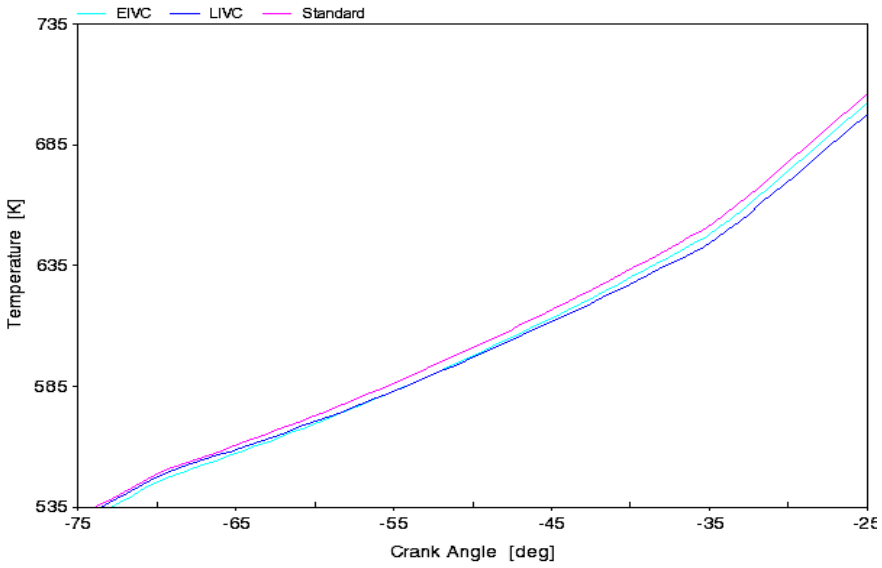

Figure 6-16 Temperature during the compression stroke

6.1.4 Summary: Comparison of EIVC vs LIVC

The results are concluded from all testing points at low, medium and high load conditions. Figure 6.17 shows the percentage difference of the knock intensity improvement between the standard and LIVC profiles, while Figure 6.18 shows the percentage difference of knock intensity improvement between the standard and EIVC profiles. By comparing both figures, it may be observed that the LIVC makes it possible to decrease knock intensity to a further extent as opposed to the EIVC for low and medium loads at all speeds. The reason why the EIVC does not yield significant improvement is because the EIVC is said to lower the turbulence in the cylinder, thus leading to slower flame propagation and may also cause poor fuel-air mixing [87].

However, at the high load condition, the EIVC is able to supress more knock intensity at 3000 and 4000 rpm, while the LIVC is characterised by higher knock intensity than the standard profile. Only at 2000 rpm has the LIVC shown better improvement compared to the EIVC. Figure 6.19 concludes the EIVC and LIVC performance at all testing points.

The results have been further analysed using the GECR factor. Referring to the GECR value, generally, the LIVC with a lower GECR value than the EIVC leads to more knock suppression. Lower GECR means a shorter compression stroke relative to the expansion stroke. This entails a reduction in temperature and pressure at the end of the compression stroke, thus making it possible to suppress knock.

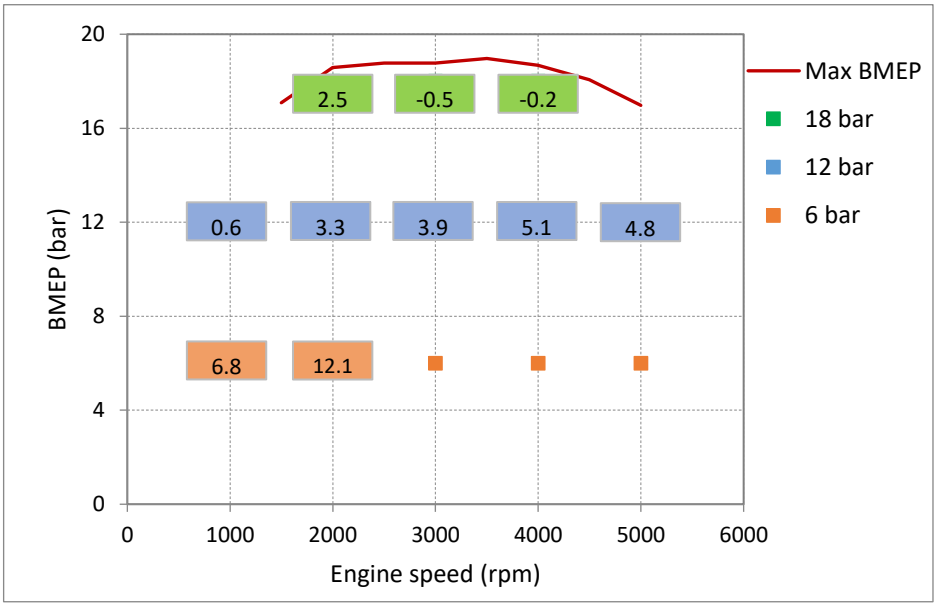

Figure 6-17 Percentage different of knock intensity: standard vs LIVC profiles

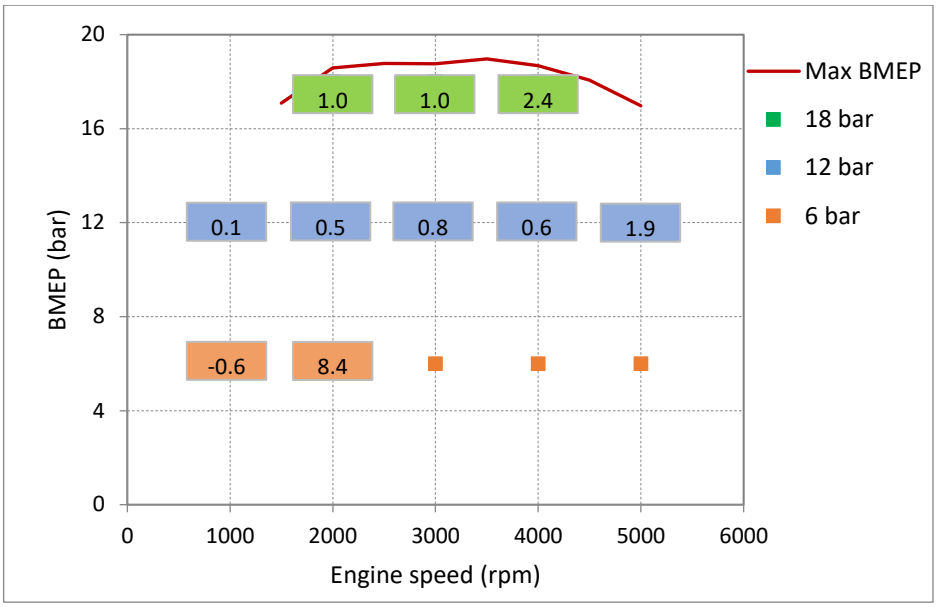

Figure 6-18 Percentage different of knock intensity: standard vs. EIVC profiles

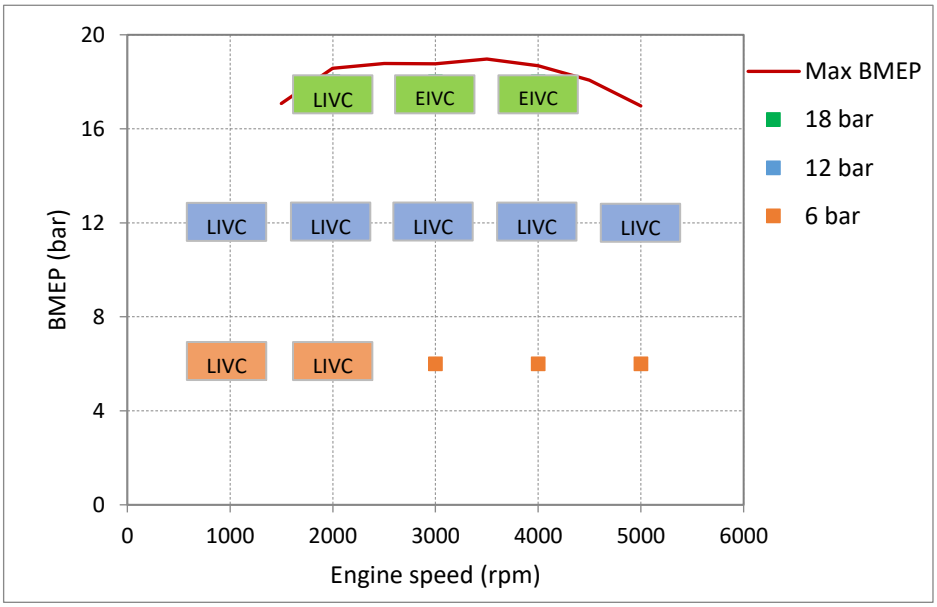

Figure 6-19 Comparison between EIVC and LIVC

6.2 Part 2: Knock Suppression with Extreme Miller Cycle

In the previous subsection, a comparison has been drawn between the EIVC and LIVC under different speed load conditions. We managed to understand that the Miller cycle behaves differently under different conditions. In this part, one operating point has been chosen and the Miller cycle valve timings have been extended to the extreme point in order to get the engine knock to be totally suppressed.

The simulation was done at an engine speed value of 1000 rpm with 6 bar BMEP using a variation in IVC timings (Figure 6.20). The IVC points cannot go beyond -100 or 100 °CA BDC, as they are not able to reach 6 bar BMEP. Figure 6.21 shows the GECR values for different EIVC and LIVC timings. The straight red line represents the standard valve closing point. The EIVC values managed to be adjusted up to 60 % from the standard IVC while maintaining the BMEP, while for the LIVC, it could go up to 20 % from the standard IVC due to the difficulty in reaching the same BMEP value.

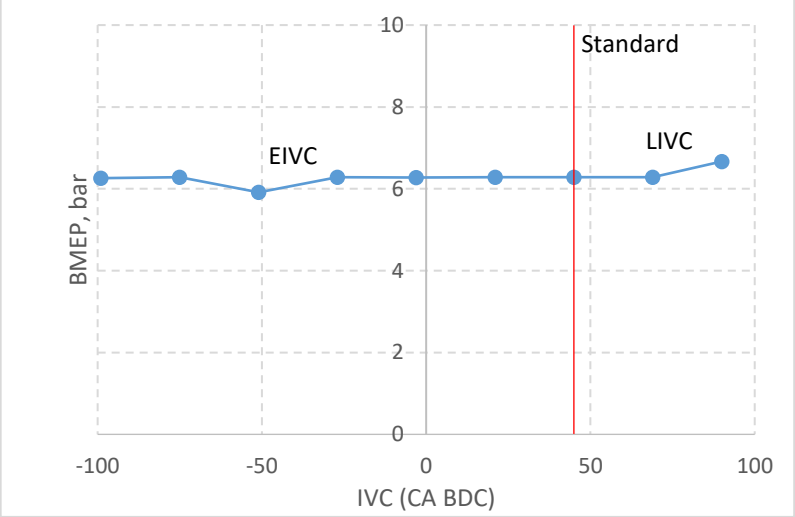

Figure 6-20 Same BMEP (6 bar) for all valve timings

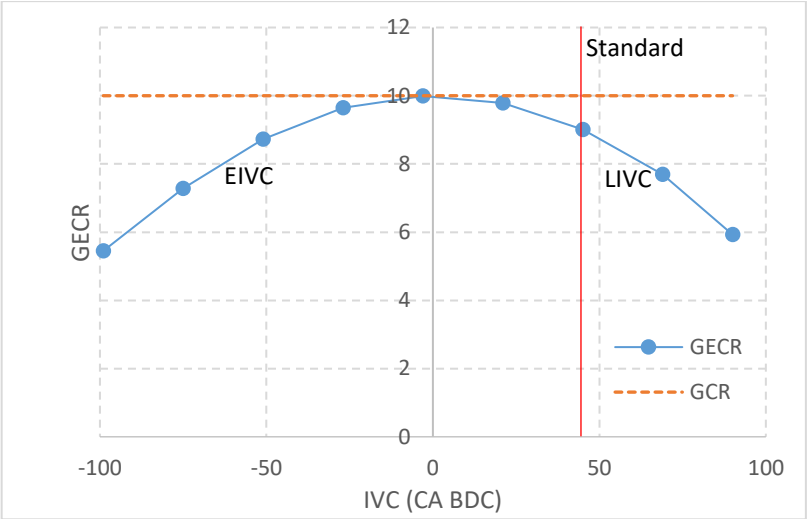

Figure 6-21 GECR values for different valve timings

Figure 6.22 shows that as the valve was closed earlier, passing the BDC points, the knock intensity decreased significantly in the downsized engine. This shows that the EIVC has greater potential to suppress knock provided that the valve system is capable of handling such timing. The boosting system is able to provide the required amount of charge in order to reach the desired power although the valves have been closed early. Extreme EIVC shows that it can suppress the knock more than the LIVC timing.

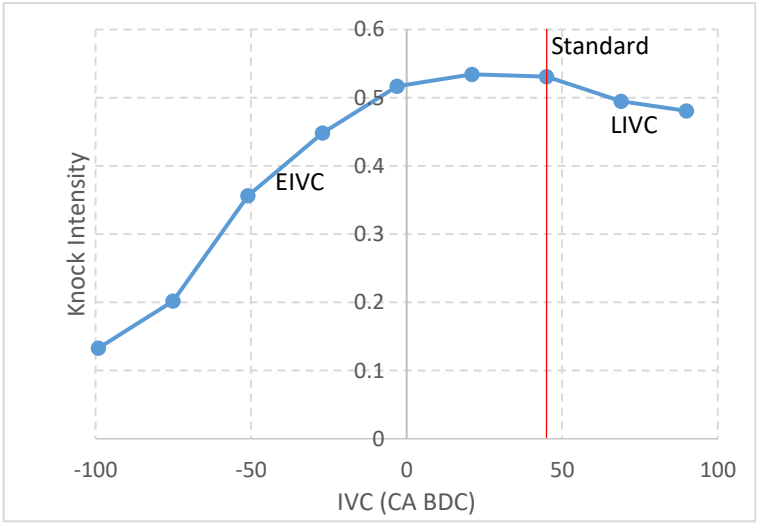

Figure 6-22 Knock intensity with variation IVC timing

Figure 6.23 shows the brake thermal efficiency at different GECR. The results have shown an improvement in thermal efficiency by lowering the geometric effective compression ratio (GECR). As the GECR decreases, the efficiency increases and improves as a result thereof. A lower GECR means that the engine is having a longer

power or expansion stroke. The EIVC and LIVC have made it possible to disconnect the expansion ratio from the effective compression ratio, thus promoting a better engine performance. [88], [89] also addressed the higher expansion effect resulted from the implementation of the Miller cycle, thus indicating better thermal efficiency and that engine knocking can also be avoided.

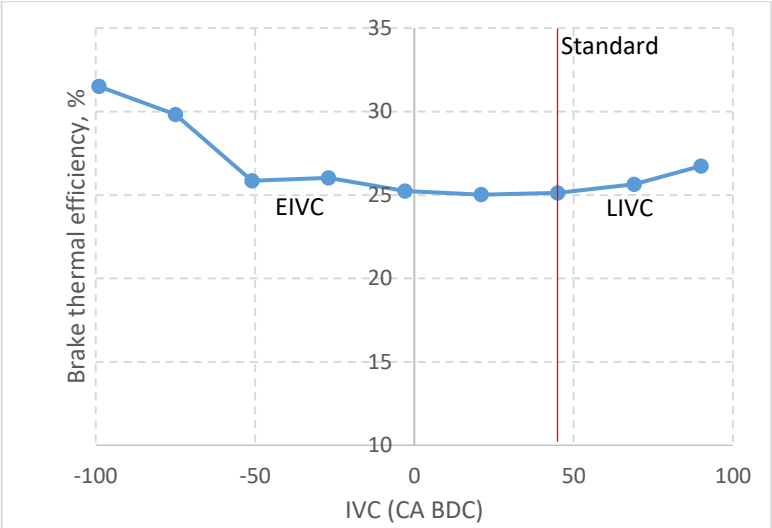

Figure 6-23 Brake thermal efficiency at different IVC timing

6.3 Part 3: Knock Analysis with Combustion Kinetics

This subsection analysed the results of knock suppression by Miller cycle which has been done using the combustion kinetics model. Table 6.2 lists down the variation of EIVC and LIVC points while other parameters are kept constant at the speed of 3000 rpm, AFR 14.7:1, and ignition timing at 32 BTDC. The IVC variations are done until the knocking was totally suppressed.

Table 6-2 Variation of the valve profiles for Miller cycle

	IVC (°CA)	IVC Constant	Duration (°CA)	Lift (mm)
EIVC5	75 BBDC	0.5	120	9.35
EIVC4	51 BBDC	0.6	144	9.35
EIVC3	27 BBDC	0.7	168	9.35
EIVC2	3 BBDC	0.8	192	9.35
EIVC1	21 ABDC	0.9	216	9.35
Standard	45 ABDC	1.0	240	9.35
LIVC1	69 ABDC	1.1	264	9.35
LIVC2	93 ABDC	1.2	288	9.35

Figure 6.24 shows the percentage of mass burned by autoignition for different intake valve closing. This mass burned by autoignition is calculated based on the mass burned in the unburned zone due to the chemical kinetic reactions of the unburned gas auto ignition. The formula could be found in section 5.4.1. EIVC5 and LIVC2 valve profiles have managed to suppress the knocking until zero percentage of mass burned by autoignition. The IVC profiles (EIVC-1,2,3) near the BDC crank angle have higher mass burned percentage as compared to the standard profile. It can be seen that, the higher

percentage of mass burned by autoignition, the higher temperature in the unburned zone (please refer to the Figure 6.25).

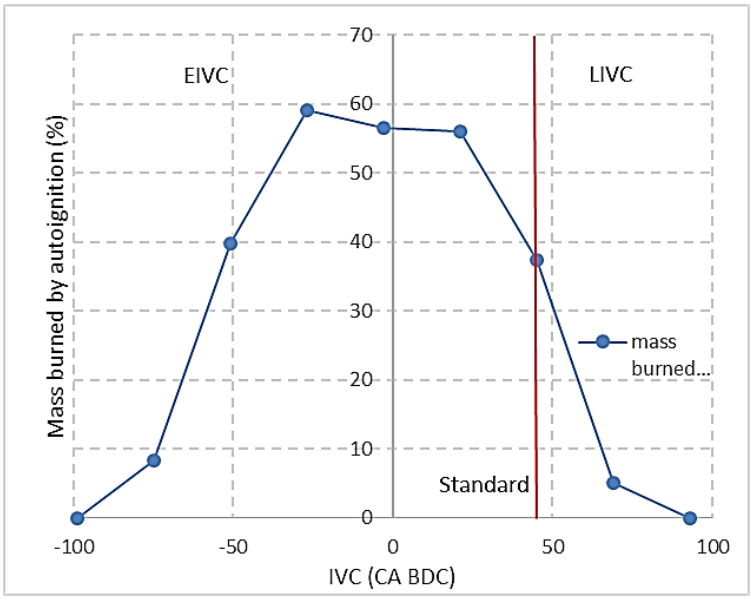

Figure 6-24 Percentage of mass burned by autoignition

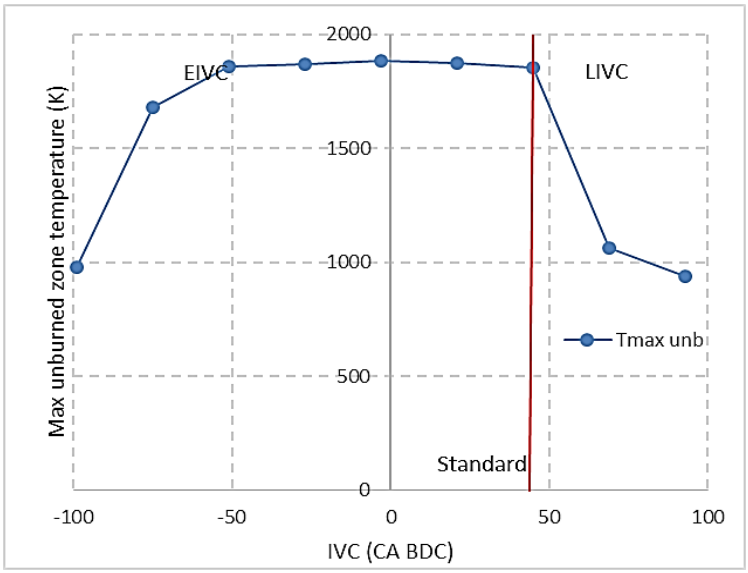

Figure 6-25 Maximum unburned zone temperature with IVC variation

During the autoignition, the mass fraction of OH species in the unburned region would suddenly shoot up. All the things that happened in the unburned zone were parallel with the in-cylinder pressure values. It was found that the knock onset by the first crank angle OH mass fraction shot up (Figure 6.26) in the unburned region was the same as knock onset by calculated based on the pressure fluctuation (Figure 6.27). The OH burned mass

fraction value in the unburned region (Figure 6.28) that used to characterise the intensity has the same trend as the knock intensity by pressure amplitude (Figure 6.29).

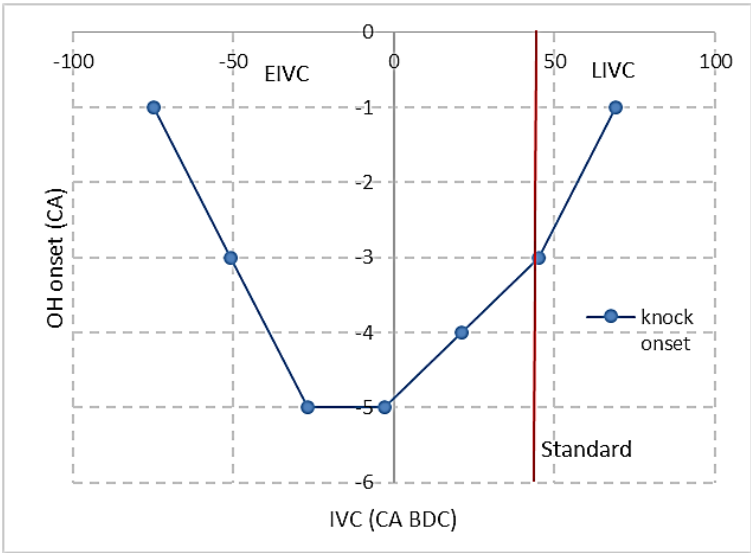

Figure 6-26 Knock onset based on the OH species

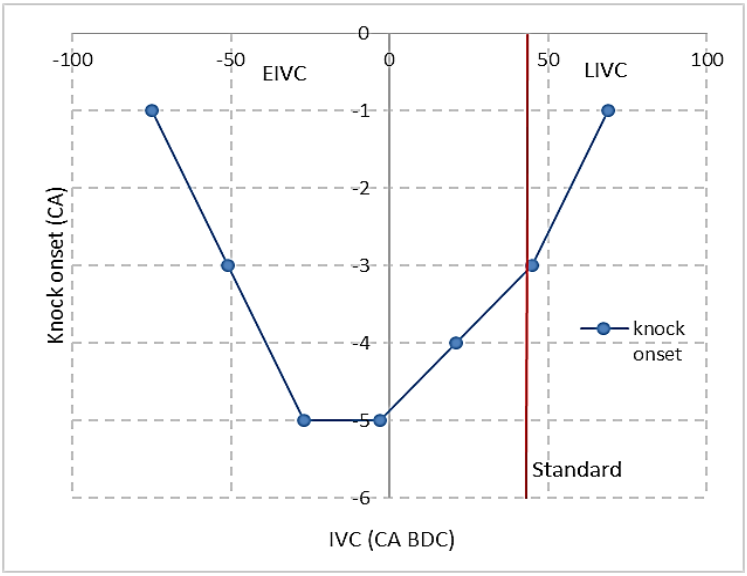

Figure 6-27 Knock onset based on the in-cylinder pressure

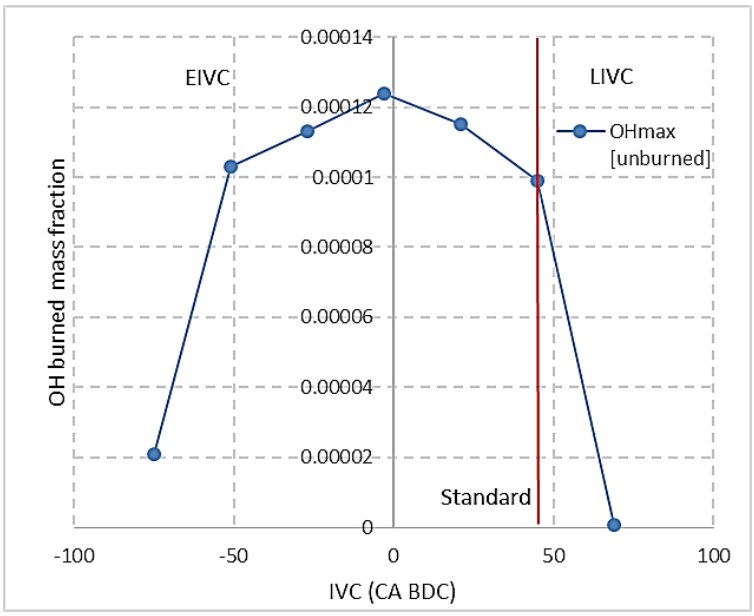

Figure 6-28 Knock intensity based on the OH mass fraction

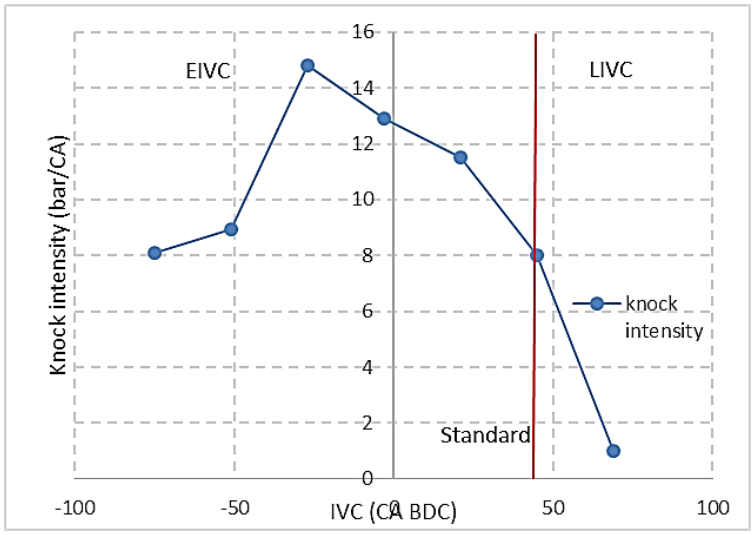

Figure 6-29 Knock intensity based on the in-cylinder pressure

Figure 6.30 shows the maximum in-cylinder pressure values for different intake valve closing timing. Generally, the in-cylinder pressures for all valve timings do not vary very much from each other. However, the values were a bit lower for the intake valve closings near the BDC crank angle.

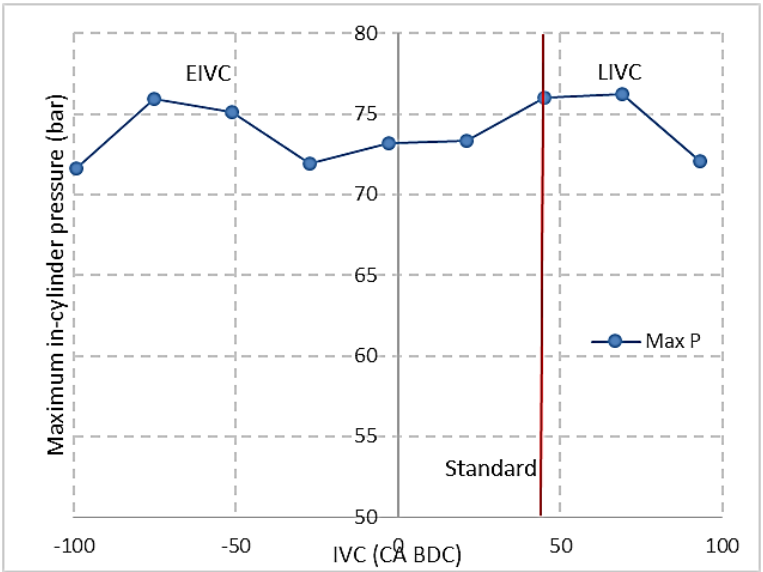

Figure 6-30 Maximum in-cylinder pressure with IVC variation

6.4 Summary

This chapter has investigated the Miller cycle effects on knock suppression in a downsized engine environment. The modelling works have been conducted in three parts, namely the Miller cycle at different speed-load, knock suppression with extreme Miller cycle, and knock analysis with combustion kinetics. Through the works, the Miller cycle has shown its capability to suppress engine knocking in a more efficient manner as opposed to the standard engine operation. This is contributed by the fact that early and late intake valve closings could affect the end gas condition at the end of the compression stroke, thus making it possible to suppress the engine knocking.

Chapter 7

RESULT & DISCUSSION II: MILLER CYCLE – LOAD CONTROL

7.0 Overview

In this chapter, the Miller cycle application has been extended to the load control strategy without using the throttle. This chapter discusses the Miller cycle effects on controlling the load based on the following questions: (1) How does the Miller cycle strategy with the EIVC profiles influence the engine performance for naturally-aspirated engines? and, (2) What is the performance comparison between naturally-aspirated and boosted engines when using the unthrottled Miller cycle strategy in order to control the load?

Using the Miller cycle as a load control mechanism is not a new strategy. However, previous works mostly focused on utilising the fully variable valve train (FVVT) as a load control strategy in the naturally-aspirated engine environment. Modern downsized engines nowadays are equipped with a boosting system, which makes it possible to achieve higher power output with a smaller size. The high intake pressure in downsized engines makes it possible to reduce the additional work or pumping losses. The gas exchange process during the part load condition requires additional work to draw in the air into the cylinder due to the decreased pressure in the intake manifold coming from the restriction of the throttle plate.

The Miller cycle potential by utilising the FVVT in controlling the load under a naturally-aspirated and boosted environment at the part load condition has been investigated in this work. The Miller cycle performance in naturally-aspirated engines has been evaluated on the basis of the experimental work conducted on the Lotus research engine. For the downsized engine condition, the evaluation has been conducted using the engine model built in the Ricardo WAVE software application, which was validated based on the Lotus research engine. One of the main reasons why the downsized engine cannot be evaluated through experimental work is that the available engine was not equipped with a boosting system. The focus of this chapter is to show how the Miller cycle with early IVC affects

the gas exchange process and the engine efficiency in naturally-aspirated and downsized engines.

7.1 Experimental Analysis of Miller Cycle in Naturally-aspirated Engine

Installing a throttle plate in the intake manifold is a standard method applied in order to control the amount of air going into the combustion chamber. This approach, however, has the drawback of lowering the manifold pressure below the atmospheric value, which then forced the engine to do additional work in order to overcome the opposite force to draw air into the cylinder. At low load, the throttle is only slightly opened, so the losses are expected to be higher as compared to the high speed associated with the wide open throttle (WOT) condition.

With the application of FVVT, the engine can be operated without throttle at part load in order to reduce the pumping losses and optimise the volumetric efficiency during the intake process. The aim of this work is to study the effect of varying the intake valve closing profiles on the combustion performance output with the throttle-less condition.

7.1.1 Experiment Procedures and Testing Points

Table 7.1 lists the testing points that have been implemented on the Lotus SCORE engine, as described in Chapter Four, under subsection 4.1. The procedure for the standard operating condition is that the opening angle of the throttle has been adjusted in order to achieve the desired load points, as mentioned in the table below. For the unthrottled Miller cycle condition, the valve closing timing was shortened and the lift has been altered so that it could trap sufficient air for the mixture to achieve the desired load points (2.0 bar and 2.7 bar IMEP) at 2000 rpm.

The difference in the valve timing duration is as illustrated in Figure 7.1. Ideally, in order to avoid the throttling loss, the valve has to be as high as possible, with the shortest possible duration [90]. Thus, in order to adopt a shorter duration with the valves, the lift should be altered as well so as to keep the valve acceleration within acceptable design limits.

Table 7-1 Testing points

	Throttled (2.0 bar)	Unthrottled (2.0 bar)	Throttled (2.7 bar)	Unthrottled (2.7 bar)
Throttle opening	2 %	100 %	4 %	100 %
IVO	345	345	345	345
IVC	585	461	585	461
Lift (mm)	9.35	1.3	9.35	1.7
Duration	240	116	240	116
GECR	9.21	7.49	9.21	7.49

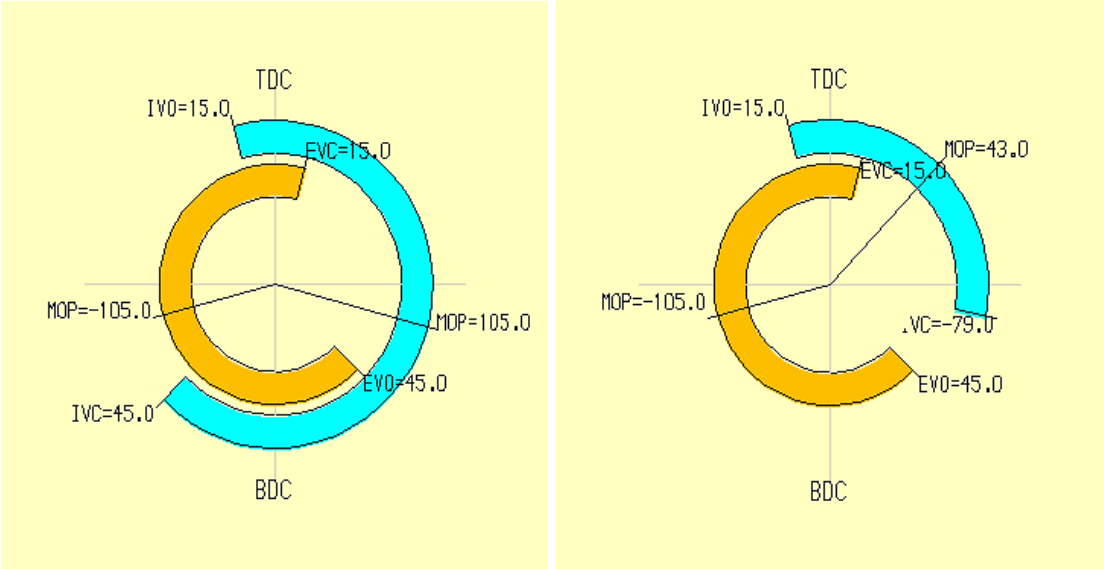

(i) Standard profile (ii) EIVC profiles

Figure 7-1 Valve timing display

The start of injection (SOI) for the tests was set at 36 °ATDC. This is based on the previous works conducted on the same engine [11], [90], [91] that found the best ISFC to be within 30 – 80 °ATDC. SOI > 80 ° gives unstable combustion because of the limited time for the mixture preparation, while SOI < 30 ° will result in fuel impingement on the piston. The ignition timing was set to the minimum advance for the best torque (MBT), which is then translated as the peak pressure being about 12 °ATDC. The unthrottled operation ignition timing was advanced to 50 °BTDC compared to the throttled profile at 35 °BTDC, in order to achieve the MBT.

7.1.2 Open Cycle Analysis [Gas Exchange Process]

Open cycle efficiency: Firstly, the results were analysed on the basis of the open cycle efficiency. Open cycle is defined as the gas exchange processes, which include the intake and exhaust strokes. The open cycle efficiency refers to determining the ability of the engine breathing system to transport the fresh charge and exhaust products into and out of the combustion chamber. Manipulating the intake and exhaust pressures will affect the fresh charge density and the air charge motion in order to promote the air-fuel mixing, while the EGR fraction will exert a direct impact on the open cycle efficiency.

The formula below describes how the open cycle efficiency has been calculated. The gross indicated mean effective pressure (GIMEP) evaluates the MEP in the cylinder during the compression and expansion strokes, while the net indicated mean effective pressure (NIMEP) is the MEP for the complete cycle including the intake and exhaust strokes. Thus, the pumping mean effective pressure (PMEP), which calculates the MEP of the work during the intake and exhaust strokes exerts a significant impact on the open cycle efficiency. Referring to Figure 7.2, by implementing the unthrottled Miller cycle strategy to control the engine load, the open cycle efficiency of the engine could be improved. For the unthrottled Miller cycle at 2.7 bar IMEP, an increase of 4.3 % in efficiency could be observed compared with the throttled operation, while the efficiency increased by 6 % for the 2.0 bar IMEP load point. The next part will explain how the unthrottled Miller cycle achieved higher open cycle efficiency through the reduction of the PMEP in greater detail.

$$\eta_{open} = \left[1 + \frac{PMEP}{GIMEP}\right] = \frac{NIMEP}{GIMEP} \tag{7.1}$$

$$PMEP = \int \frac{PdV}{V_d} \tag{7.2}$$

$$NIMEP = GIMEP + PMEP \tag{7.3}$$

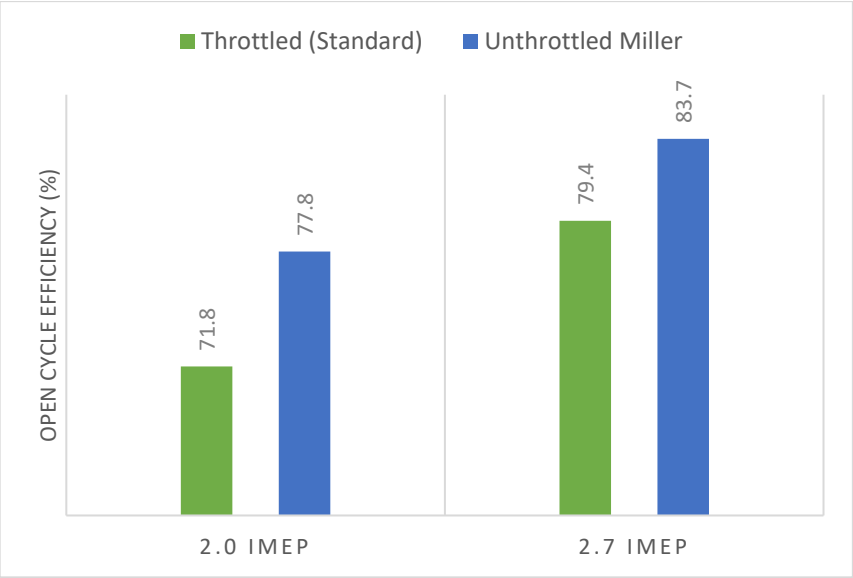

Figure 7-2 Open cycle efficiency comparison (in percentage)

Pumping losses: The improvement of the open cycle efficiency by means of the unthrottled Miller cycle strategy was gained from a reduction in the pumping mean effective pressure (PMEP) (please refer to Table 7.2). For the 2.0 bar IMEP test point, the unthrottled Miller cycle PMEP decreased by 30 % compared with the standard throttled version. While for the 2.7 bar IMEP, the PMEP decreased by 25.4 %. These reductions were achieved by using the Miller cycle on the basis of the early intake valve closing strategy in order to control the load instead of the butterfly valve.

Table 7-2 PMEP reduction over the standard profile

		NIMEP (bar)	**GIMEP (bar)**	**PMEP (bar)**	**PMEP reduction (%)**
2.0 bar IMEP	Throttled	2.04	2.84	0.80	-
	Unthrottled	1.96	2.52	0.56	30
2.7 bar IMEP	Throttled	2.74	3.45	0.71	-
	Unthrottled	2.72	3.25	0.53	25.35

The PV-diagram in Figure 7.3 indicates how much negative work has been alleviated by implementing the Miller cycle unthrottled strategy in comparison with the conventional throttled operation. Figure 7.4 illustrates that the intake manifold pressure for the unthrottled operation is consistently at atmospheric pressure (0.99 – 1.01 bar), while the

throttled operation has an atmospheric pressure of 0.35 bar (2 % throttle opening at 2.0 bar IMEP) and 0.443 bar (4 % throttle opening at 2.7 bar IMEP). By applying the Miller cycle strategy, no additional work is needed by the piston in order to draw the fresh air into the cylinder to compensate the effect of sub-atmospheric pressure due to the throttle opening restriction at low load.

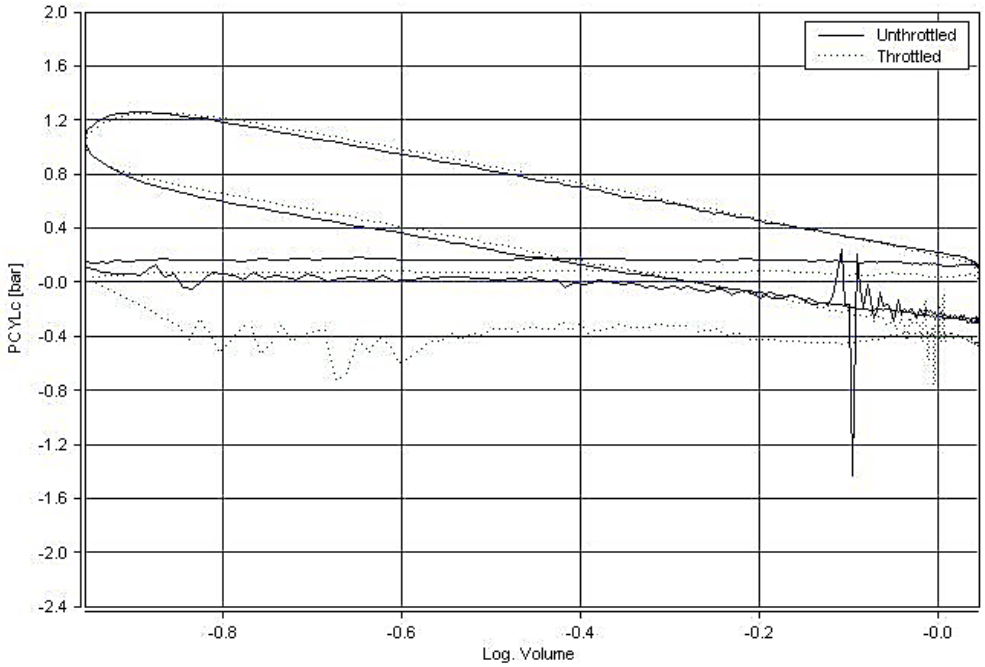

Figure 7-3 Log PV-diagram

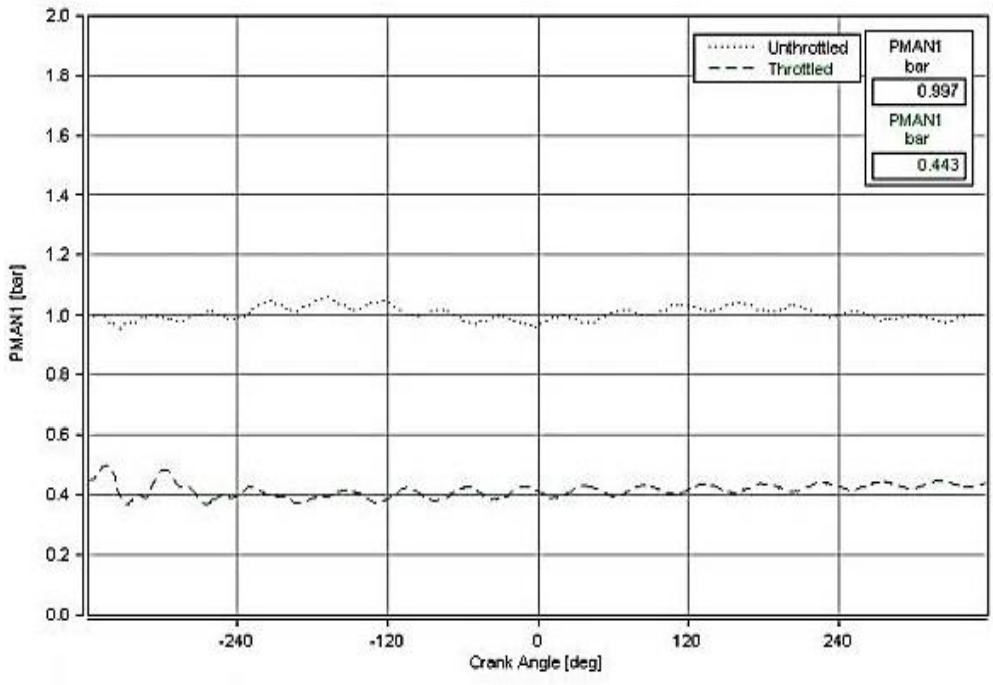

Figure 7-4 Intake manifold pressures at 2.7 bar IMEP

Volumetric efficiency: A measure of the effectiveness of the engine's induction system. The overall volumetric efficiency is evaluated at atmospheric condition.

$$\eta_v = \frac{\dot{m}_a}{\rho_a V_d \, N/2} = \frac{m_a\,(percycle)}{\rho_a V_d} \tag{7.4}$$

where:

ρ_a = at ambient condition

V_d = swept volume, 0.000498 m^3

The intake valves' lift and timing are other factors that contribute to the engine breathing efficiency. An unthrottled Miller cycle at 2.0 bar IMEP operation has the lowest lift and shortest intake stroke duration, thus giving a lower volumetric efficiency value (please refer Figure 7.5). This means that the amount of the fresh charge available in the cylinder is also less than 2.7 bar IMEP, thus giving better volumetric efficiency because it has a higher fluid flow momentum compared to the 2.0 bar IMEP, with lower ECR values.

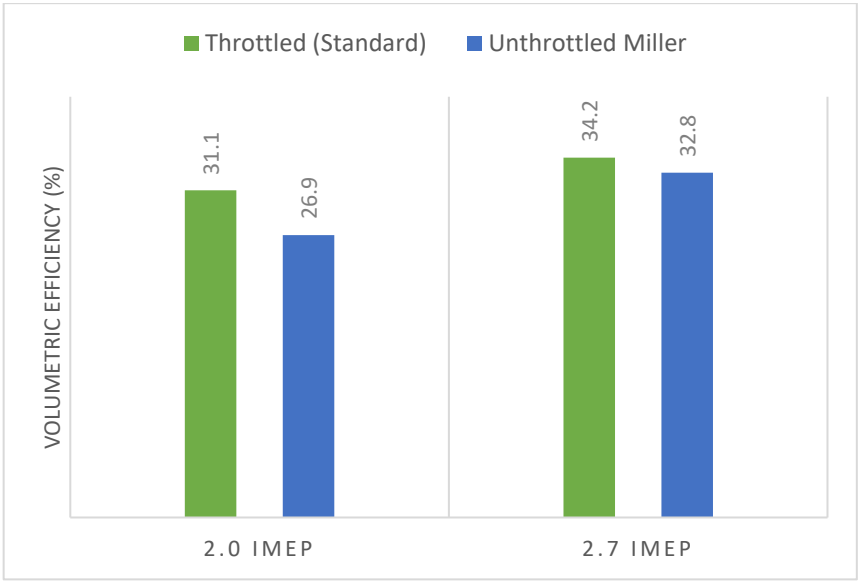

Figure 7-5 Volumetric efficiency for NA engine

7.1.3 Closed Cycle Analysis [Combustion Process]

Closed cycle efficiency: The closed cycle analysis is referring to the processes when the valves are fully closed, which includes the compression, ignition and expansion stroke. It is evaluated based on the gross indicated power (*grossIP*) over the fuel power (*FuelPower*) provided to the engine. Two of the main factors which determine the closed-cycle efficiency are combustion and heat transfer. The rate of the fuel's chemical energy,

also known as the heat release rate (HRR), can be used in order to understand the combustion phenomena occurring in the engine.

Table 7.3 listed the indicated power and fuel power for both throttled and unthrottled operations. The values for the unthrottled Miller strategy are less than those for the throttled ones. At 2.7 bar IMEP, the unthrottled Miller strategy *grossIP* is 6 %, while the *FuelPower* is 3 % less than the standard operation. The unthrottled Miller cycle strategy does not show any good improvement in terms of the closed cycle efficiency, as indicated in Figure 7.6. At 2.0 bar IMEP, it only increased slightly at 0.4 %, while at 2.7 bar IMEP, the efficiency dropped by 0.9 % compared with the throttled one. This situation might be due to the in-cylinder combustion instability, as discussed in the next section.

$$\eta_{closed} = \frac{GIMEP}{\left(\dot{m}_{fuel} \cdot Q_{LHV} \Big/ C \cdot N \cdot V_d\right)} = \frac{grossIP}{FuelPower} \tag{7.5}$$

Table 7-3 Indicated power and fuel power

	2.0 bar IMEP		2.7 bar IMEP	
	Throttled	Unthrottled	Throttled	Unthrottled
Gross IP (kW)	2.36	2.10	2.87	2.70
Fuel power (kW)	8.97	7.86	9.89	9.62

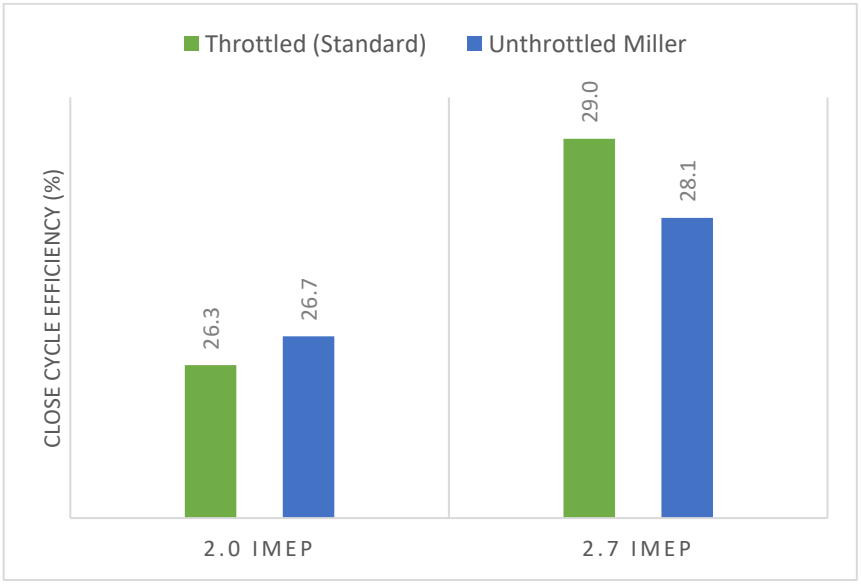

Figure 7-6 Closed cycle efficiency

Mass burned fraction (MBF): According to the graph in Figure 7.7, the low load operation (2.0 bar) has a slower combustion, as compared to the higher load operation (2.7 bar). However, the MBF curves for the two different loads have indicated similar trends, as discussed below:

- The standard throttled intake has much faster combustion phasing compared with the unthrottled EIVC. The unthrottled operation ignition delay is 40.1 % more than the standard operation timing for 2.0 bar IMEP and 32.9 % for 2.7 bar IMEP. If we refer to the in-cylinder pressure during ignition timing in Table 7.4, the standard profile has a much higher value, which promoted a faster combustion duration compared to the lower in-cylinder pressure for the unthrottled profile.
- The previous work in [11] has demonstrated that the air velocity for the unthrottled EIVC is lower than the standard profile from 50 °BTDC to 30 °ATDC, which encompasses the ignition, flame initiation and flame propagation phases. This might explain why the unthrottled operation requires a longer time to burn the mixture.
- Another finding, as discussed in [11], found that the bulk motion and turbulence were deteriorated when applying EIVC timing. They concluded that the reduction in the in-cylinder gas motion affected the longer time required for MBF. Other research studies ascribe this longer MBF duration and combustion instability to the lower compression temperatures.
- The findings in [10] also support the fact that the in-cylinder turbulence would become lower at the end of the compression stroke because of the lower valve lift for the EIVC timing. This leads to the decreased laminar flame speed.
- It also mentioned that the longer combustion duration by the unthrottled Miller cycle might be caused by the reduced mixture temperature at ignition [10].

Table 7-4 In-cylinder pressure values

		Max in-cylinder pressure (bar)	Ignition pressure (bar)
2.0 bar IMEP	Throttled	13.40	2.482
	Unthrottled	12.80	1.572
2.7 bar IMEP	Throttled	17.47	2.935
	Unthrottled	17.58	1.652

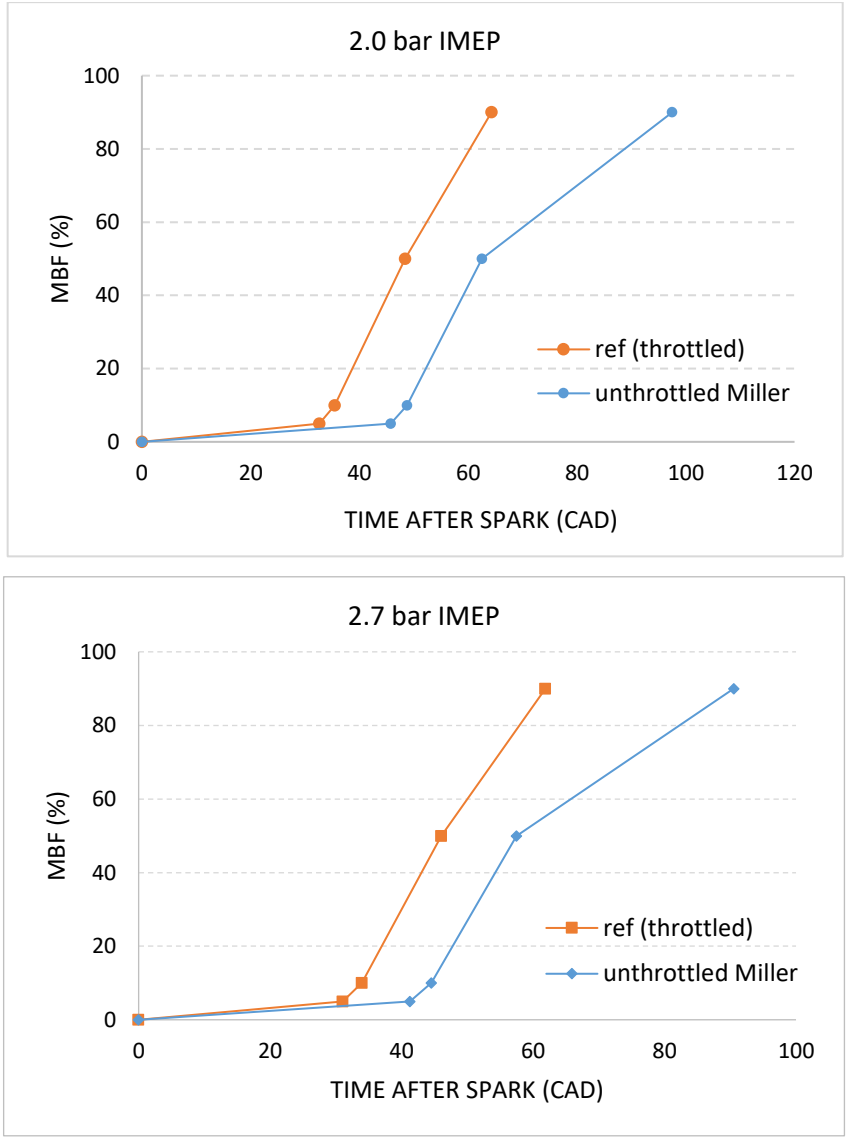

Figure 7-7 Mass burned fraction (MBF) curves

Cumulated heat release: With reference to Figure 7.8, the cumulated heat release for the unthrottled operation is quicker than the throttled operation before the peak in-cylinder pressure location (~12 °CA). After that, the throttled intake operation has a higher heat release until both lines meet again at the 100 % burn point.

A faster heat release might be gained from the advanced ignition timing of the unthrottled EIVC timing, but then the longer ignition delay might explain why it has a lower heat release compared with the throttled operation. Turbulence decayed once the intake valve closed early, so this phenomenon does not help promote the faster combustion progress of the unthrottled EIVC operation.

Instantaneous heat release: The throttled operation shows that the end of combustion is about 40 °CA, while the unthrottled operation is about 60 °CA. The longer combustion duration, which could imply a slower flame propagation, might be the reason why the unthrottled operation needed a longer time for the mixture to burn completely.

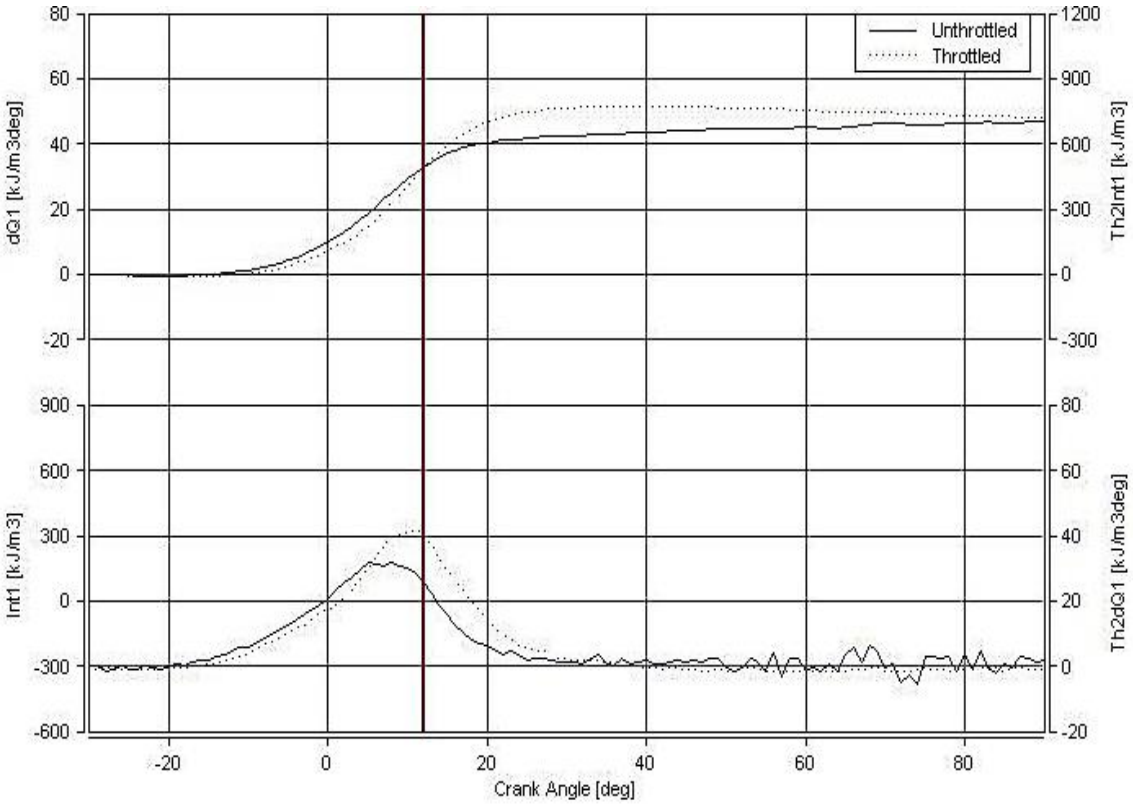

Figure 7-8 Heat release curves

Fuel injection: The amount of the fuel in this engine is estimated from the analysis of the fuel injection duration using the Akribis fuel mass meter output, as shown in Figure 7.9. The volume and mass of the fluid can be calculated based on the Akribis measurement, which was conducted using the same injector used in the Lotus SCORE engine [92]. The injection duration of the incompressible fluids can be directly linked to the volume flow of fuel through the injector. The fuel mass is then calculated based on the density of the fuel. The mass of fuel for different conditions is determined by integrating the area under the curve (please refer to Figure 7.10). Two assumptions were therefore made:

i) The start and end of duration will follow the same pattern regardless of the duration
ii) The differences in fuel duration will only affect the steady part of the curve

The assumptions are considered reasonable because the fuel rail pressure is maintained constant for all conditions. The mass of air can also be estimated since the testing is held under the stoichiometric condition.

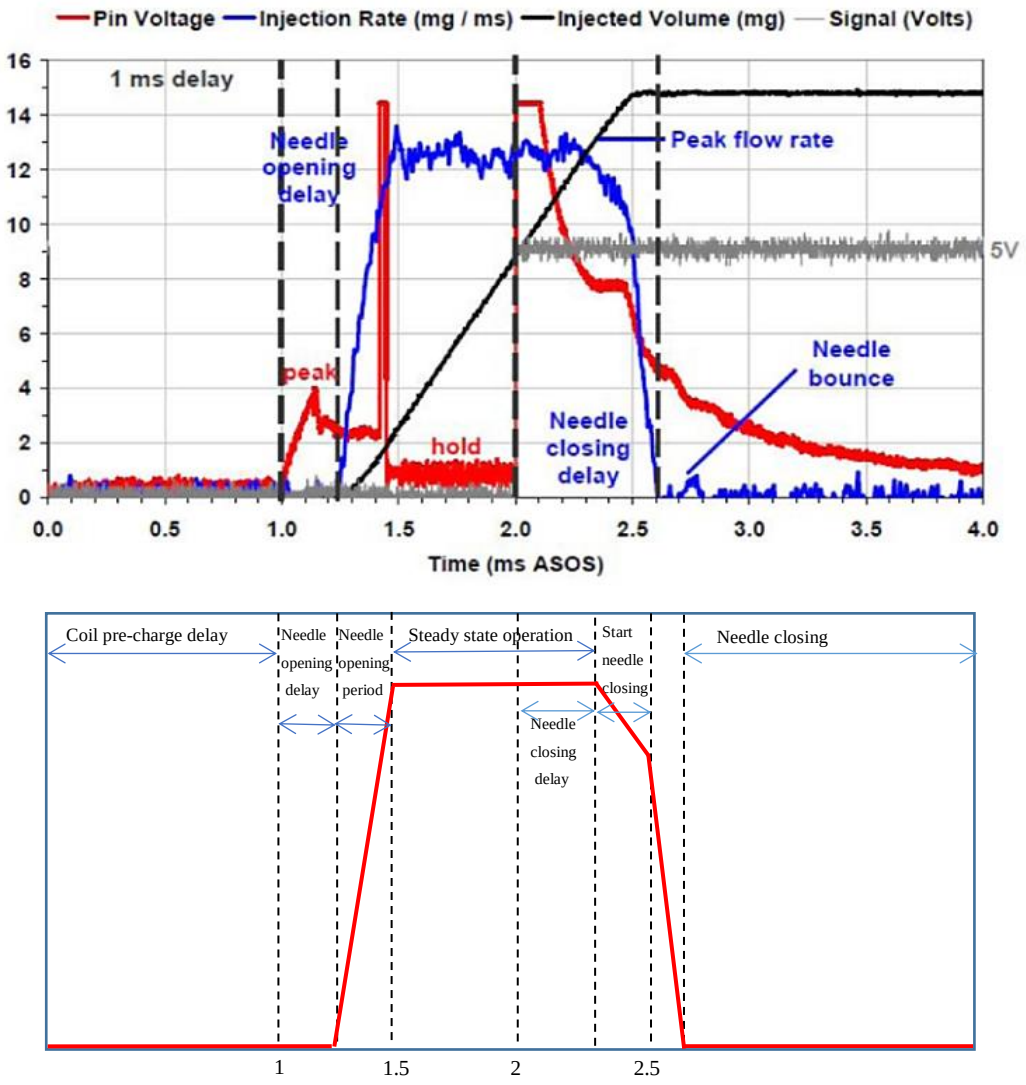

Figure 7-9 Graphical output from Akribis flow meter and simplified graph

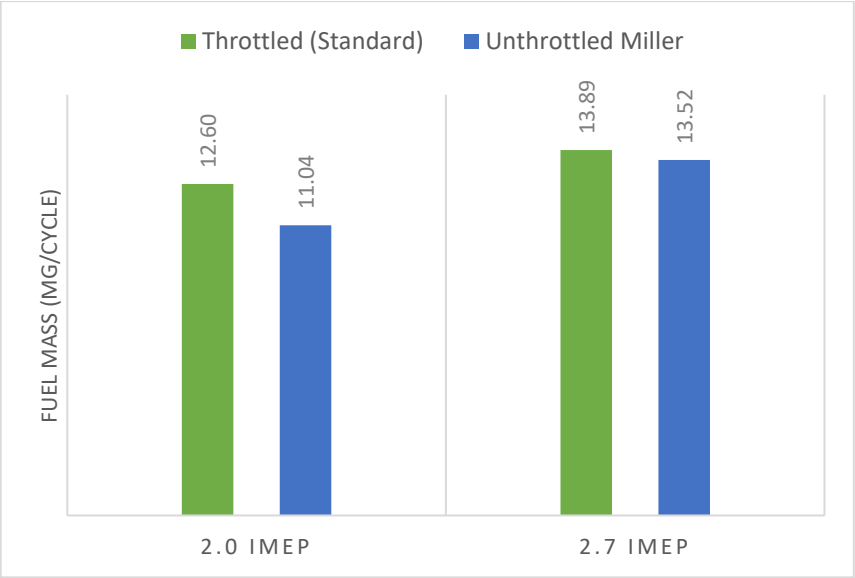

Figure 7-10 Fuel mass estimation based on Akribis data

From the fuel mass determined through the Akribis meter output, the ISFC values were computed. Figure 7.11 shows the improvement of ISFC for the unthrottled Miller cycle case from the standard throttled case. At 2.0 bar IMEP, the unthrottled Miller strategy ISFC improved by 8.8 % compared to the throttled case. While at 2.7 bar IMEP, the unthrottled Miller strategy ISFC improved by 1.9 %.

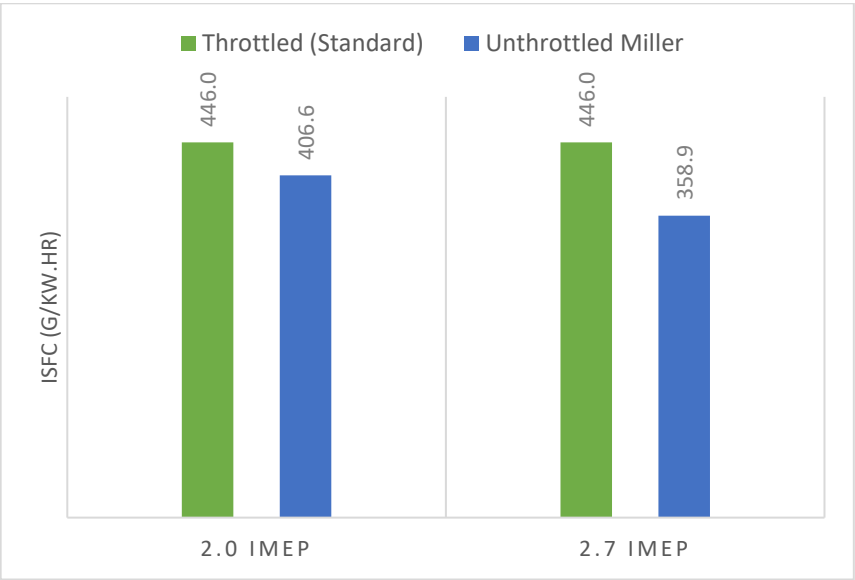

Figure 7-11 ISFC values

7.2 Modelling Analysis of Miller Cycle in Downsized Engine

This section discusses the unthrottled Miller cycle strategy used in controlling the load tested for the downsized engine environment. The Lotus research engine has no boosting

system to serve as a downsized engine. Thus, the work was simulated using the downsized engine model in the WAVE software. The validation for the engine model has been done as in Section 5.2.

7.2.1 Open Cycle Analysis [Gas Exchange Process]

Open cycle efficiency:

By implementing the unthrottled Miller cycle strategy to control the engine load, this has improved the open cycle efficiency of the engine, as shown in Figure 7.12. For the unthrottled Miller at 2.7 bar IMEP, it has gained 4.5 % more efficiency than the throttled version, and 2.0 bar IMEP has increased the efficiency by 6.2 %. The efficiency values for the downsized engine are slightly higher than the NA engine model (please refer to Figure 7.2). At 2.0 bar IMEP, the NA engine has 77.8 % efficiency, while the downsized engine has an efficiency of 78.8 %. Thus, applying the unthrottled Miller cycle strategy would provide better benefits for the downsized engine.

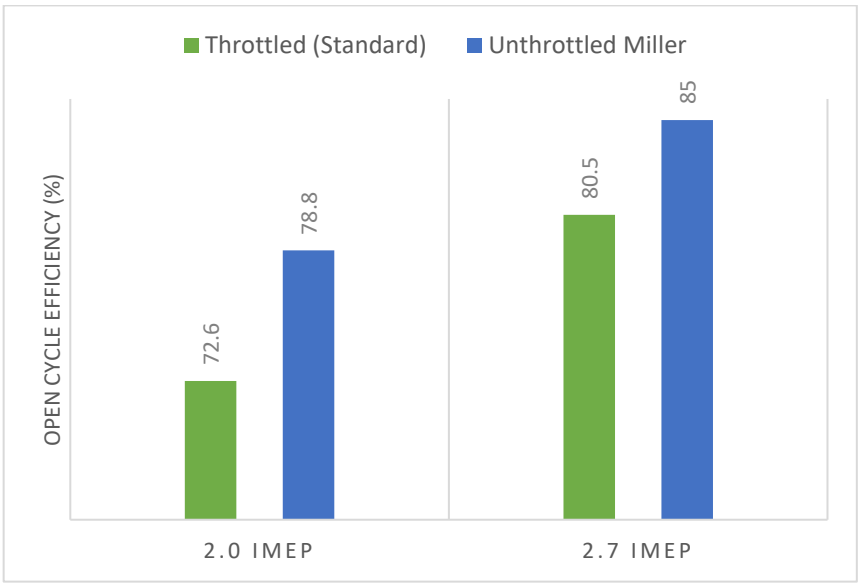

Figure 7-12 Open cycle efficiency for downsized engine

Pumping losses: The increment in the open cycle efficiency is contributed by the reduction in the pumping losses. The downsized model shows lower PMEP values than the NA engine (please refer to Table 7.5). This shows that having a boosting system makes it possible to reduce the flow resistance during the throttling process. Figure 7.13 shows how much the pumping losses area has been reduced by using the unthrottled Miller cycle strategy.

The boosted intake pressure was increased in order to achieve the targets with the lower lift. This is required in order to apply a sufficient charge and it helped to reduce the pumping losses [10].

Table 7-5 Pumping losses reduction for downsized engine

		NIMEP (bar)	GIMEP (bar)	PMEP (bar)	PMEP reduction (%)
2.0 bar IMEP	Throttled	1.91	2.62	0.71	-
	Unthrottled	2.08	2.64	0.56	21.13
2.7 bar IMEP	Throttled	2.74	3.41	0.67	-
	Unthrottled	2.72	3.20	0.48	28.36

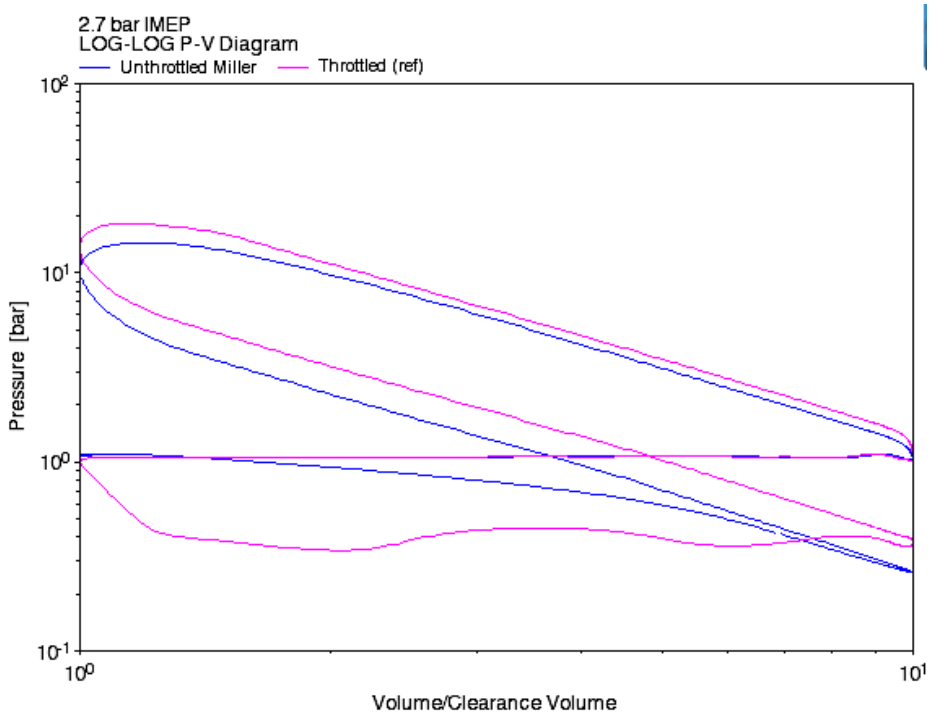

Figure 7-13 Log PV-diagram for downsized engine

7.2.2 Closed Cycle Analysis [Combustion Process]

Closed cycle efficiency: The closed cycle efficiency for downsized engines shows a different trend than the NA engine counterpart. The NA engine close cycle efficiency does not show any good improvement. As for the downsized engine, the unthrottled Miller cycle shows an increment in the efficiency (Figure 7.14). This must be from a better combustion

assisted by the boosting system. More turbulence occurs. Table 7.6 shows that the fuel power values for the downsized engine are lower than those for the NA engine. This shows that less fuel is used in order to gain the gross indicated power. In other words, it enables the engine to achieve higher efficiency. The efficiency for 2.0 bar IMEP increases by 6.4 % and 2.7 bar IMEP has a 3 % increment compared to the throttled operation.

Table 7-6 Indicated power and fuel power for downsized engine

	2.0 bar IMEP		2.7 bar IMEP	
	Throttled	Unthrottled	Throttled	Unthrottled
Gross IP (kW)	2.18	2.19	2.83	2.66
Fuel power (kW)	6.14	5.23	7.46	6.49

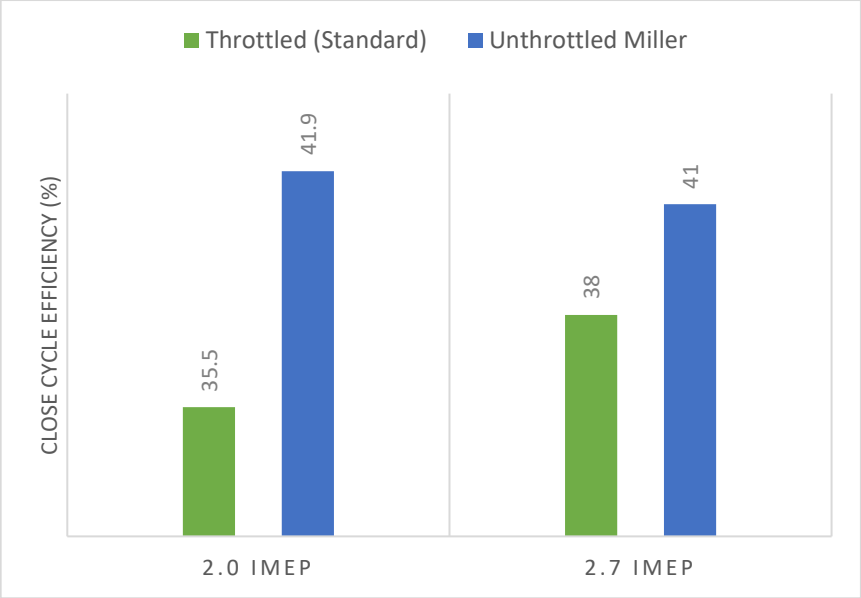

Figure 7-14 Closed cycle efficiency for downsized engine

The maximum in-cylinder pressure for the unthrottled Miller cycle operations has lower values compared to the throttled operations (Table 7.7). The trend is similar with the naturally-aspirated engine output, as stated in the previous Table 7.4.

Table 7-7 Maximum in-cylinder pressure for downsized engine

		Max in-cylinder pressure (bar)
2.0 bar IMEP	Throttled	14.87

	Unthrottled	12.02
2.7 bar IMEP	Throttled	18.30
	Unthrottled	14.45

ISFC: Table 7.8 shows the ISFC values for the downsized engine model. The unthrottled Miller cycle strategy shows an improvement in terms of fuel consumption. Comparing the ISFC values with the NA engine, the downsized engine appears to have better ISFC. For the unthrottled Miller cycle at 2.0 bar IMEP, the downsized engine shows an improvement of 37.1 % for the ISFC, compared to the NA engine. While at 2.7 bar IMEP, the ISFC for the downsized engine improved by 32.4 %.

Table 7-8 ISFC values for downsized engine

IMEP	Throttled	Unthrottled Miller
2.0 bar	0.326 kg/kW/hr	0.255 kg/kW/hr
2.7 bar	0.276 kg/kW/hr	0.242 kg/kW/hr

7.3 Summary

This chapter has explained the Miller cycle application through early intake valve closing for the load control strategy at the part load condition. The work has been conducted experimentally for the naturally-aspirated engine condition. It has been proven that by eliminating the throttle and applying the Miller cycle strategy, the engine has performed better compared to the standard throttle load control. The downsized engine condition, which has been evaluated via modelling work, also showed the same better performance trend with the unthrottled Miller cycle strategy.

Chapter 8

CONCLUSION & FUTURE WORKS

8.0 Overview

This research work has explored the application of the Miller cycle combustion strategy in downsized gasoline engines. The contribution of this work primarily seeks to establish a Miller cycle combustion strategy in downsized gasoline engines. Two areas of focus in this respect are the Miller cycle strategy for engine knock suppression and the Miller cycle strategy for load control under a downsized environment. The following conclusions have been reached based on the research objectives stated below.

8.1 Knowledge Contributions

The first objective is to compare the efficiency of the Miller cycle with other engine cycles of the Otto, Diesel, Dual, and Atkinson cycles under naturally-aspirated and boosted conditions on the basis of the ideal gas cycle modelling. An analytical analysis of ideal gas cycle modelling was carried out based on the efficiency comparison between Otto, Diesel, Dual, Diesel and Miller cycles. The boosted gas cycles model was also compared to represent the downsized engines condition. It was found out that, the supercharged Miller cycle can be utilised in the engine as a more efficient combustion strategy as opposed to other cycles based on the air standard cycles' comparison.

Another finding was that the efficiency increment for all the cycles was significant for a compression ratio range from 5 to 15, which is the most common compression ratio range used in commercialised engines. The supercharged Miller cycle has the highest efficiency compared to the supercharged Otto cycle. At a compression ratio of 10, it has a greater efficiency by 11.2 % than its naturally-aspirated counterpart.

The second objective is to investigate the Miller cycle performance through the implementation of early intake valve closing (EIVC) and late intake valve closing valve (LIVC) timings in order to determine how it affects the compression process, thus influencing the knock phenomenon during the combustion process in the downsized

engine. A downsized engine model was developed in Ricardo WAVE software based on a Lotus research engine. The engine model was integrated with an in-house MATLAB code referred to as LUCKS2 (Loughborough University Chemical Kinetics Simulation 2) to simulate the combustion system with chemical kinetics in order to have a thorough and in-depth analysis of the engine knocking. The works were divided into three major parts.

Part 1: The comparison of the Miller cycle behaviours that was achieved either through EIVC or LIVC at different speed-load conditions in a downsized gasoline engine was studied extensively in the first part. It was found out that, at low load condition, the engine knocking only happened under the low speed condition. Cylinder temperature values higher than 2500 K for the unburned zone result in knocking occurring at 1000 rpm and 2000 rpm. The EIVC has no significant improvement in knock intensity and BSFC at all speeds while the LIVC is able to reduce the engine knock at low speeds but does not show consistency in the BSFC values. The BSFC values were increasing at higher engine speeds for 4000 rpm and 5000 rpm.

For the medium load condition, knock intensity reached its highest value which was about 80 % of mass fraction by autoignition at 1000 rpm. Neither the EIVC nor the LIVC were able to suppress the knock at that point. The LIVC has shown an improvement in knock suppression and BSFC at 2000 rpm to 5000 rpm, while the EIVC did not have any effect at any speed. As for high load condition, the EIVC has shown better potential than the LIVC on suppressing the engine knocking. Only at 2000 rpm, the LIVC was able to suppress more knock, however, it consumed more fuel than the EIVC.

Part 2: In this part, the engine knocking was totally suppressed using the extreme Miller cycle strategy. As we closed the valve early, passing the BDC points for extreme EIVC, the knock intensity was greatly reduced. This shows that the EIVC has a greater potential to suppress knock provided that the valve system is fully flexible. When the geometric effective compression ratio value decreases for the EIVC, this indicates that the expansion stroke is longer than the compression stroke. Thus, this has improved the brake thermal engine efficiency. However, for LIVC, it could not reach the desired BMEP if it went beyond 20 % more than the standard IVC which might be due to the combustion instability.

Part 3: An understanding of the chemical process that occurred using the chemical kinetics mechanism is achieved in order to better understand the detailed process during the engine knocking. During the autoignition, the mass fraction of OH species in the unburned region would suddenly shoot up. It was found that the knock onset by the first crank angle OH mass fraction shot up in the unburned region was the same as knock onset by calculated based on the pressure fluctuation. The OH burned mass fraction value in the unburned region that used to characterise the intensity has the same trend as the knock intensity by pressure amplitude.

The third objective is to study the potentials of the load control strategy by the Miller cycle without throttle by varying the intake valve closing profiles in naturally-aspirated and downsized engines via engine modelling and experimental works. Experimental work of Miller cycle was done for the naturally-aspirated engine. The targeted IMEP was achieved by early intake valve closing instead of using the throttle.

The open cycle efficiency for the unthrottled Miller cycle strategy has shown an improvement. This improvement is gained from the major pumping losses reduction. The unthrottled Miller cycle strategy however does not show any good improvement in terms of close cycle efficiency. The standard throttled intake has much faster combustion phasing compared with the unthrottled EIVC. Higher in-cylinder pressure during the ignition timing for the standard profile also promotes a faster combustion duration. The unthrottled operation has a much longer ignition delay, which contributes to the slower combustion phasing. The ISFC for the unthrottled Miller cycle case are lower compared to the standard throttled case.

The application of the unthrottled Miller cycle for engine load control in the downsized gasoline engine is done as an extension to the study completed in the naturally aspirated engine. Under a downsized environment, the unthrottled Miller cycle strategy has improved the open cycle efficiency. The values are slightly better than the naturally-aspirated environment. The increment in efficiency is contributed by the reduction in the pumping losses. Although a naturally-aspirated engine is having a higher PMEP reduction, the downsized model shows lower PMEP values. This indicates the presence of a boosting system able to reduce the flow resistance during the throttling process. The closed cycle efficiency for the downsized engine shows a different trend compared to its

naturally-aspirated engine counterpart. The unthrottled Miller cycle shows an increment in terms of efficiency. This must be from a better combustion assisted by the boosting system.

8.2 Future Recommendations

This research has shown that a further increment in engine efficiency can be achieved with a downsized gasoline engine downsizing using the Miller cycle combustion strategy. Further works can be done in order to attain higher engine efficiency and better fuel economy with fewer emissions.

Recommendation 1

As an alternative, having a two-stroke cycle on a four-stroke engine platform is regarded as a promising alternative to produce greater torque and high power output based on its doubled firing frequency. The most significant difference between two-stroke and four-stroke cycles is represented by their gas exchange processes. The gas exchange and scavenging processes strongly affect the two-stroke engine performance, fuel economy and emissions. It is not easy to achieve a great balance between these two processes in order to obtain the best efficiency. Further research can be done to evaluate different valve strategies of achieving a two-stroke cycle on a four-stroke engine platform in order to achieve better engine performance.

Recommendation 2

The conventional four-stroke cycle is exposed to great thermal losses. On average, only about 30 % of the energy efficiency is utilised. It is important to compensate for those losses in order to have better engine efficiency. However, the recovering process can be complicated and less effective than what it is supposed to be. The six-stroke cycle is not new for the compression ignition diesel engine. It has great potential in producing higher efficiency and reducing emissions. However, this concept is new for gasoline engines and it could also bring great prospects in compensating for the heat losses, thus gaining an increased power output. A study to find the possibility of a new six-stroke cycle concept in order to improve the fuel efficiency and convert the waste heat into usable work might be a good solution for the thermal losses.

Recommendation 3

An engine is usually adopting a single strategy for all engine operations. Combining a few cycles as multi-cycle operations based on the thermodynamics sweet spots is expected to improve the overall engine performance. However, the optimisation process ensuring that different speed-load regions of the engine map are at their highest efficiency and benefit from the best fuel economy is a complicated process. Thus, more works could be done to adopt multi-cycle strategies based on the efficiency and fuel economy results for different speed-load regions.

APPENDIX A: Wave Engine Model Specifications

Table 1: Intake ducts & junctions

LABEL	ELEMENT	SPECIFICATIONS
intake	Intake ambient	Diameter (mm): 50 Pressure (bar): 1 Temperature (K): 298.15
p1	Duct	Left diameter (mm): 50 Right diameter (mm): 39 Overall length (mm): 40 Roughness height (mm): 0.0015 Maximum taper angle (deg): 7.83 Wall friction: 1 Wall heat transfer: 1 Discharge coefficient: auto Thickness (mm): 1 Conductivity (W/m/K): 204 Heat capacity ($J/m^3/K$): 2538000
orif1	Orifice	Diameter (mm): auto
intplenum1	Intake plenum	Diameter (mm): 305 Right diameter (mm): 305 Overall length (mm): 855 Wall friction: 1 Wall heat transfer: 1 Discharge coefficient: auto
orif2	Orifice	Diameter (mm): auto
p2	Duct	Diameter (mm): 48 Overall length (mm): 80 Roughness height (mm): 0.0015 Wall friction: 1 Wall heat transfer: 1 Discharge coefficient: auto Thickness (mm): 1 Conductivity (W/m/K): 204 Heat capacity ($J/m^3/K$): 2538000
orif3	Orifice plate	Diameter (mm): 45
p3	Duct	Diameter (mm): 47.3 Overall length (mm): 635 Roughness height (mm): 0.0015 Wall friction: 1 Wall heat transfer: 1

		Discharge coefficient: auto Thickness (mm): 1.3 Conductivity (W/m/K): 48 Heat capacity (J/m^3/K): 3871000
butterflyvalve	Throttle valve	Plate angle (deg): 0-90 Bore diameter (mm): 38 Shaft diameter (mm): 10
p4	Duct	Diameter (mm): 45.7 Overall length (mm): 180 Roughness height (mm): 0.0015 Wall friction: 1 Wall heat transfer: 1 Discharge coefficient: auto Thickness (mm): 1 Conductivity (W/m/K): 204 Heat capacity (J/m^3/K): 2538000
orif4	Orifice	Diameter (mm): auto
intplenum2	Intake plenum	Diameter (mm): 150 Overall length (mm): 143 Roughness height (mm): 0.0015 Wall friction: 1 Wall heat transfer: 1 Discharge coefficient: auto Thickness (mm): 1 Conductivity (W/m/K): 48 Heat Capacity (J/m^3/K): 3871000
orif5	Orifice	Diameter (mm): auto
p5	Duct	Diameter (mm): 49 Overall length (mm): 30 Roughness height (mm): 0.0015 Wall friction: 1 Wall heat transfer: 1 Discharge coefficient: auto Thickness (mm): 1.3 Conductivity (W/m/K): 48 Heat Capacity (J/m^3/K): 3871000
orif6	Orifice	Diameter (mm): auto
p6	Duct	Diameter (mm): 49 Overall length (mm): 137.5 Roughness height (mm): 0.0015 Wall friction: 1 Wall heat transfer: 1 Discharge coefficient: auto

		Thickness (mm): 1.3 Conductivity (W/m/K): 48 Heat Capacity (J/m^3/K): 3871000
orif7	Orifice	Diameter (mm): auto
p7	Duct	Left diameter (mm): 49 Right diameter (mm): 45.44 Overall length (mm): 130 Roughness height (mm): 0.008 Maximum taper angle (deg): 0.78 Wall friction: 1 Wall heat transfer: 1 Discharge coefficient: auto Thickness (mm): 1.63 Conductivity (W/m/K): 48 Heat capacity (J/m^3/K): 3871000
orif8	Orifice	Diameter (mm): auto
p8	Duct	Left diameter (mm): 45.44 Right diameter (mm): 43.84 Overall length (mm): 75 Roughness height (mil): 0.0015 Maximum taper angle (deg): 0.61 Wall friction: 1 Wall heat transfer: 1 Discharge coefficient: auto Thickness (mm): 4 Conductivity (W/m/K): 204 Heat capacity (J/m^3/K): 2538000
yjun1	Complex Y-junction	Diameter (mm): 31 Wall friction multiplier: 1 Heat transfer multiplier: 1 Thickness: 4 Conductivity (W/m/K): 204 Heat capacity (J/m^3/K): 2538000 Openings: X Y Z int1 0 90 90 int3 0 90 90 p12 180 90 90

Table 2: Exhaust ducts & junctions

LABEL	ELEMENT	SPECIFICATIONS

yjun2	Complex Y-junction	Diameter (mm): 26 Wall friction multiplier: 1 Heat Transfer multiplier: 1 Thickness (mm): 4 Conductivity (W/m/K): 204 Heat capacity (J/m^3/K): 2538000 Openings: X Y Z int1 180 90 90 int3 180 90 90 p12 0 90 90
p9	Duct	Left diameter (mm): 34.64 Right diameter (mm): 42.66 Overall length (mm): 70 Roughness height (mm): 0.0015 Maximum taper angle (deg): 3.28 Wall friction: 1 Wall heat transfer: 1 Discharge coefficient: auto Thickness (mm): 1 Conductivity (W/m/K): 204 Heat capacity (J/m^3/K): 2538000
orif9	Orifice	Diameter (mm): auto
p10	Duct	Left diameter (mm): 42.66 Right diameter (mm): 40 Overall length (mm): 101 Roughness height (mm): 0.0015 Maximum taper angle (deg): 0.75 Wall friction: 1 Wall heat transfer: 1 Discharge coefficient: auto Thickness (mm): 1.63 Conductivity (W/m/K): 48 Heat capacity (J/m^3/K): 3871000
orif10	Orifice	Diameter (mm): auto
p11	Duct	Diameter (mm): 40 Overall length (mm): 30 Roughness height (mm): 0.0015 Wall friction: 1 Wall heat transfer: 1 Discharge coefficient: auto Thickness (mm): 1.63 Conductivity (W/m/K): 48

		Heat capacity (J/m^3/K): 3871000
orif11	Orifice	Diameter (mm): auto
p12	Duct	Diameter (mm): 80 Overall length (mm): 222.06 Roughness height (mm): 0.0015 Wall friction: 1 Wall heat transfer: 1 Discharge coefficient: auto Thickness (mm): 2 Conductivity (W/m/K): 48 Heat capacity (J/m^3/K): 3871000
orif12	Orifice	Diameter (mm): auto
p13	Duct	Diameter (mm): 40 Overall length (mm): 30 Roughness height (mm): 0.0015 Wall friction: 1 Wall heat transfer: 1 Discharge coefficient: auto Thickness (mm): 1.63 Conductivity (W/m/K): 48 Heat capacity (J/m^3/K): 3871000
orif13	Orifice	Diameter (mm): 31
p14	Duct	Diameter (mm): 31 Overall length (mm): 1
exhaust	Exhaust ambient	Diameter (mm): auto Pressure (bar): 1.05 Temperature (K): 800

Table 3: Engine & Injector

LABEL	ELEMENT	SPECIFICATIONS
SCORE		Bore (mm): 87.9998 Stroke (mm): 82.1 Clearance height: 9.12 Connecting rod length (mm): 142 Engine type: Spark-ignition
Injector1	Fuel/Air Trapped Mass per Hour	Air/Fuel ratio: 14.53 Start of injection (deg): 421.2 -Electronic pulse (deg): 396 -Pre-charge time + Delay (deg):25.2 Mixture temperature (K): 350 Nozzle diameter (mm): 0.1 Spray spread angle (deg): 40

<table>
<tr><td></td><td></td><td>Injection duration: ~
Injection rate & pressure profile:<table><tr><td>Crank angle</td><td>Rate</td><td>Pressure (bar)</td></tr><tr><td>{SOI}</td><td>1</td><td>120</td></tr><tr><td>{inj_rate}</td><td>1</td><td>120</td></tr></table></td></tr>
</table>

Chen-Flynn Friction Correlation Tool v2

Comments:	

Stroke	82.1	mm

P_{max}	Engine Speed	Measured FMEP	Predicted FMEP	Error
bar	rpm	bar	bar	%
Use Fixed Value	Calculate Linear Term			
0.005	65.26403			
	0.2			
71.01	1997.97	1.4839476	1.616	-8.88
71.1	1999.89	1.754106	1.617	7.84
62.06	3002.42	1.859576	1.812	2.55
62.58	3001.54	1.81418	1.815	-0.03
63.71	3001.05	1.8187312	1.820	-0.08
62.05	3001.35	1.7733352	1.812	-2.18
55.73	4001.73	2.1099352	2.027	3.91
57.18	4002.27	2.0223744	2.035	-0.61
57.83	4002.36	1.9995444	2.038	-1.93
56.6	4001.94	1.9694916	2.032	-3.16
57.21	4998.28	2.305838	2.288	0.79

ACF	0.8009	bar
BCF	0.0050	
CCF	544.1776	Pa*min/m
QCF	0.2000	$Pa*min^2/m^2$
Adj. R^2	0.8779	-
Error %	7.84	Max.
	-8.88	Min.

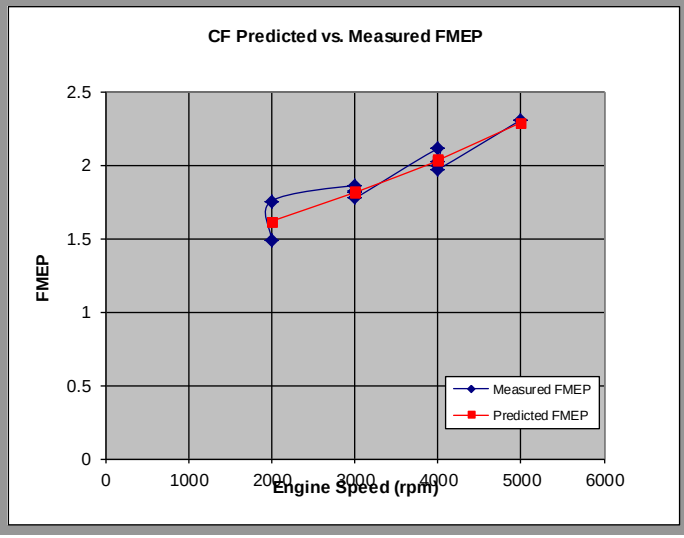

Otto Cycle

Otto cycle is assumed to have combustion process at constant volume. Typical compression ratio is from 9 to 11. The four basic processes are:

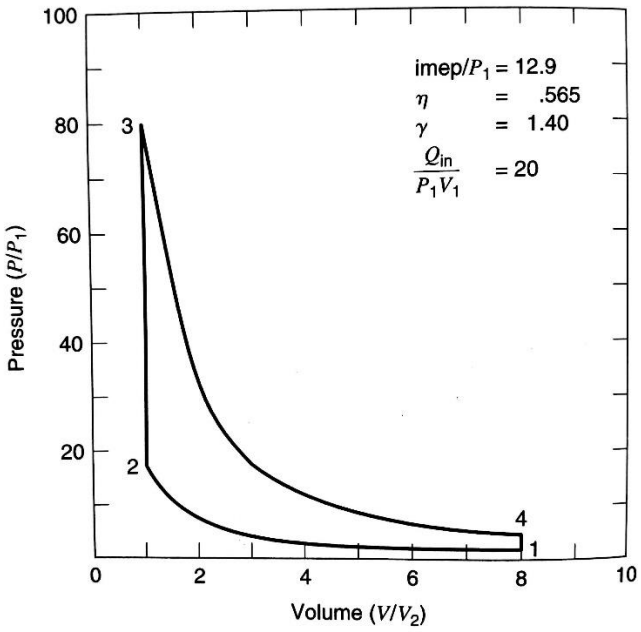

Figure 8-1 The Otto cycle [42]

- 1 to 2: Isentropic compression

$$\frac{T_2}{T_1} = R_c^{\gamma-1} \qquad \frac{P_2}{P_1} = R_c^{\gamma}$$

- 2 to 3: Constant volume heat addition

$$Q_{in} = mC_v(T_3 - T_2)$$

- 3 to 4: Isentropic expansion

$$\frac{T_4}{T_3} = \left(\frac{1}{R_c}\right)^{\gamma-1} \qquad \frac{P_4}{P_3} = \left(\frac{1}{R_c}\right)^{\gamma}$$

- 4 to 1: Constant volume heat rejection

$$Q_{out} = mC_v(T_4 - T_1)$$

- Indicated efficiency

$$\eta_{Otto} = 1 - R_c^{1-\gamma}$$

Diesel Cycle

Diesel cycle is assumed to have combustion process at constant pressure. The common compression ratio is from 15 to 20, higher from Otto cycle because it needs to reach cylinder temperature that is high enough for the mixture to auto-ignite. The different part of the process from Otto cycle will be the heat addition and expansion stroke.

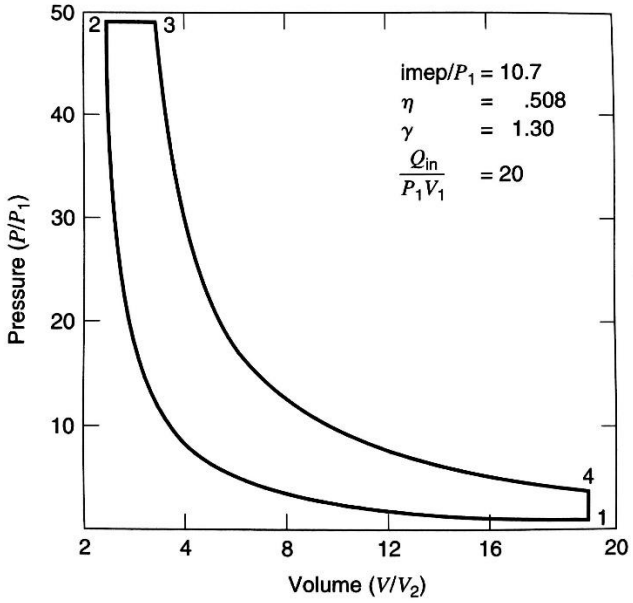

Figure 8-2 The Diesel cycle [42]

- 2 to 3: Constant pressure heat addition

$$Q_{in} = mC_p(T_3 - T_2)$$

- 3 to 4: Isentropic expansion

$$\frac{T_4}{T_3} = \left(\frac{\beta}{R_c}\right)^{\gamma-1} \qquad \frac{P_4}{P_3} = \left(\frac{\beta}{R_c}\right)^{\gamma}$$

- Indicated efficiency

$$\eta_{Diesel} = 1 - \frac{1}{R_c{}^{\gamma-1}} \cdot \frac{\beta^{\gamma} - 1}{\gamma(\beta - 1)}$$

- Parameter, β

$$\beta = \frac{T_3}{T_2} = \frac{V_3}{V_2}$$

Dual Cycle

Dual cycle represents the modern engine which is working at neither constant volume nor constant pressure. Part of the heat is added at constant volume process while the

remaining is added during constant pressure process. The distribution of the heat is influenced by the fuel injection, fuel type and engine geometry.

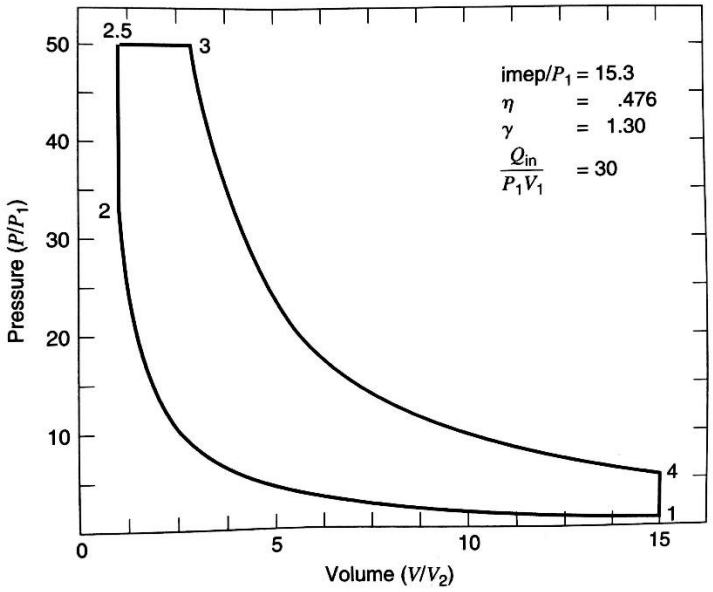

Figure 8-3 The Dual cycle [42]

- 2 to 2.5 & 2.5 to 3: Heat addition

$$Q_{in} = mC_v(T_{2.5} - T_2) + mC_p(T_3 + T_{2.5})$$

- Indicated efficiency

$$\eta_{Dual} = 1 - \left(\frac{1}{R_c}\right)^{\gamma-1} \cdot \frac{\alpha\beta^{\gamma} - 1}{(\gamma - 1) + \alpha\gamma(\beta - 1)}$$

- Parameters, β and α

$$\beta = \frac{T_3}{T_{2.5}} = \frac{V_3}{V_{2.5}} \qquad \alpha = \frac{P_3}{P_2}$$

Miller Cycle

One of the ways to increase the cycle efficiency is by having expansion ratio greater than compression ratio as adopted by Miller cycle through early and late intake valve closing.

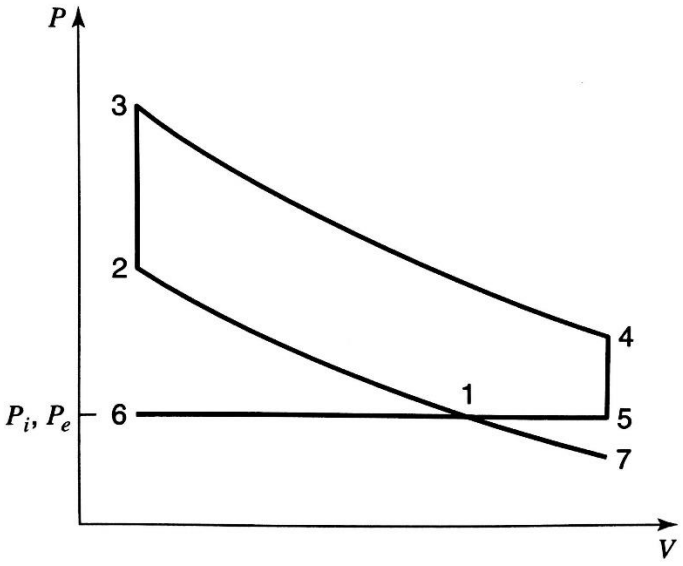

Figure 8-4 The Miller cycle [42]

- Effective compression ratio, R_c

$$R_c = \frac{V_1}{V_2}$$

- Expansion ratio, R_e

$$R_e = \frac{V_4}{V_3}$$

- Ratio of expansion ratio to the compression ratio, λ

$$\lambda = \frac{R_e}{R_c}$$

- 4 to 5 & 5 to 1: Heat rejection

$$Q_{out} = mC_v(T_4 - T_5) + mC_p(T_5 + T_1)$$

- Indicated efficiency

$$\eta_{Miller} = 1 - (\lambda R_c)^{1-\gamma} - \frac{\lambda^{1-\gamma} - \lambda(1-\gamma) - \gamma}{\gamma - 1} \cdot \frac{P_1 V_1}{Q_{in}}$$

Atkinson Cycle

Atkinson cycle is applying a similar concept with Miller cycle but the expansion stroke continues until it reaches the atmospheric pressure.

- Indicated efficiency

$$\eta_{Atkinson} = 1 - \gamma \cdot \frac{R_e - R_c}{R_e^{\gamma} - R_c^{\gamma}}$$

Otto Cycle + Turbocharging [93]

```
%1 - compressor
```

$$P_1 = P_r \times P_{atm}$$ P_r = Pressure ratio

$$T_1 = T_{in}\left(\frac{P_1}{P_{atm}}\right)^{\frac{\gamma-1}{\gamma}}$$

$$W_{compressor} = m \times C_p \times \left(T_1 - T_{in}\right)$$

```
%2 - turbine
```

$$T_{turbine} = T_{exhaust}\left(\frac{P_1}{P_{atm}}\right)^{\frac{\gamma-1}{\gamma}}$$

$$W_{turbine} = m \times C_p \times \left(T_{turbine} - T_4\right)$$

$$W_{otto} = Q_{in} - Q_{out}$$

$$W_{turbocharger} = W_{turbine} - W_{compressor}$$

$$\eta_{turbocharger} = \frac{\left(W_{otto} + W_{turbo}\right)}{Q_{in}}$$

$$\eta_{overall} = \eta_{otto} + \eta_{turbocharger}$$

BIBILIOGRAPHY

[1] A. E. Atabani, I. A. Badruddin, S. Mekhilef, and A. S. Silitonga, "A review on global fuel economy standards, labels and technologies in the transportation sector," *Renew. Sustain. Energy Rev.*, vol. 15, no. 9, pp. 4586–4610, Dec. 2011.

[2] M. Maria, R. Fernandez, and E. M. Tomanik, "Comparison of the potential to reduce fuel consumption by engine," *SAE Tech. Pap.*, no. 2013-36–0221, 2013.

[3] J. D. Miller and C. Facanha, "The state of clean transport policy - A 2014 synthesis of vehicle and fuel policy vevelopments," Washington DC, 2014.

[4] "ERTRAC research and innovation roadmaps," European Road Transport Research Advisory Council, 2011.

[5] R. Golloch and G. P. Merker, "Internal combustion engine downsizing: Fundamentals, state of the art and future concepts," *MTZ Worldw.*, vol. 66, pp. 20–22, 2005.

[6] M. Knopf, "How low can we go? Downsizing the internal combustion engine," *Ingenia*, London, Dec-2011.

[7] J. W. G. Turner *et al.*, "Ultra boost for economy: Extending the limits of extreme engine downsizing," *SAE Int. J. Engines*, vol. 7, no. 1, pp. 387–417, 2014.

[8] W. P. Attard, E. Toulson, H. Watson, and F. Hamori, "Abnormal combustion including mega knock in a 60 % downsized highly turbocharged PFI Engine," *SAE Tech. Pap.*, 2015.

[9] A. C. Clenci, G. Descombes, P. Podevin, and V. Hara, "Some aspects concerning the combination of downsizing with turbocharging, variable compression ratio, and variable intake valve lift," *Proc. Inst. Mech. Eng. Part D J. Automob. Eng.*, vol. 221, no. 10, pp. 1287–1294, 2007.

[10] Y. Li, H. Zhao, P. Stansfield, and P. Freeland, "Synergy between boost and valve timings in a highly boosted direct injection gasoline engine operating with Miller cycle experimental set-up," *SAE Tech. Pap.*, no. 2015-01–1262, 2015.

[11] R. Patel *et al.*, "Un-throttling a direct injection gasoline homogeneous mixture engine with variable valve actuation," *Int. J. Engine Res.*, vol. 11, no. 6, pp. 391–411, 2010.

[12] N. Fraser, H. Blaxill, G. Lumsden, and M. Bassett, "Challenges for increased efficiency through gasoline engine downsizing," *SAE Int. J. Engines*, vol. 2, no. 1,

pp. 991–1008, 2009.

[13] A. Isenstadt, J. German, M. Dorobantu, D. Boggs, and T. Watson, “Downsized , boosted gasoline engines,” *ICCT Internaltional Counc. Clean Transp.*, no. 21, p. 23, 2016.

[14] M. B. Çelik and B. Özdalyan, *Gasoline direct injection*. InTech, 2010.

[15] M. Haase and T. Piecyk, “Get ready for the combustion strategies of tomorrow: Variable Valvetrain,” in *Schaeffler Symposium 2014*, Schaeffler Technologies GmbH & Co. KG, 2014, pp. 188–201.

[16] G. Lumsden, D. Oudenijeweme, N. Fraser, and H. Blaxill, “Development of a turbocharged direct injection downsizing demonstrator engine,” *SAE Int. J. Engines*, vol. 2, no. 1, pp. 1420–1432, 2009.

[17] D. Hancock, N. Fraser, M. Jeremy, R. Sykes, and H. Blaxill, “A new 3 cylinder 1.2L advanced downsizing technology demonstrator engine,” *SAE Tech. Pap.*, no. 2008-01–0611, 2008.

[18] “All-new, fuel-efficient 1.0-litre Ford Ecoboost engine to debut in european Focus range,” 2011. [Online]. Available: http://www.ford.co.uk/experience-ford/AboutFord/News/VehicleNews/2011/Ecoboost-in-Focus.

[19] S. Bickerstaffe, “Ford 1.0 Ecoboost,” *Automotive Engineer*, 2012. [Online]. Available: http://ae-plus.com/features/ford-10-ecoboost/page:1.

[20] “17th international engine of the year awards,” *Engine Technology International Magazine*, 2015. [Online]. Available: http://ukipme.com/engineoftheyear/about.php.

[21] “FIAT air technologies.” [Online]. Available: http://www.fiat.co.uk/uk/air-technologies.

[22] “Panda natural power earns title of ‘Most Eco-friendly Car,’” 2012. [Online]. Available: http://www.fiat.com/com/news/panda-eco-friendly-2013.

[23] D. Coltman *et al.*, “Project Sabre : A close-spaced direct injection 3-cylinder engine with synergistic technologies to achieve low CO2 output,” *SAE Tech. Pap.*, no. 2008-01–0138, 2008.

[24] J. W. G. Turner, R. J. Pearson, R. Curtis, and B. Holland, “Sabre : A cost-effective engine technology combination for high efficiency, high performance and low CO2 emissions,” Norfolk, 2009.

[25] A. Eichhorn, D. Lejsek, A. Kulzer, A. Kufferath, E. Wizgall, and R. Centmayer, “Design of a boosted 2-cylinder SI-engine with gasoline direct injection to define

the needs of future powertrains," *SAE Tech. Pap.*, no. 2012-01–0832, 2012.

[26] T. Inoue, Y. Inoue, and M. Ishikawa, "Abnormal combustion in a highly boosted SI engine - The occurrence of Super Knock," *SAE Tech. Pap.*, no. 2012-01–1141, 2012.

[27] X. Zhen *et al.*, "The engine knock analysis – An overview," *Appl. Energy*, vol. 92, pp. 628–636, 2012.

[28] J. Taylor, N. Fraser, R. Dingelstadt, and H. Hoffmann, "Benefits of late inlet valve timing strategies afforded through the use of intake Cam-In-Cam applied to a gasoline turbocharged downsized engine," *SAE Tech. Pap.*, no. 2011-01–0360, 2011.

[29] P. Smith, J. Heywood, and W. Cheng, "Effects of compression ratio on spark-ignited engine efficiency," *SAE Tech. Pap.*, no. 2014-01–2599, 2014.

[30] M. Sjerić, I. Taritaš, R. Tomić, M. Blažić, D. Kozarac, and Z. Lulić, "Efficiency improvement of a spark-ignition engine at full load conditions using exhaust gas recirculation and variable geometry turbocharger – Numerical study," *Energy Convers. Manag.*, vol. 125, pp. 26–39, 2016.

[31] T. G. Leone *et al.*, "The effect of compression ratio, fuel octane rating, and ethanol content on spark-ignition engine efficiency," *Environ. Sci. Technol.*, vol. 49, pp. 10778–10789, 2015.

[32] J. Chang, Y. Viollet, A. Alzubail, A. F. N. Abdul-Manan, and A. Al Arfaj, "Octane-on-Demand as an enabler for highly efficient spark ignition engines and greenhouse gas emissions improvement," *SAE Tech. Pap.*, no. 2015-01–1264, 2015.

[33] V. S. B. Shankar *et al.*, "Antiknock quality and ignition kinetics of 2-phenylethanol, a novel lignocellulosic octane booster," *Proc. Combust. Inst.*, vol. 0, pp. 1–8, 2015.

[34] K. Kumano and S. Yamaoka, "Analysis of knocking suppression effect of cooled EGR in turbo-charged gasoline engine," *SAE Tech. Pap.*, no. 2014-01–1217, Apr. 2014.

[35] L. Francqueville and J.-B. Michel, "On the effects of EGR on spark-ignited gasoline combustion at high load," *SAE Int. J. Engines*, vol. 7, no. 4, pp. 1808–1823, 2014.

[36] F. Bozza, V. De Bellis, and L. Teodosio, "Potentials of cooled EGR and water injection for knock resistance and fuel consumption improvements of gasoline

engines," *Appl. Energy*, vol. 169, pp. 112–125, 2016.

[37] Y. Zhuang and G. Hong, "Effects of direct injection timing of ethanol fuel on engine knock and lean burn in a port injection gasoline engine," *Fuel*, vol. 135, pp. 27–37, 2014.

[38] N. Kim, S. Cho, and K. Min, "A study on the combustion and emission characteristics of an SI engine under full load conditions with ethanol port injection and gasoline direct injection," *Fuel*, vol. 158, pp. 725–732, Oct. 2015.

[39] D. Takahashi, K. Nakata, and Y. Yoshihara, "Engine thermal control for improving the engine thermal efficiency and anti-knocking quality," *SAE Tech. Pap.*, no. 2012-01–0377, 2012.

[40] J. Harishchandra *et al.*, "Optimisation of engine cooling for knock suppression of turbocharged gasoline engine," in *International Conference on Engineering and Meta-Engineering*, 2010.

[41] T. Nishano, H. Senba, and N. Murakami, "Study of engine cooling technologies for knock suppression in spark ignition engines," *Mitsuhibishi Mot. Tech. Rev.*, no. 16, pp. 17–22, 2004.

[42] C. R. Ferguson and A. T. Kirkpatrick, *Internal Combustion Engines: Applied Thermosciences*, Second. United States of America: John Wiley & Sons, Inc., 2001.

[43] R. Miller, "Supercharged Engine," 1957.

[44] O. M. F. Junior, "Impact of the miller cycle in the efficiency of an FVVT (Fully variable valve train) engine during part load operation," *SAE Tech. Pap.*, no. 2009-36–0081, 2009.

[45] B. Ribeiro and J. Martins, "Direct comparison of an engine working under Otto , Miller and Diesel cycles : Thermodynamic analysis and real engine performance," *SAE Tech. Pap.*, no. 2007-01–0261, 2007.

[46] A. Al-Sarkhi, J. O. Jaber, and S. D. Probert, "Efficiency of a Miller engine," *Appl. Energy*, vol. 83, pp. 343–351, 2006.

[47] J. B. Heywood, *Internal combustion engine fundamentals*. Singapore: McGraw-Hill Book Company, 1988.

[48] J. Zhao, "Research and application of over-expansion cycle (Atkinson and Miller) engines – A review," *Appl. Energy*, vol. 185, pp. 300–319, 2017.

[49] G. Gonca, "Thermodynamic analysis and performance maps for the irreversible Dual – Atkinson cycle engine (DACE) with considerations of temperature-

dependent specific heats , heat transfer and friction losses," *Energy Convers. Manag.*, vol. 111, pp. 205–216, 2016.

[50] Kazuyuki Okudaira, "The story behind the Prius," 2015. [Online]. Available: https://asia.nikkei.com/Business/Companies/The-story-behind-the-Prius.

[51] "Honda Introduces the 'INSIGHT', a Hybrid Car that Offers the World's Lowest Fuel Consumption for a Mass-Produced Gasoline-Powered Vehicle," 1999. [Online]. Available: http://world.honda.com/worldnews/1999/4990906c.html.

[52] R. Brown, "Sustainability Report 2012/13," 2012.

[53] W. Gottschalk, U. Lezius, and L. Mathusall, "Investigations on the potential of a variable Miller cycle for SI knock control," *SAE Tech. Pap.*, no. 2013-01–1122, 2013.

[54] Y. Mito, K. Tanzawa, M. Watanabe, and Y. Eiyama, "Advanced combustion performance for high efficiency in new I3 1.2L supercharged gasoline engine by effective use of 3D engine simulation," *SAE Tech. Pap.*, no. 2012-01–0422, 2012.

[55] R. Flierl and M. Kluting, "The third generation of valvetrains – New fully variable valvetrains for throttle-free load control," *SAE*, pp. 2000-01–1227, 2000.

[56] R. Osborne, T. Downes, S. O'Brien, K. Pendlebury, and M. Christie, "A Miller Cycle Engine without Compromise - The Magma Concept," *SAE Int. J. Engines*, vol. 10, no. 3, pp. 2017-01–0642, 2017.

[57] O. A. Kutlar, H. Arslan, and A. T. Calik, "Methods to improve efficiency of four stroke, spark ignition engines at part load," *Energy Convers. Manag.*, vol. 46, pp. 3202–3220, 2005.

[58] Y. Wang *et al.*, "Application of the Miller cycle to reduce NOx emissions from petrol engines," *Appl. Energy*, vol. 85, no. 6, pp. 463–474, Jun. 2008.

[59] J. Zhao, M. Xu, M. Li, B. Wang, and S. Liu, "Design and optimization of an Atkinson cycle engine with the Artificial Neural Network Method," *Appl. Energy*, vol. 92, pp. 492–502, 2012.

[60] L. Miklanek, V. Klir, O. Vitek, and O. Gotfryd, "Study of unconventional cycles (Atkinson and Miller) with mixture heating as a means for the fuel economy improvement of a throttled SI engine at part load," *SAE Int. J. Engines*, vol. 5, no. 4, pp. 1624–1636, 2012.

[61] P. A. Stansfield, "The control of an unthrottled homogeneous DISI engine through reduced valve lift and duration," Loughborough University, 2008.

[62] J. W. G. Turner *et al.*, "The HOTFIRE homogeneous GDI and fully variable valve

train project - An initial report," *SAE Tech. Pap.*, no. 2006-01–1260, 2006.

[63] M. A. R. S. Al-baghdadi, "A simulation model for a single cylinder four-stroke spark ignition engine fueled with alternative fuels," *Turkish J. Eng. Env. Sci.*, vol. 30, pp. 331–350, 2006.

[64] "Ricardo WAVE Software," *Version 2015.1*. .

[65] "MATLAB and statistics toolbox," *Release 2016a,* 2016. [Online]. Available: https://www.mathworks.com/products/simulink.html.

[66] D. G. Goodwin, H. K. Moffat, and R. L. Speth, "Cantera: An object- oriented software toolkit for chemical kinetics, thermodynamics, and transport processes," *Version 2.2.1,* 2016. [Online]. Available: http://www.cantera.org.

[67] A. M. Douaud and P. Eyzat, "Four-Octane-Number method for predicting the anti-knock behavior of fuels and engines," *SAE Tech. Pap.*, no. 780080, 1979.

[68] Z. Liu and R. Chen, "A Zero-Dimensional Combustion Model with Reduced Kinetics for SI Engine Knock Simulation," *Combust. Sci. Technol.*, vol. 181, no. 6, pp. 828–852, Jun. 2009.

[69] L. Liang, R. D. Reitz, C. O. Iyer, and J. Yi, "Modeling Knock in Spark-Ignition Engines Using a G -equation Combustion Model Incorporating Detailed Chemical Kinetics," *SAE Tech. Pap.*, pp. 2007-01–0165, 2007.

[70] P. Eckert, S. Kong, and R. D. Reitz, "Modeling Autoignition and Engine Knock Under Spark Ignition Conditions," *SAE Tech. Pap.*, no. 2003-01–0011, 2003.

[71] D. Linse, A. Kleemann, and C. Hasse, "Probability density function approach coupled with detailed chemical kinetics for the prediction of knock in turbocharged direct injection spark ignition engines," *Combust. Flame,* vol. 161, no. 4, pp. 997–1014, Apr. 2014.

[72] S. Fontanesi, G. Cicalese, A. d'Adamo, and G. Cantore, "A Methodology to Improve Knock Tendency Prediction in High Performance Engines," *Energy Procedia,* vol. 45, pp. 769–778, 2014.

[73] Z. Liu, "Chemical Kinetics Modelling Study on Fuel Autoignition in Internal Combustion Engines," Loughborough University, 2010.

[74] H. J. Curran, P. Gaffuri, W. J. Pitz, and C. K. Westbrook, "A comprehensive modeling study of n-heptane oxidation," *Combust. Flame,* no. 114, pp. 149–177, 1998.

[75] H. J. Curran, P. Gaffuri, W. J. Pitz, and C. K. Westbrook, "A comprehensive modeling study of iso-Octane oxidation," *Combust. Flame*, no. 129, pp. 253–280,

2002.

[76] H. Wang, M. Yao, and R. D. Reitz, “Development of a Reduced Primary Reference Fuel Mechanism for Internal Combustion Engine Combustion Simulations,” *Energy Fuels*, vol. 27, pp. 7843–7853, 2013.

[77] S. Petrakides, “On the combustion of premixed natural gas-gasoline dual fuel blends in SI engines,” Loughborough University, 2016.

[78] G. Shu, J. Pan, and H. Wei, “Analysis of onset and severity of knock in SI engine based on in-cylinder pressure oscillations,” *Appl. Therm. Eng.*, vol. 51, pp. 1297–1306, 2013.

[79] A. J. Shahlari and J. B. Ghandhi, “A Comparison of Engine Knock Metrics,” *SAE Tech. Pap.*, pp. 2012-32–7, Oct. 2012.

[80] S. S. Merola and B. M. Vaglieco, “Knock investigation by flame and radical species detection in spark ignition engine for different fuels,” *Energy Convers. Manag.*, vol. 48, no. 11, pp. 2897–2910, Nov. 2007.

[81] N. Kawahara, E. Tomita, and Y. Sakata, “Auto-ignited kernels during knocking combustion in a spark-ignition engine,” *Proc. Combust. Inst.*, vol. 31, no. 2, pp. 2999–3006, Jan. 2007.

[82] X. Zhen, Y. Wang, and Y. Zhu, “Study of knock in a high compression ratio SI methanol engine using LES with detailed chemical kinetics,” *Energy Convers. Manag.*, vol. 75, pp. 523–531, Nov. 2013.

[83] T. Li, Y. Gao, J. Wang, and Z. Chen, “The Miller cycle effects on improvement of fuel economy in a highly boosted, high compression ratio, direct-injection gasoline engine: EIVC vs. LIVC,” *Energy Convers. Manag.*, vol. 79, pp. 59–65, 2014.

[84] P. Ferrey, Y. Miehe, C. Constensou, and V. Collee, “Potential of a variable compression ratio Gasoline SI engine with very high expansion ratio and variable valve actuation,” *SAE Int. J. Engines*, vol. 7, no. 1, 2014.

[85] J. J. G. Martins, K. Uzuneanu, B. S. Ribeiro, and O. Jasasky, “Thermodynamic analysis of an over-expanded engine,” *SAE Tech. Pap.*, no. 2004-01–0617, 2004.

[86] V. De Bellis, “Performance optimization of a spark-ignition turbocharged VVA engine under knock limited operation,” *Appl. Energy*, vol. 164, pp. 162–174, 2016.

[87] S. Luisi *et al.*, “Experimental investigation on early and late intake valve closures for knock mitigation through Miller cycle in a downsized turbocharged engine,” *SAE Tech. Pap.*, no. 2015-01–0760, 2015.

[88] T. Goto, K. Hatamura, S. Takizawa, N. Hayama, H. Abe, and H. Kanesaka,

"Development of V6 Miller cycle gasoline engine," *SAE Tech. Pap.*, no. 940198, 1994.

[89] H. Sakai, H. Noguchi, M. Kawauchi, and Hiros, "A new type of Miller supercharging system for high speed engines- Part 1 fundamental considerations and application to gasoline engines," *SAE Tech. Pap.*, no. 851522, 1985.

[90] R. Patel *et al.*, "Comparison between unthrottled , single and two-valve induction strategies utilising direct gasoline injection : Emissions , heat-release and fuel consumption analysis," *SAE Tech. Pap.*, no. 2008-01–1626, 2008.

[91] P. A. Stansfield *et al.*, "Unthrottled engine operation using variable valve actuation : The impact on the flow field , mixing and combustion," *SAE Tech. Pap.*, pp. 2007-01–1414, 2007.

[92] G. Pitcher, J. W. G. Turner, and R. J. Pearson, "GEM ternary blends of Gasoline, Ethanol and Methanol: An initial investigation into fuel spray and combustion characteristics in a direct-injected spark-ignition optical engine using Mie Imaging," *SAE Tech. Pap.*, no. 2012-01–1740, 2012.

[93] V. Ganesan, *Internal combustion engines*, 2nd ed. Singapore: Mc Graw Hill, 2004.